

https://dspace.org/

Fatigue crack growth behaviour of tungsten carbide-cobalt hardmetal alloys

Fry, Peter Ryan

2015-03-13
http://hdl.handle.net/10539/17280

Downloaded from a DSpace repository. https://dspace.org/

FATIGUE CRACK GROWTH BEHAVIOUR OF TUNGSTEN CARBIDE-COBALT HARDMETAL ALLOYS

Peter Ryan Fry

A Dissertation submitted to the Faculty of Engineering, University of the Witwatersrand, Johannesburg in fulfilment of the requirements for the Degree of Master of Science in Engineering.

Department of Metallurgy
University of the Witwatersrand
June 1982

DECLARATION

I declare that this dissertation is my own, unaided work. It is being submitted for the degree of Master of Science in Engineering at the University of the Witwatersrand, Johannesburg. It has not been submitted before for any degree or examination in any other university.

PETER RYAN FRY

22nd day of June, 1982.

ABSTRACT

THE FATIGUE CRACK GROWTH BEHAVIOUR OF TUNGSTEN CARBIDE-COBALT ALLOYS

For many engineering materials fatigue crack growth plays a dominant role in determining component life. In general terms this can be considered to be true for many applications of tungsten carbide-cobalt hardmetal alloys, which are used almost universally in variable loading situations. By implication, therefore, there is a substantial design requirement for quantitative fatigue data and a need for a greater understanding of the nature and mechanisms of fatigue crack propagation in these alloys.

However, the determination of fatigue crack growth data in ostensibly brittle materials has always presented problems due to their particular sensitivity to catastrophic failure. It is almost essential in such studies to utilise a constant stress intensity specimen geometry, and the recently developed double torsion test has been used very successfully throughout the test programme described in this thesis. Crack growth has been monitored throughout using a dye penetrant technique with an optical travelling microscope system.

Fatigue data have been obtained in the form of crack growth rate versus stress intensity range (da/dN vs K_I) graphs, for six different alloys of varying grain size and cobalt content. The effects of testing variables such as mean stress intensity, stress intensity amplitude and frequency have been explored. Subcritical crack growth under monotonic loading has also been determined in two alloys in order to provide a comparison to the corresponding crack growth behaviour under fatigue

loading. Further, some preliminary investigations have been made into the effect of elevated temperature on fatigue crack growth.

The results show that fatigue crack growth obeys a so-called, Paris 'law' of the form $da/dN = C'(\Delta K_I)^m$, but propagation rates increase as the mean stress intensity increases. The value of the exponent 'm' varies in the range 20 to 10, decreasing as the cobalt content and grain size (i.e. the mean free path) increase. Static crack growth does not occur below a stress intensity of $0,9K_{IC}$, with the exponent 'n' in $da/dt = A(K_I)^n$, having values in the range 125 to 200. There is no significant influence of frequency on the crack advance per cycle, but there is some indication that fatigue crack growth rates increase with temperature, although further work is required to substantiate this effect.

It has been unequivocally proven that true cyclic crack growth mechanisms operate in hardmetal alloys at room temperature despite the fact that, fractographically, fatigue and fast fracture are indistinguishable.

A model is proposed which attempts to explain this apparent anomaly through consideration of the local fracture events at, and ahead of, an extending crack tip.

ACKNOWLEDGEMENTS

I am indebted to the following people and institutions for their invaluable assistance, advice, use of equipment and, particularly, their encouragement:

Professor Geoff Garrett, who persuaded me to embark on this project, for his interest and enthusiastic supervision of the work.

Members of Boart International, especially R. Cooper Dr C. Peters, T. Hack and V. Motuba at the Krugersdorp Research Centre and N. Dent, A. Paxton and H. de Villiers at the Springs production plant.

T. Dean, Dr N. Pipkin and T. Elworthy of the de Beers Research Laboratories.

Members of staff of the Electron Microscope Unit of the University of the Witwatersrand.

Dr S. Luyckx, who was always ready to discuss my problems and who through her overseas contacts kept me in touch with the most recent work on WC-Co alloys.

My friends and fellow students in the Fracture Research Laboratory, particularly R. Tait, for useful discussions.

Finally, to Boart International, the Council for Scientific and Industrial Research and to the Bursaries Fund of the University of the Witwatersrand, for their financial support for the duration of my work.

CONTENTS

	Declaration	i
	Abstract	ii
	Acknowledgements	iii
	Contents	iv
	Nomenclature	x
1	INTRODUCTION	1
	1.1 Fatigue Crack Growth and Fracture Mechanics	1
	1.2 Anvil Failures	6
2	MATERIAL DESCRIPTION	10
	2.1 Introduction	10
	2.2 Summary of Manufacturing Process	11
	2.3 Properties of the Individual Constituents	13
	2.4 Inter-relationship between Tungsten, Carbon and Cobalt	17
	2.4.1 Tungsten-carbon phase diagram	17
	2.4.2 Tungsten carbide-cobalt phase relationships	18
	2.4.3 Alloying of the binder by tungsten & carbon	19
	2.4.4 Alloying of the binder by other elements	19
	2.5 Wetting of the Carbide Grains by the Binder	20
	2.6 Residual Stresses	21
	2.7 Microstructural Variables	24
	2.7.1 Cobalt binder phase	24
	2.7.2 Tungsten carbide grains	25
	2.7.3 Contiguity	25
	2.7.4 Porosity and defects	28
	2.7.5 Summary	28
	2.8 Mechanical Properties of WC-Co Alloys	29
	2.8.1 Introduction	29
	2.8.2 Hardness	30
	2.8.3 Uniaxial compressive strength	33
	2.8.4 Transverse rupture and tensile strength	37
	2.8.5 Fracture toughness	43
	2.8.6 Poisson's ratio and Young's modulus	48
	2.8.7 Summary	49

2.9 Slow Crack Growth under Static Load 50
2.10 Fatigue 52
2.10.1 S-N data 52
2.10.1.1 Rotating beam in bending (R = -1) 53
2.10.1.2 Three-point bend tests (R = 0,1) 54
2.10.1.3 Compression tests (R < 0,05) 55
2.10.1.4 Elevated temperature fatigue 56
2.10.2 da/dN vs ΔK_I data 56
2.10.3 Frequency effects 61
2.10.4 Fractography and the mechanisms of fatigue 61
2.10.5 Summary 65

3 REVIEW OF THE DOUBLE TORSION TEST METHOD 68
3.1 Introduction 68
3.2 Theoretical Analysis 71
3.2.1 Description of test 71
3.2.2 Derivation of the stress intensity at the crack tip 73
3.3 Influence of Specimen Geometry on the Fracture Mechanics Measurements 78
3.3.1 Mode of fracture 78
3.3.2 Specimen geometry and dimensions 80
3.3.3 Thickness 83
3.3.4 Grooves 84
3.3.5 Variation of stress intensity with crack length 86
3.3.6 Crack front shape and growth rate correction factors 89
3.4 Experimental Techniques 93
3.4.1 Pre-cracking 93
3.4.2 Direct measurement of crack length (Position of crack tip) 95
3.4.3 Use of compliance to measure crack length 96
3.4.4 Applications of the compliance relationship to determine crack growth rates indirectly 100
3.4.4.1 Constant displacement methods 101
3.4.4.2 Constant displacement rate 105

3.4.4.3 Constant load methods 107
3.4.4.4 Displacement rate and constant displacement combination 109
3.5 Summary 112

4 EXPERIMENTAL DETAILS 115
4.1 Introduction 115
4.2 Material Properties 115
4.3 Double Torsion Specimen 118
4.3.1 Geometry 118
4.3.2 Notch preparation 121
4.3.3 Crack front shape 123
4.4 Procedure for Obtaining Centre Line Fracture 125
4.4.1 Loading system 125
4.4.2 Alignment 128
4.4.3 Pre-cracking 130
4.5 Crack Length Measurement 132
4.5.1 General background 132
4.5.2 Fatigue crack growth rate measurement 133
4.5.3 Static crack growth data 136
4.6 Double Torsion and Fracture in a Scanning Electron Microscope 137
4.7 Elevated Temperature Investigation 140
4.8 Preparation of SEM Samples 145

5 RESULTS 147
5.1 Crack Growth under Static Loading 147
5.1.1 Static load crack growth rate 147
5.1.2 Fracture observations in SEM 149
5.2 Fatigue 155
5.2.1 Fatigue crack growth rates for R ratio < 0,1 155
5.2.2 Fatigue at constant mean stress intensity 161
5.2.3 Fatigue at constant stress intensity range 167
5.2.4 Constant R values 172
5.2.5 Frequency effects at R < 0,1 176
5.2.6 Fatigue fracture path 185

5.2.7 Fatigue at elevated temperatures 188
5.2.7.1 Effect of thermal cycling 188
5.2.7.2 Elevated temperature fatigue testing 189
5.3 Fracture Toughness 198
5.4 Fractography 201

6 DISCUSSION 209
6.1 Introduction 209
6.2 Crack Growth under Static Loading 212
6.2.1 Background 212
6.2.2 Static crack growth rate 212
6.2.3 Observations in SEM 212
6.3 Fatigue Crack Propagation 214
6.3.1 Fatigue mechanisms in metals 214
6.3.2 Fatigue crack growth rate results in WC-Co alloys 215
6.4 Fracture Toughness 222
6.5 Model of the Crack Tip 225
6.6 Model for Static Crack Growth 228
6.7 Model for Fatigue Crack Growth 229
6.8 Anvil Failure 233

7 CONCLUSIONS AND RECOMMENDATIONS FOR FUTURE WORK 237
7.1 Conclusions 237
7.1.1 Experimental technique 237
7.1.2 Static crack growth 237
7.1.3 Fatigue crack growth 238
7.1.4 Fractography 239
7.1.5 Model for fatigue crack propagation 239
7.2 Recommendations for Future Work 240
7.2.1 Double torsion test geometry 240
7.2.2 Crack length measurement 240
7.2.3 Inert atmosphere and elevated temperature tests 241
7.2.4 Fracture toughness 241
7.2.5 In situ SEM studies of fracture 242

7.2.6 Fractography 242
7.2.7 General 242

REFERENCES 244

APPENDIX 1 - K_{Ic} data extracted from literature 253

APPENDIX 2 - Microstructural details 259

APPENDIX 3 - Examples of defects in specimens 265

APPENDIX 4 - Drawings of test rig 267

APPENDIX 5 - Indirect measurement of crack growth 272

APPENDIX 6 - da/dN vs ΔK_I at R ratio < 0,1 281

NOMENCLATURE

a	crack length
a_c	critical crack length
a_f	final crack length
a_i	initial crack length
A	area of crack
C	compliance
C	constant of proportionality in equation $da/dN = C(\Delta K_I)^m$
d	double torsion specimen thickness
d_w	double torsion specimen thickness in plane of crack
$\bar{d}$	mean tungsten carbide grain size
E	elastic (Young's) modulus
f_{Co}	volume fraction of cobalt
f_{WC}	volume fraction of carbide
G	shear modulus
HV	Vicker's hardness
K_I	stress intensity for mode I opening
K_{IC}	critical stress intensity for mode I opening
ΔK_I	stress intensity range in fatigue $(K_{Imax} - K_{Imin})$
L	length of double torsion specimen
m	exponent in fatigue crack growth equation $da/dN = C(\Delta K_I)^m$

n	exponent in static crack growth equation $da/dt = A(K_I)^n$
N	number of cycles
N_f	number of cycles to failure
P	load
R	ratique ratio = K_{Imin}/K_{Imax} or P_{min}/P_{max}
t	time
T	temperature
v	velocity
w	double torsion specimen width
w_m	moment arm of double torsion specimen
y	displacement
$\dot{y}$	displacement rate, w.r.t time

G_{IC}	critical strain energy release rate
ξ	thickness correction factor used in double torsion stress intensity calculation
θ	torsional strain
λ_{nom}	nominal mean free path
λ_{true}	true mean free path
ν	Poisson's ratio
μm	microns (10^{-6} metre)
σ_{app}	applied static stress
$\Delta\sigma_{app}$	applied cyclic stress
σ_y	yield stress
σ_{UTS}	ultimate tensile strength

1 INTRODUCTION

1.1 FATIGUE CRACK GROWTH AND FRACTURE MECHANICS

Fatigue crack propagation remains a major cause for failure in engineering components. This is despite a considerable improvement in the understanding of fatigue mechanisms and the development of fracture mechanics methods for the quantitative assessment of failure.

For many materials fracture toughness values are either commonly available or can be readily determined by standard laboratory procedures. Corresponding fatigue crack propagation data, however, are, relatively speaking, much less available and this is particularly the case for nominally 'brittle' materials, for which conventional specimen geometries are totally inappropriate.

Tungsten carbide-cobalt hardmetal alloys typify this situation. There is a wealth of information available on fracture toughness but only limited work has been directed at measuring fatigue crack growth behaviour and identifying the mechanisms of cyclic crack propagation.

The majority of hardmetal alloy components consist of the tungsten carbide-cobalt combination but other carbide and binder systems are not uncommon. Almost all are commonly subject to fatigue loading. (Table 1.1).

Table 1.1

TYPICAL APPLICATIONS OF WC-CO COMPONENTS

Composition ranges		Grain structure	Application categories		Typical applicatons
WC	Co		Abrasion	Shock	
97-93	2-3	fine	extreme	none	wire-drawing dies, shot-blast nozzles, plug gauges, machine parts
95-97	3-5	fine or medium	very severe	very low	drawing and compacting dies, machine parts, lathe centres, bushes, thread guides, pen balls
92-95	5-8	fine			
94-95	5-6	medium	severe	low	masonry and glass drills, scribers, tyre studs, rolls, woodworking routers, machine parts, mechanical seals
90-92	8-10	fine			
90-94	6-10	medium	medium	medium	extrusion dies, rolls, scrapers, work rest blades, mandrels, forming blades
92-95	5-8	coarse	moderate to medium	medium to severe	twist and guide rolls, plane irons and other woodworking cutters, grinding mill components punching and blanking dies
86-90	10-14	fine or medium			
87-92	8-13	coarse	moderate	severe	heading and forming dies, anvils, crushers, hammers
70-85	15-30	medium or coarse			

For many applications the criterion for alloy composition selection may not include fatigue life. Hardness, wear resistance, toughness, elevated temperature deformation, yield strength may all supersede the resistance to fatigue. However, the fact that failures arising from subcritical crack growth do occur in these materials (Figures 1.1 and 1.2) is a clear indication that fatigue needs to be more seriously investigated and should be integrated into the application and alloy selection process.

The most rational approach to the problem of dealing with fatigue is the determination of cyclic crack growth rate as a function of operating stresses and prevailing flaw sizes, i.e. the stress intensity range. The data

obtained not only characterise the alloys tested but enable a fracture mechanics evaluation of a component's expected service performance.

The basis for failure prediction is the ability to calculate the stress intensity (K_I) or, in the case of cyclic loading, the stress intensity range (ΔK_I) acting at a crack tip. The 'worst case' philosophy associated with fracture mechanics assumes that cracks of some nature will exist in all components, these are either inadvertently designed-in or result from flaws and defects produced in the material during fabrication or service. The stress intensity equations combine the stress in the component and the crack length:

$$K_I = \phi(\sigma_{app})(\pi a)^{\frac{1}{2}} \qquad \text{static loading}$$

$$\Delta K_I = \phi(\Delta\sigma_{app})(\pi a)^{\frac{1}{2}} \qquad \text{fatigue loading}$$

where:

K_I = stress intensity (mode I, or tensile crack opening)
ΔK_I = stress intensity range
σ_{app} = monotonic stress
$\Delta\sigma_{app}$ = cyclic stress
ϕ = constant of proportionality, depends on geometry of component
a = crack length

Under static loads, when the stress intensity at a crack tip reaches a critical value, the fracture toughness of the material, K_{IC}, catastrophic failure occurs. This can happen when either the applied stress or the crack length (or both) increase.

Fatigue crack growth has been defined by the well established Paris 'law':

$$\frac{da}{dN} = C(\Delta K_I)^m$$

where:

N = number of cycles
m = growth rate exponent
C = constant

Since ΔK_I increases continuously as the crack propagates the equation has to be integrated to estimate anticipated life (N_f):

$$N_f = \int_0^{N_f} dN = \frac{1}{C} \int_{a_i}^{a_c} \frac{da}{(\Delta K_I)^m}$$

$$N_f = \frac{1}{C} \int_{a_i}^{a_c} \frac{da}{\{\phi(\Delta\sigma_{app})(\pi a)^{\frac{1}{2}}\}^m}$$

$$N_f = \frac{1}{C\phi^m \pi^{m/2}(\Delta\sigma_{app})^{m(1-m/2)}} \left[a_c^{(1-m/2)} - a_i^{(1-m/2)} \right]$$

where:

N_f = number of cycles to failure
a_i = initial crack length
a_c = critical crack length

The investigation of fatigue in any material system represents a vast area for research in which numerous variables: frequency, wave form, environments, temperature, alloying and mean loading can be explored.

The objective of this research programme has been to develop a viable and reproducible technique for measuring fatigue crack growth in tungsten carbide-cobalt alloys, and to quantify some of the many microstructural and operational factors which influence its magnitude.

1.2 ANVIL FAILURES

The nature of failures reported for the high pressure anvils used in the manufacture of synthetic diamonds indicates that fatigue is a likely mechanism: the life of a unit is variable and unpredictable.

Unfortunately, the service conditions are largely unknown. The extent of hydraulic load transfer to the anvil is obscured by the pressure-absorbing friction created between the various components in the system. The diamonds are synthesised at high temperature but the temperature in the anvils can only be roughly approximated. Thus, it is estimated that the synthesis capsule is subjected to a pressure of 6000 MPa and temperature of 1500°C, so that the anvil stress would therefore be in the range 3000 - 6000 MPa[1] depending on the cross sectional area, at temperatures of about 500°C.

Due to the industrial secrecy that surrounds diamond manufacture it is not known whether each cycle an anvil unit experiences is precisely the same; both pressure and temperature conditions may be changed. In spite of this the range of performance indicates that defects in the material must exist, that initially they are subcritical and the anvil performs satisfactorily, but that the defect subsequently grows, presumably by fatigue, eventually reaching a critical size which precipitates failure. (Table 1.2).

Blumenthal[1] has calculated the stresses in anvils and shown that tensile circumferential stresses occur close to the surface about half way down the nose cone of the anvils. Evidence from fractured anvils indicates that these regions of tensile stress cause or contribute to the final failure of the component.

Fatigue crack growth data, together with stress analysis and non-destructive testing of anvils, and in fact all components used under cyclic loading, should

enable a more rational approach to alloy selection, which at present is based almost entirely on trial and error methods.

Table 1.2

SUMMARY OF TYPICAL ANVIL LIFE[2]

LIFE CYCLES	DESCRIPTION OF FAILURE
8	Failure by nose chips reducing nose area.
30	Vertical fracture, with beach markings, followed by horizontal fast fracture.
83	Horizontal fracture at the level of the shoulder.
325	'Cake slice' fracture in nose cone, Figure 1.1 taken from horizontal crack at shoulder level.
635	Vertical fracture with 'beach markings', Figure 1.2.
685	Not known.
735	Vertical fracture with 'beach markings'.

(A description of the use of anvils in diamond synthesis, stress analysis and typical failures can be found in Blumenthal's thesis.[1]).



Figure 1.1 Smooth flat fracture surface typical of fatigue.



Figure 1.2 Typical beach markings from fractured anvil.

The following literature survey is divided into two chapters. The first is a brief review of tungsten carbide-cobalt hardmetal and the second an assessment of the experimental techniques available for studying crack growth in brittle materials. The double torsion geometry, selected for this investigation, is discussed in detail as it is still a little-known technique.

The object of this survey is to provide readers and future workers in this area of research with the information necessary for a thorough understanding of the tungsten carbide-cobalt alloy system and the double torsion technique used in the test programme.

2 MATERIAL DESCRIPTION

2.1 INTRODUCTION

Tungsten carbide-cobalt hardmetal is a composite manufactured using powder metallurgical and sintering procedures. The two constituents, having vastly different properties, contribute to one of the most technically successful combinations currently in use in composite materials. A wide variety of alloy grades can be obtained by varying the proportions of hard, brittle tungsten carbide grains and soft, ductile cobalt-rich binder. In order to obtain an understanding of the bulk material the properties of the two phases, their interaction and established mechanical behaviour are briefly reviewed. Exner[3] has recently published a comprehensive paper on cemented carbides which should be consulted for further details on most of the topics mentioned here.

2.2 SUMMARY OF THE MANUFACTURING PROCESS

(i) Tungsten:

Raw materials used for obtaining tungsten are the ores wolframite $Fe/MnWO_4$ and scheelite $CaWO_4$. These are chemically processed to produce tungsten trioxide, WO_3, tungsten hydratic acid, H_2WO_4 and blue tungsten, W_4O_{11}, and then via hydrogen reduction to tungsten metal powder.[3]

(ii) Cobalt:

Cobalt metal is extracted from the ore electrolytically and is purchased as impure 'cathode metal'. The metal is dissolved in concentrated acid and the impurities precipitated out. Cobalt oxides, Co_3O_4, CoO are produced from the cobalt carbonate which has also been precipitated out, these are hydrogen reduced to Co metal powder.

(iii) Tungsten carbide

Tungsten metal powder and carbon black are blended together in stoichiometric proportions (1 to 1 atomic %, equivalent to 6,12 wt% carbon) pressed into blocks and heated to 1400 - 1500°C in a non-oxidising, H_2 atmosphere. After carburising the blocks are crushed, the WC crystals are then size graded.

(iv) Tungsten carbide-cobalt

The two powders are milled together for several hours and, after drying waxed. The waxed powder can then be pressed to the required component shape and will have sufficient strength for handling but not machining. The component is then put through dewaxing (~400°C) and pre-sintering (~800°C) furnaces. Machining operations are carried

out on the presintered article allowing for approximately 20% shrinkage during final sintering, depending on the alloy grade.

Final sintering takes place at 1400 - 1500^{0}C; the cobalt fuses and forms a molten eutectic alloy which wets the carbide grains and binds the whole together.

2.3 PROPERTIES OF THE INDIVIDUAL CONSTITUENTS

Several of the current theories concerning the processes of deformation and fracture in WC-Co hardmetal under stress relate to the properties of the individual constituents. For example,[4-7] the f.c.c to h.c.p transformation of cobalt, the slip systems in WC, the yield stress of the binder and dislocation densities and movement are frequently quoted.

It will be seen from the following tables (Tables 2.1, 2.2) that the properties of the two phases are vastly different. The binder has small amounts of alloyed tungsten and carbon and will therefore have slightly different properties to pure cobalt. Despite the anisotropy of both the tungsten carbide and cobalt the bulk composite is considered isotropic since both the constituents are randomly orientated.

Table 2.1

PROPERTIES OF TUNGSTEN CARBIDE GRAINS

Material Property	Units	Value	Notes	Ref.
Density	gms/cms^3	15,7		3
Elastic modulus	GPa	696		3
Poisson's ratio		0,20		8
Melting point	°C	2870	Dissociation	3
Elongation at fracture			brittle	3
Microhardness HV 50 gms	kg/mm^2	2400	(0001)	3
		2300	(20$\bar{1}$3)	3
Yield strength			Not well established	9
			Yield and fracture strength reported to decrease as particle size increases.	10,11
Coefficient of thermal expansion	$10^{-6}K^{-1}$	5,2	(0001)	3
		7,3	(10$\bar{1}$0)	
Crystal structure		hexagonal		3
Lattice constants	nm	a = 0,291		3
		c = 0,284		3
Stress required for slip	MPa	2500		12,13
Slip planes		(0$\bar{1}$1)		14,15
Burgers vectors		[0001]	slip plane (10$\bar{1}$0)	16
		1/3[11$\bar{2}$0]	slip plane (10$\bar{1}$0)	16
		1/3[11$\bar{2}$3]-	[0001] + 1/3[11$\bar{2}$0]	16
			1/6[11$\bar{2}$3]+1/6[11$\bar{2}$3]	16
		1/3[11$\bar{2}$3]-	or	
			1/6[20$\bar{2}$3]+1/6[02$\bar{2}$3]	16

Cobalt is not soluble in the WC monocarbide.[3]

Table 2.2

PROPERTIES OF COBALT (ALPHA)

Material Property	Units	Value	Notes	Ref
Density	gms/cms^3	8,9		17
Elastic modulus	GPa	206,8		17
Poisson's ratio		0,32		17
Melting point	°C	1495		18
Elongation at fracture	%	12		17
Hardness	Kg mm^{-2}	250	Cobalt sintered from powder	17
[illegible]	MPa	759	Tension	18
		586	Compression	18
Coefficient of thermal expansion	10^{-6}°C^{-1}	A + BT	A°C^{-1} / B°C^{-2}	7
			Exp. // to axis: 13,4 / 0,0128	
			Exp. $\perp$ to axis: 11,9 / 0,0075	
Crystal structure		h.c.p.	T < 417°C	24
		f.c.c.	T > 417°C	3
Lattice constants	Å	a = 0,2507	h.c.p.	17
		c = 0,4069	h.c.p.	17
		a = 0,3544	f.c.c.	7

Cobalt in WC-Co alloys:

The dimensions of cobalt grains in WC-Co alloys cannot be determined by metallographic techniques.[18] X-ray diffraction, however, shows that lattice orientation is constant over distances as large as 50 - 100 μm [4] while other authors[19-23] have reported cobalt grain size to be in the order of 1mm. Clearly the effective grain size of the binder is much larger than that of the carbide.

At high temperatures (>417°C) cobalt is f.c.c, but at 417°C it undergoes a transformation such that at room temperature the structure is h.c.p.[24] In sintered alloys

containing WC, however, the cobalt has a cubic lattice. This has been attributed to the thin film mechanical constraints imposed on the dislocation movement necessary for the transition.[25,26] It is more probable that the cubic modification is stabilised by dissolved tungsten and carbon.[27] Heavy deformation results in stacking faults and partial transformation.[28,29]

2.4 INTER-RELATIONSHIP BETWEEN TUNGSTEN, CARBON AND COBALT

The properties of sintered WC-Co alloys are known to be critically dependent upon their final composition and structure.[30] It is therefore useful to review briefly the inter-relationship between tungsten, carbon and cobalt.

2.4.1 Tungsten-carbon Phase Diagram

The important feature of the tungsten-carbon phase diagram is the very small range of homogeneity of WC, (Figure 2.1). The carbon content corresponds to the theoretical value of the stoichiometric composition,[3] (50 at % or 6,13 wt% C).

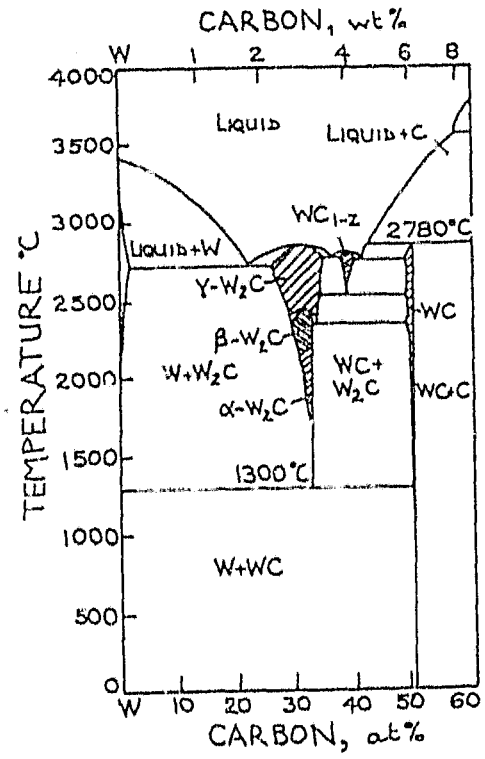


Figure 2.1 Tungsten carbon phase diagram[3]

2.4.2 Tungsten Carbide-cobalt Phase Relationships

Cobalt, tungsten and carbon form a complicated ternary phase diagram. Isothermal sections at 1400°C, determined by three investigators,[31-33] are all different particularly in the tungsten-rich corner. The most recent investigations[34-36] do not agree with any of these results.

Certain principles are, however, common to all the proposed sections (Figure 2.2). For a W/C ratio of 1, the phases: WC, liquid and β are stable (β being the Co-rich binder); at lower carbon contents a ternary phase, eta (η) occurs. Eta is a complex carbide with a variable composition of the type $W_{4-x}Co_{2+x}C$, $0 \leqslant x \leqslant 2$, most commonly indicated to be W_3Co_3C.[37]

At higher carbon contents than the stoichiometric value, primary carbon precipitates and remains in equilibrium with WC and β phases.[3]

In general, both free carbon and the ternary compound eta (η) are highly undesirable and are detrimental to the mechanical properties. The carbon content therefore has to be maintained within very narrow limits.[37]

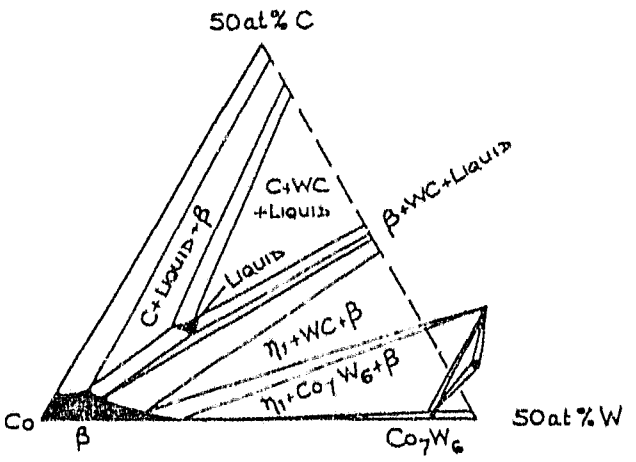


Figure 2.2 Isothermal section at 1260°C of cobalt rich part of W-C-Co ternary phase diagram.

2.4.3 Alloying of the Binder by Tungsten and Carbon

An extremely important parameter controlling mechanical properties is the composition of the cobalt-rich β phase. For WC-Co alloys it has been shown that the tungsten content in the binder is between 2 and 20% and the corresponding carbon content between 0,04 and 0,12%, with a lower tungsten content being associated with a higher carbon content.[3,38]

Interestingly, cobalt alloys have been prepared with compositions corresponding to the binder phase in WC-Co hardmetal, obviously without the carbide grains. The alloys show yield strengths between 250 and 850 MPa with ultimate tensile strengths in the range 400 to 1300 MPa.[39] These dramatic changes in the properties of the binder phase with varying alloy content can profoundly affect the properties of hardmetal alloys. Control of the carbon content is obviously of great importance in obtaining the required properties from tungsten carbide-cobalt alloys.

2.4.4 Alloying of Binder by other Elements:

Certain elements (Cr, Al, Mo, Sn)[40,41] have been added to the cobalt binder, typically producing increases in hardness but reducing the transverse rupture strength (TRS) at room temperature. At elevated temperatures the TRS is increased by the addition of small amounts of molybdenum, chromium, aluminum or chromium bromide but is reduced by larger additions.[41]

2.5 WETTING OF TUNGSTEN CARBIDE GRAINS BY BINDER

Solid-state and liquid phase sintering, the formation of the microstructure and the mechanical properties of hardmetal alloys, all depend critically on the energy of the carbide phase to binder metal interface. They also depend on the grain boundary energy of the carbide.[3]

The most obvious effect of the interfacial energy is its influence on the wetting behaviour of the liquid binder on the solid carbide. Exner[3] has provided details of the considerable volume of work that has gone into attempts to understand the atomistic nature of wetting but there is currently no consistent theoretical approach to the wetting behaviour of carbides. It is concluded that a strong chemical bond exists at the interface between carbides and the iron group metals, a bonding which is especially favourable in the case of tungsten carbide and cobalt. This results in a very low interfacial energy for this combination,[42] nearly perfect wetting and good adhesion in the solid state. It has been assumed, as a result of this near perfect wetting, that a thin cobalt layer exists between all tungsten carbide crystals in WC-Co alloys. It is now generally accepted,[43] however, that grain boundaries between carbide crystals (presumably enriched with cobalt) also exist.

2.6 RESIDUAL STRESSES

The pronounced difference in the thermal expansion coefficients of the cobalt and tungsten carbide results in considerable stresses developing in the mocrostructure during cooling from the sintering temperature. The thermal contraction of cobalt is approximately three times that of tungsten carbide. Experimental investigations and theoretical analyses have been used to calculate the sign and magnitude of these stresses.[44,45-53]

Early work[46,47] measured tensile stresses in the carbide phase of low cobalt alloys. It has subsequently been determined that thermal stresses in the carbide are compressive for all alloy compositions, and that the early results were in error. The stresses in the binder are therefore tensile.

As the alloy is cooled there is a temperature above which no thermal stresses are developed since the cobalt binder is too soft to carry load and residual stresses disappear by local creep deformation. This temperature (T_o) has been well established to be about 800°C. (Figure 2.3).

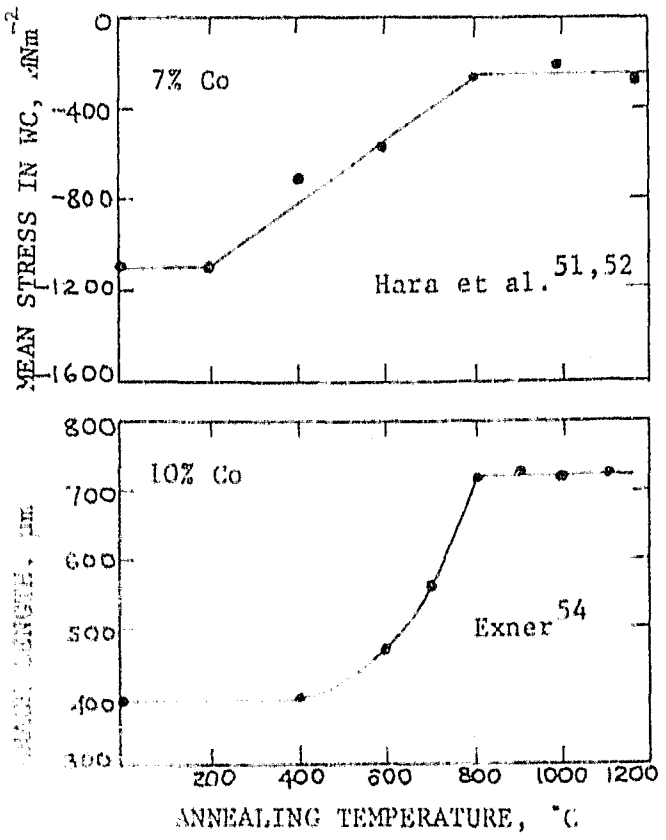
Theoretical considerations predict an approximately linear increase of the compressive stress in WC with increasing cobalt content[44,53] of the form $\sigma = 13X_{Co}$ (where: σ = residual compressive stress, MPa, in the carbide, X_{Co} = wt% cobalt in the alloy). The corresponding tensile stresses in the binder have been theoretically estimated to be in excess of 1000 MPa over the entire range of compositions decreasing only slightly as cobalt content increases. (Figure 2.4.) (It is interesting to compare this value with the yield and tensile strengths of cobalt alloyed with tungsten in the range 2 to 20% and carbon 0,04 to 0,12%, i.e. σ_y = 250 to 850 MPa, σ_{UTS} = 400 to 1300 MPa.[39])

There is controversy as to whether these residual

stresses influence mechanical properties. Some authors consider them negligible,[40,44,55,56] whereas others[57,58] take the opposite view and lay great emphasis on the effect. Kreimer[18] has discussed the various arguments at length and concludes that the relative proportions of the carbide and binder and not thermal stresses control the fracture process.

Either way, since it is not possible to prepare alloys without these microstructural stresses, it would seem reasonable to assume that they could play a role in the mechanisms of fracture but that the fundamental properties and proportions of the two constituents in hardmetals are of more primary significance in attempting to understand their behaviour.

Residual stresses can also be artifically introduced into the surface of the material by mechanical grinding but these are not considered important here because WC-Co hardmetal components are not normally ground.



Residual stresses and crack length at Vickers indentations as a function of annealing temperature.[51,52,54]

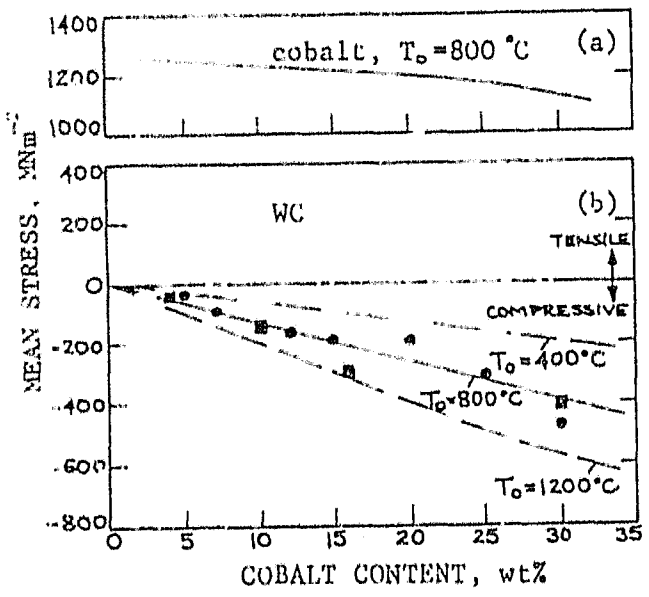


Figure 2.4 (a) Tensile stresses in cobalt, calculated.[3]

(b) Compressive stresses in WC, data points from double X-ray exposure results of:

▪ Öhman et al.[44]

• Hara et al.[51,52]

Theoretical curves after:

Amberg[53] and Öhman[44]

2.7 MICROSTRUCTURAL VARIABLES

Numerous parameters have been devised in an attempt to quantify the microstructure and composition of hardmetal alloys. In general these concentrate on the size of the carbide grains, the thickness of cobalt layers and the degree to which a continuous skeleton of carbide exists.

2.7.1 Cobalt Binder Phase

The cobalt binder phase exists as a continuous network of varying thickness. The true mean free path (also called the true mean linear intercept) has begun to replace the nominal mean free path,[59] which assumes a binder layer between all carbide grains, to describe the binder layer thickness. The true mean free path takes into account only the visible regions of cobalt[57,60] (i.e.: cobalt free WC-WC boundaries exist in the microstructure) and is inversely proportional to the specific surface of the binder phase (carbide/binder interface per unit volume of binder). It is thus a most important parameter for characterising the binder phase.

Both the true and nominal mean free path are still widely used.

$$\text{Nominal mean free path} = \frac{(\text{vol fraction cobalt})(\text{mean WC grain size})}{(1 - \text{vol fraction cobalt})}$$

$$\lambda_{nom} = \frac{f_{Co}\,\bar{d}}{(1 - f_{Co})}$$

True mean free path =

$$\frac{\text{(vol fraction cobalt)(mean WC grain size)}}{\text{(1 - vol fraction cobalt)(1 - contiguity)}}$$

$$\lambda_{true} = \frac{f_{Co}\,\bar{d}}{(1-f_{Co})(1-C)}$$

(Contiguity describes the degree to which carbide-carbide interfaces exist, see Section 2.7.3.)

(These equations have been rigorously derived by Pickens.[61])

2.7.2 Tungsten Carbide Grains

The size and distribution of the carbide grains is obviously of primary importance but cannot be determined prior to sintering because of grain growth during the sintering process. The varying shape of the carbide makes it difficult to apply conventional procedures for establishing the true spatial size distribution from polished sections.[62]

2.7.3 Contiguity

One of the important aspects of the microstructure of cemented carbides is the degree to which a continuous skeleton of carbide phase exists. The degree of skeleton formation can be quantitatively defined by the ratio of the carbide-carbide grain-boundary area to the total surface area of the carbide grains and is termed 'contiguity'.[60,63,64]

The contiguity decreases with increasing volume percentage of binder. The amount of binder phase at which the carbide phase becomes discontinuous is a matter

of some controversy.[65] In early work[63] it was assumed that the tungsten-carbide skeleton breaks down at a binder-phase as low as 10 vol%. In Exner's[3] opinion continuous carbide-carbide boundaries exist throughout the range of most commercial hardmetal alloy compositions, to well above 30 vol% cobalt.

At constant sintering conditions, contiguity is independent of carbide grain size.[3] This implies that cemented carbides of constant composition show geometrical similarity in their microstructure and one parameter (mean carbide grain size or mean free path of cobalt) is sufficient to describe the microstructure quantitatively.

The volume fraction of cobalt has been shown[66] to have a unique relationship to the contiguity, but results reported in the literature have considerable scatter. The value of contiguity is required to calculate the true mean free path and must either be (tediously) determined by quantitative microscopy or estimated using the work of other investigators.[61,66-70] Lindau[67] has reported that the relationship can be approximated by a circular segment. Most other results with the notable exception of Chermant and Osterstock's[68] very high contiguity values (deduced from Table 1 and Figure 14 of reference 68) fall below this curve.

Lee and Gurland's graph[66] in particular appears to be representative of the data determined by others, and has been used in this thesis to estimate contiguity values for the alloys tested, (Figure 2.5).

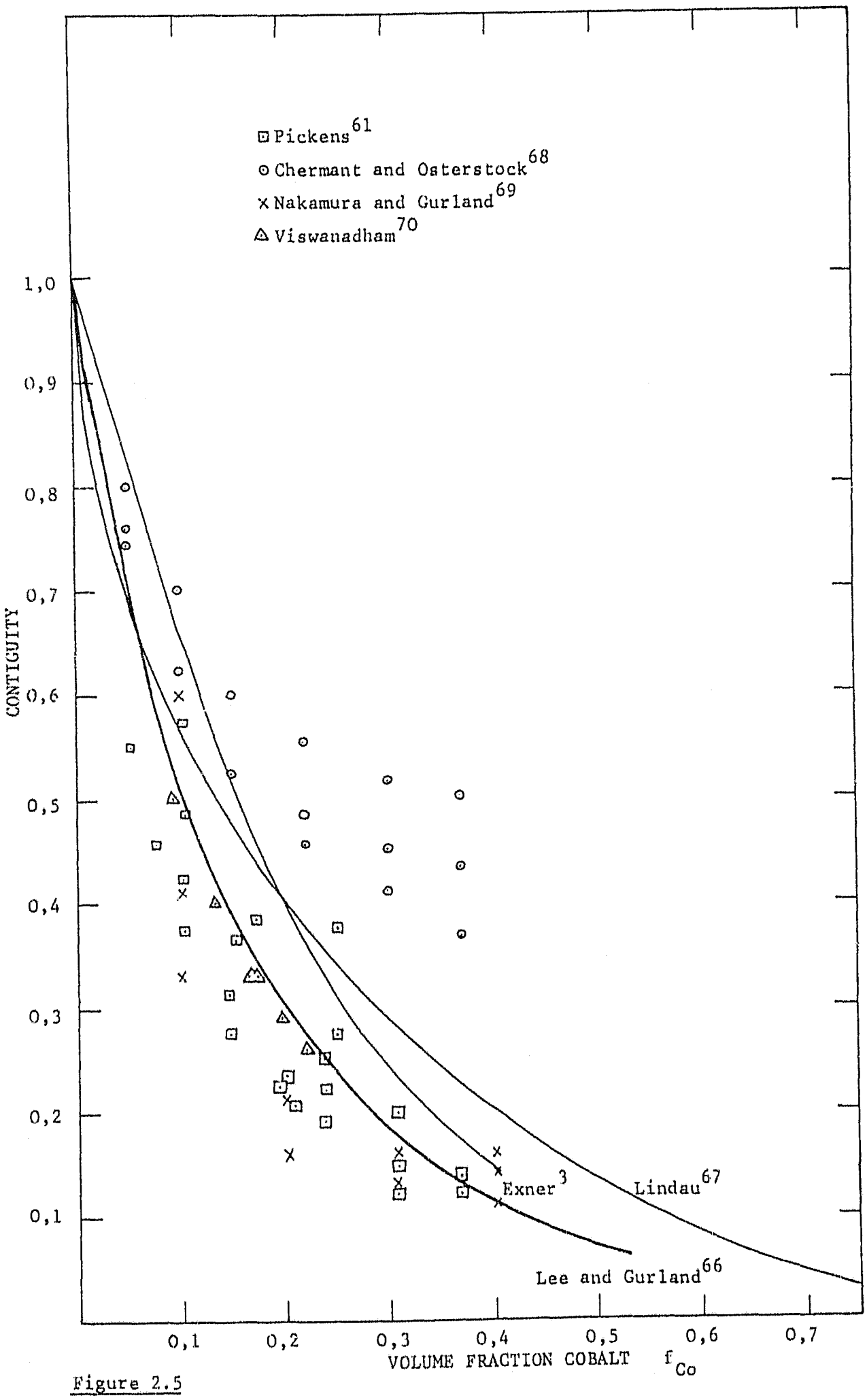

⊡ Pickens[61]
⊙ Chermant and Osterstock[68]
× Nakamura and Gurland[69]
△ Viswanadham[70]
CONTIGUITY
1,0
0,9
0,8
0,7
0,6
0,5
0,4
0,3
0,2
0,1
Exner[3]
Lindau[67]
Lee and Gurland[66]
0,1
0,2
0,3
0,4
0,5
0,6
0,7
VOLUME FRACTION COBALT f_{Co}

Figure 2.5

2.7.4 Porosity and Defects

Although modern cemented carbide production techniques are directed toward eliminating flaws in sintered components, pores, cracks and inclusions are usually present to some extent in the microstructure. The causes and effects of porosity have been discussed in detail elsewhere.[71-74] There is little doubt that strength is related intimately to these flaws, as predicted by fracture mechanics considerations.

Isostatic hot pressing (HIP) processes are used to reduce porosity.[71,75-79] The flaws cannot be eliminated completely but the effective strength and quality of ground surfaces is considerably improved.

2.7.5 Summary

For varying binder phase content and sintering conditions the parameters which describe the microstructure are not independent. The following equation holds.[57] (λ_{nom}, as previously quoted, is also commonly used.)

$$\lambda_{true} = \frac{f_{Co}\,\bar{d}}{(1-f_{Co})(1-C)}$$

λ_{true} = mean free path of binder
$\bar{d}$ = mean linear size of carbide grains
C = contiguity
f_{Co} = volume fraction of the binder

It is generally accepted that both the phases are themselves continuous in the microstructure.

2.8 MECHANICAL PROPERTIES OF WC-Co ALLOYS

2.8.1 Introduction

There is a vast amount of information available on the mechanical properties of cemented carbides, particularly the tungsten carbide-cobalt system. An outline of these properties is necessarily limited to those which characterise the material and which have relevance to a fracture mechanics approach to the strength, toughness and fatigue life of hardmetal alloy components. Kreimer's book 'Strength of Hard Alloys'[18] contains a comprehensive summary and discussion of many of the mechanical properties, and should be consulted for additional information.

The mean free path of the binder, is the most important variable in producing cemented carbides with different mechanical properties. As described previously (Section 2.7.1), the mean free path is a function of both the percentage cobalt and the carbide grain size. It will be seen therefore that the effect of these two variables on mechanical properties can essentially be summarized by the effect of the mean free path.

Numerous models have been proposed to explain the mechanical behaviour of hardmetal alloys. Many of these have been described by Kreimer.[18] The principles on which the most reasonable are based are that:

(i) the cobalt exists as a continuous network;
(ii) the tungsten carbide forms a contiguous skeleton of hard particles in contact with each other (the contiguity decreasing as cobalt content increases, Section 2.7.3).
(iii) the cobalt behaves as a constrained thin film, in which the yield strength decreases as the constraint is reduced (i.e. as thickness increases);

(iv) plastic deformation of the carbide grains, and hence the entire skeleton, is possible.

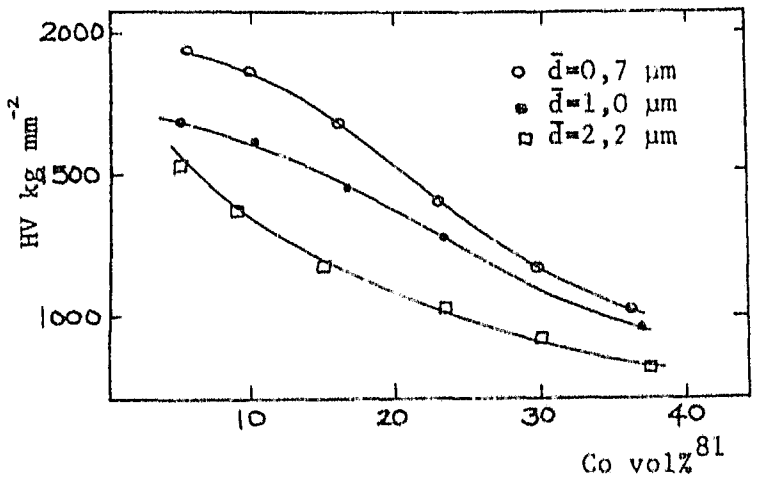
In most technical applications of WC-Co alloys the range of cobalt content used is approximately 5 to 25 wt% (8 to 32 vol%).[41] Investigations in the literature rarely therefore use alloys with cobalt contents exceeding 30 wt%.

2.8.2 Hardness

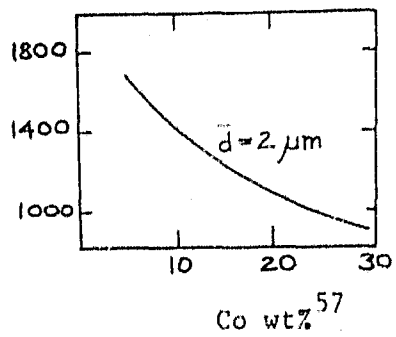
Hardness can be measured easily and accurately, and although it is not an outstanding indicator of an alloy's mechanical properties it remains an extremely useful and widely used test in the hardmetal alloy industry.

Hardness decreases as cobalt content[57,80,81] and grain size[59] increase, and consequently decreases as mean free path[57,59,82] is increased. (Figure 2.6 (a)(b)(c)). This is fully expected since as the proportion of relatively ductile binder phase is increased the material will, as a whole, plastically deform more easily. On a more microstructural scale as the mean free path increases the triaxial constraint and hence the local yield stress of the binder is reduced.

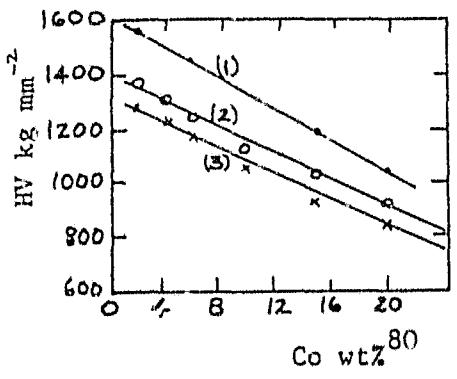
The decrease in hardness with temperature[56,83] (Figure 2.6 (d)) can also be explained by the reduced yield stress of the binder at elevated temperatures.



[81]



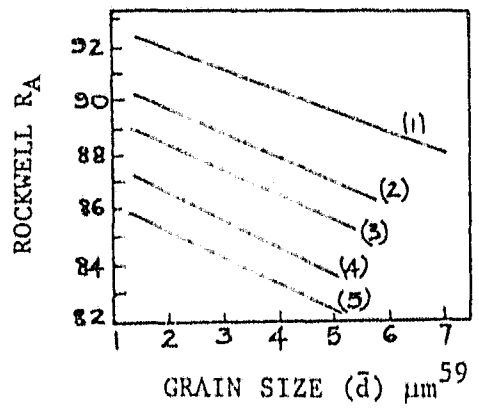
[57]



[80]

(1) $\bar{d}$=1,64 μm
(2) $\bar{d}$=3,30 μm
(3) $\bar{d}$=4,95 μm

(a) Variation in hardness with cobalt content.[57,80,81]



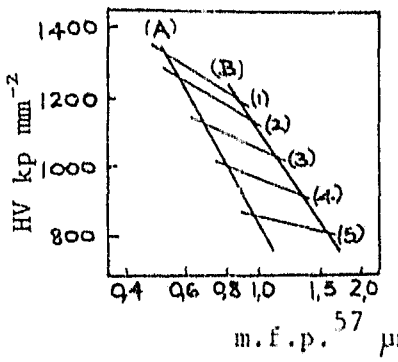
[59]

(1) 6wt% Co
(2) 12wt% Co
(3) 16wt% Co
(4) 20wt% Co
(5) 25wt% Co

(b) Variation in hardness with WC grain size.[59]

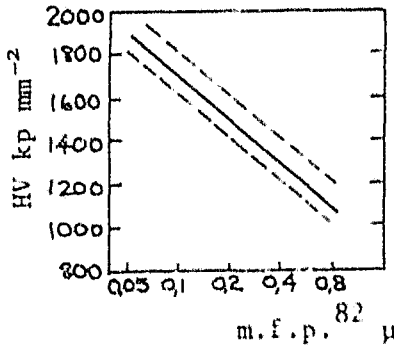
Figure 2.6

[1 kg mm^{-2} = 10 N mm^{-2}
HV load not quoted in references]

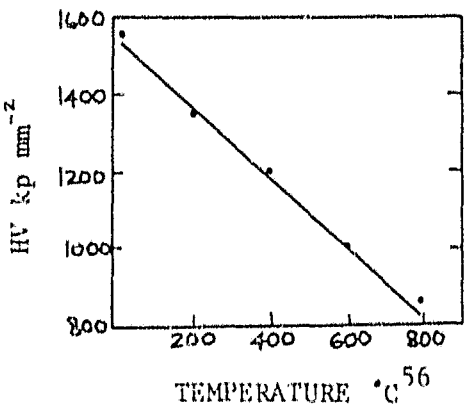


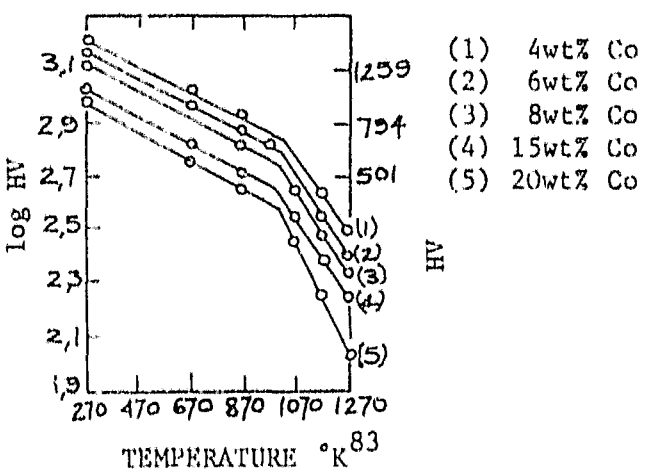
(A) $\bar{d}$=1,1 µm
(B) $\bar{d}$=2,1 µm

(1) 10wt% Co
(2) 12wt% Co
(3) 15wt% Co
(4) 20wt% Co
(5) 25wt% Co



(c) Variation in hardness with mean free path of the cobalt binder.[57,82]





(1) 4wt% Co
(2) 6wt% Co
(3) 8wt% Co
(4) 15wt% Co
(5) 20wt% Co

(d) Variation in hardness with temperature.[56,83]

Figure 2.6 [1 kp mm^{-2} = 10 N mm^{-2} HV load not quoted in references]

2.8.3 Uniaxial Compressive Strength

Although it is generally recognised that fracture, by physical separation, can only occur in the presence of tensile stresses, compressive loading is used to test a wide variety of materials. Ultimate failure in compression is due to local tensile and shear stresses in the material.

Compressive strength decreases as cobalt content[84-86] grain size[86], and hence mean free path of the binder,[6] increase (Figure 2.7(a)(b)(c)). The ultimate compressive strength and compressive yield strength both show a maximum at approximately 5wt% cobalt.[84-85] Surprisingly, this maximum has not been reported to occur when compressive strengths are plotted as a function of carbide grain size or mean free path.

There are two main factors which contribute to the decrease in compressive strength with increasing cobalt content and grain size. As the mean free path increases:

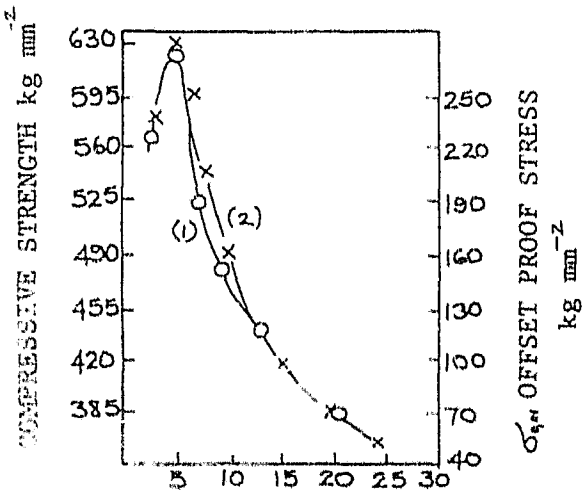
(i) the triaxial constraint and hence yield stress of the binder is reduced
(ii) the contiguity of the continuous carbide skeleton, which is largely responsible for carrying compressive load, is reduced.

At a low mean free path the applied stress is transferred through the microstructure primarily by the contiguous carbide grains, limited relaxation of local stress concentrations by dislocation movement and flow of the highly constrained binder is possible and this results in a high strength low ductility stress-strain curve.[6] As the mean free path increases the contiguity is reduced and the applied stress is increasingly carried by the binder. The degree of constraint in the binder and hence flow stress is, however, also reduced so that strength decreases and since local stress relaxation by

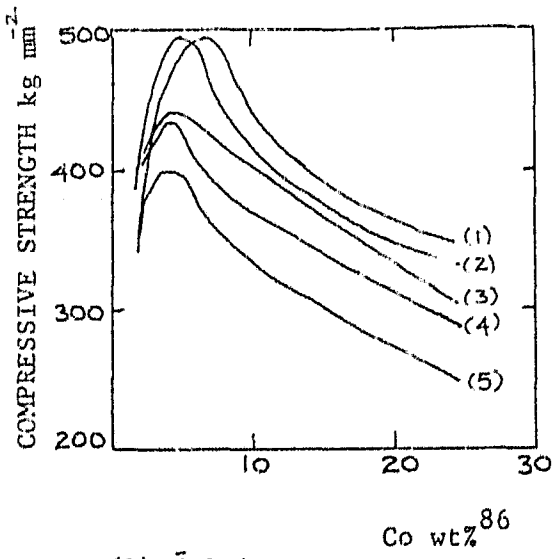
binder flow is easier ductility increases. Compressive fracture has been ascribed by Doi et al.[6] to the cumulative generation of microcracks by intergranular shear rupture at WC-WC and WC-Co boundaries.

The reduction in strength at cobalt contents below the peak strength value is probably the result of there being insufficient binder to compensate adequately for the local contact stresses generated in the carbide skeleton resulting in low strength, low ductility fracture.

The decrease in compressive strength with temperature (Figure 2.7(d))[86] is explained by the increased ductility of the binder at elevated temperatures.



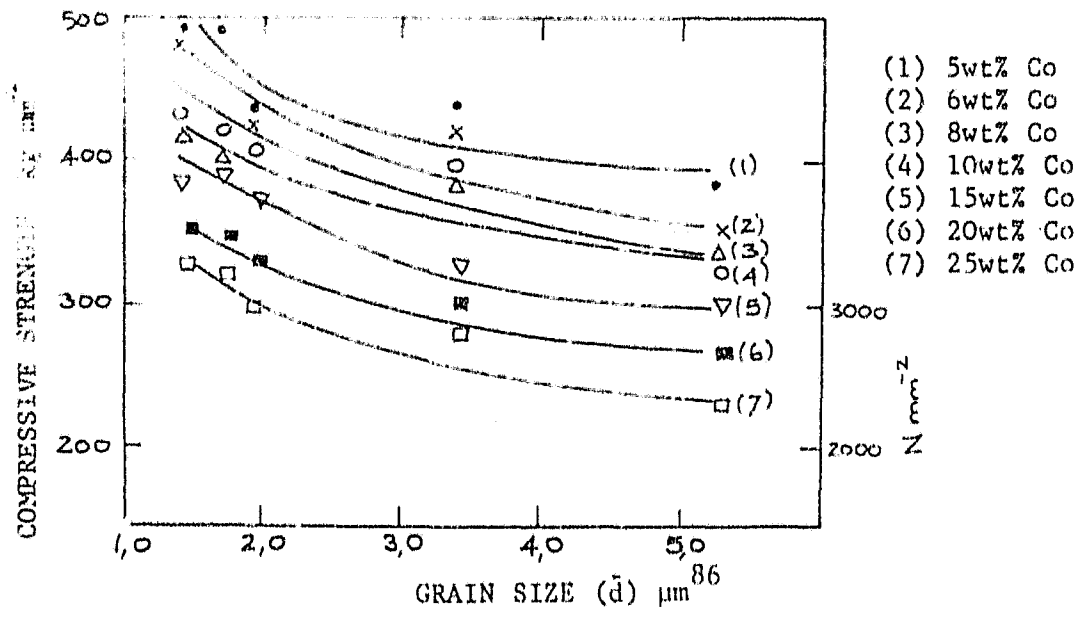
(1) Compressive strength[85]
(2) Compressive proof strength[84]



[86]

(1) $\bar{d}$=1,4 μm
(2) $\bar{d}$=1,7 μm
(3) $\bar{d}$=1,9 μm
(4) $\bar{d}$=3,3 μm
(5) $\bar{d}$=5,3 μm

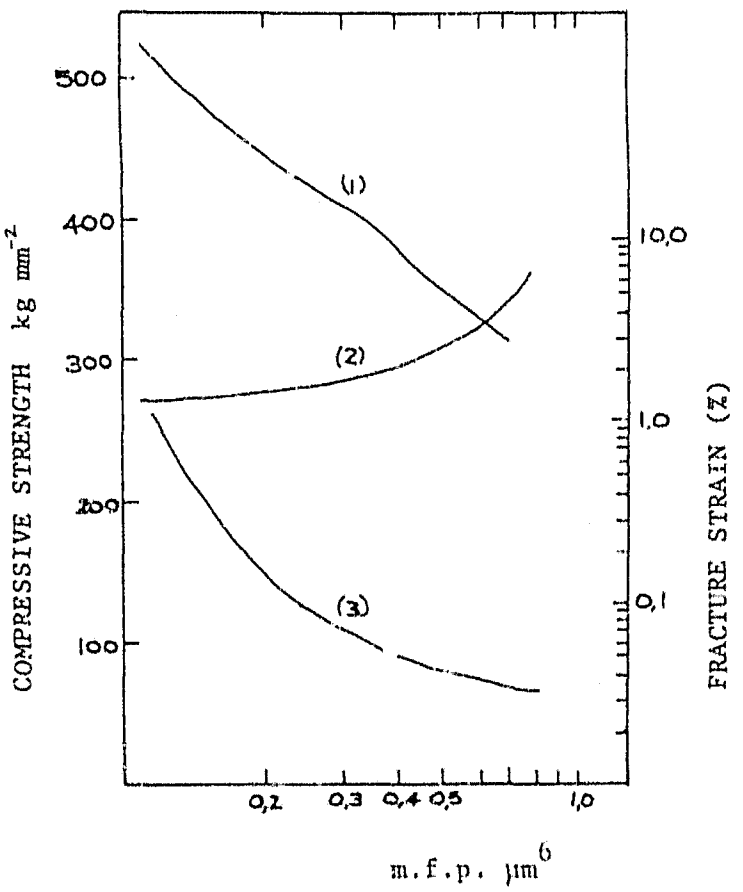
Variation in compressive strength with cobalt content.[85,86]



[86]

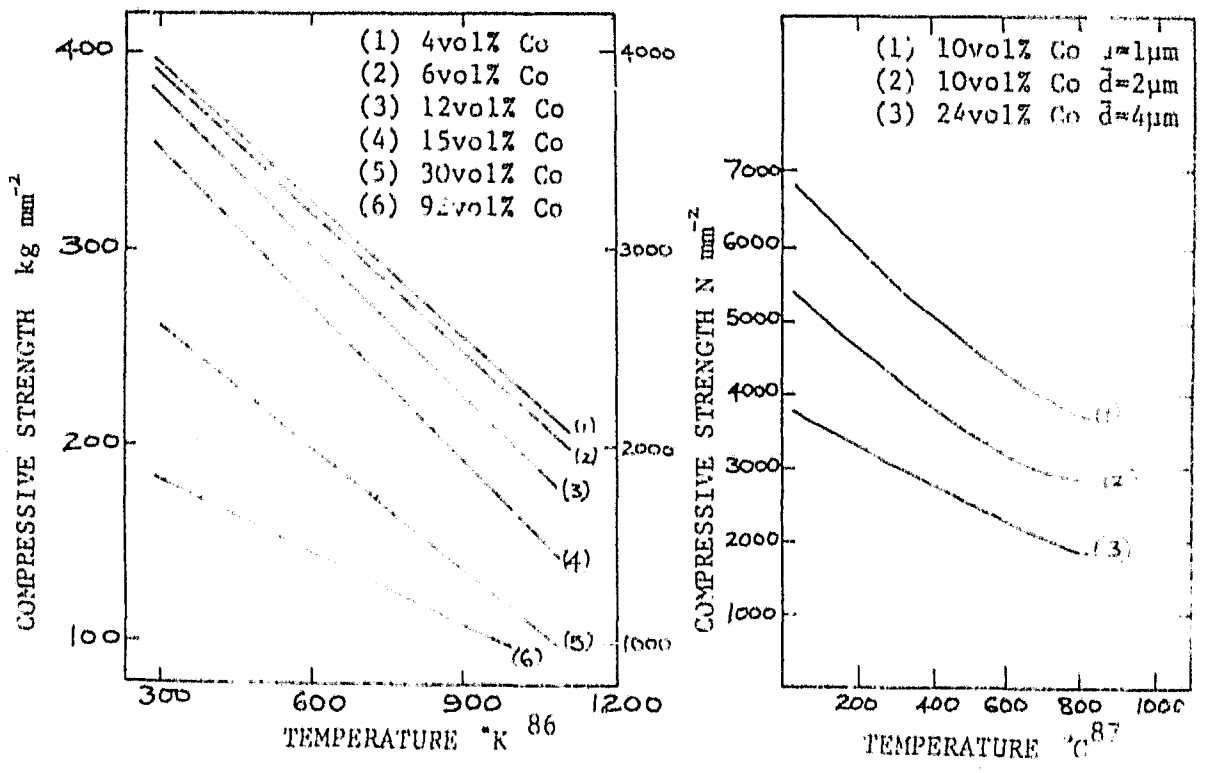
(b) Variation in compressive strength with WC grain size.[86]

Figure 2.7 $\left[1 \text{ kg mm}^{-2} = 10 \text{ N mm}^{-2}\right]$



(1) Compressive strength
(2) Compressive fracture strain
(3) Yield strength compression=tension

(c) Variation in compressive strength with mean free path of the cobalt binder.[6]



(d) Variation in compressive strength with temperature.[86,87]

Figure 2.1 [1 kg mm^{-2} = 10 N mm^{-2}]

2.8.4 Transverse Rupture and Tensile Strength

The simple three or four-point bend test for evaluating fracture strength has been widely used in both research and as a control test in industry. It remains one of the most popular tests due to its simplicity and the ease of specimen manufacture, and although it does not measure any intrinsic material property, fracture strengths are dependent on the toughness and tensile properties of the material.

Pure tensile tests on the other hand can be experimentally difficult to perform on high strength, low ductility materials. Doi et al.[6] for example, have brazed strain-gauged WC-Co rods of diameter 4mm into tubular steel adapters in order to determine stress-strain behaviour in tension.

Since transverse rupture and tensile strengths are essentially tensile property dependent it is appropriate to discuss failure mechanisms in one section.

In all reported results the transverse rupture and tensile strengths increase as factors which increase the mean free path (i.e. cobalt content[18,59] and grain size[59]) increase, reaching a maximum at a mean free path of approximately 0,4 µm.[6,59] Thereafter further increases in the binder layer thickness (m.f.p) lead to a decrease in strength (Figure 2.8 (a)(b)(c)). The explanation for this behaviour is based on the principles outlined in the introduction to the section (Section 2.8.1).

In the ascending portion of the curve, as the mean free path of the cobalt rich binder increases, the degree of plastic constraint decreases. As plastic deformation and flow by dislocation motion become easier, local stress concentrations are relieved and tensile crack initiation is impeded, the toughness of the binder is increased and crack propagation is energetically less favourable i.e. the increasing material fracture

toughness (described in Section 2.8.5) leads to increasing transverse rupture and tensile strength.

In the descending portion of the curve a dispersion hardening model is appropriate. The fracture mechanism is essentially one of ductile failure of the binder. Plastic constraint is considerably reduced and the effective flow strength of the binder decreases[55-57,89] and although the toughness continues to increase the maximum strengths attained are decreased. In addition, for a given cobalt content the increasing mean free path is associated with increasing grain size and the strength of individual tungsten carbide particles is reported to decrease[11,90,91] with increasing size. Therefore the cumulative effect of large fractured grains regions of decohesion by ductile tearing or WC-WC and WC-Co debonding can cause formation of relatively large flaws and hence contribute to reduced strength despite the increased toughness of the binder.[96]

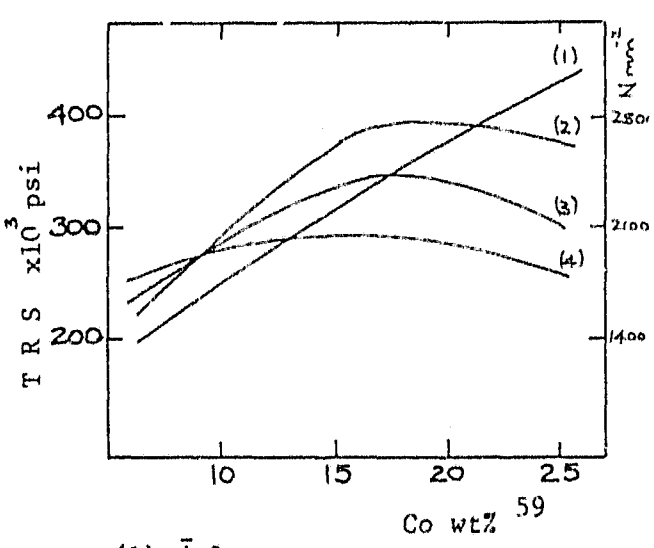
Consideration of the two extreme cases of the WC particles having no binder and hence almost no strength and pure cobalt metal with an ultimate tensile strength of 703 MPa,[18] (alloyed with W and C, σ_{UTS} 400-1300 MPa[39]) illustrate the effect. As the mean free path increases, the toughness is increased and intially ultimate strength is also increased, however, beyond the maximum the strength decreases as the hard metal tends to a low strength, high ductility behaviour.

At a mean free path of approximately 0,4 μm,[6,59] the effects of the triaxial stress constraint on the binder and its ability to flow and cause local stress relaxation are optimised and maximum transverse rutpure and tensile strength is obtained.

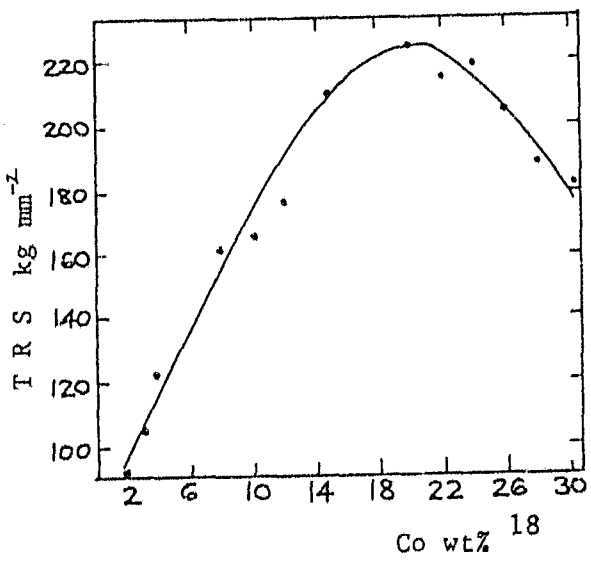
The variation in transverse rupture strength with temperature[88] (Figure 2.8(d)) is also explained by the model described. Initially as the binder becomes more ductile with increasing temperature, toughness and hence strength are slightly increased. However, beyond the

maximum the effect of increasing binder ductility with temperature is equivalent to the increasing ductility with mean free path.

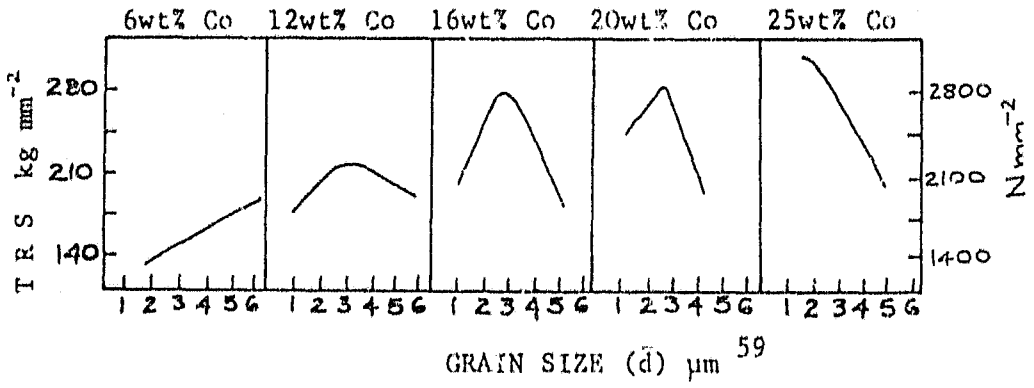
As previously discussed the correct carbon content is necessary to prevent the formation of free carbon or brittle eta phase in the microstructure. The presence of either of these phases in the hardmetal alloy causes a reduction in the transverse rupture and tensile strength.[6,30,92-94] (Figure 2.8(e)).



(1) $\bar{d}$=2 μm
(2) $\bar{d}$=3 μm
(3) $\bar{d}$=4 μm
(4) $\bar{d}$=5 μm

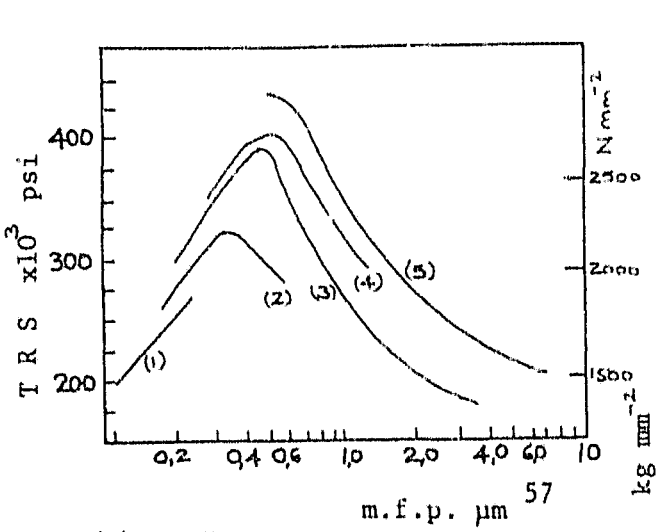


(a) Variation in transverse rupture strength with cobalt content. [18,59]

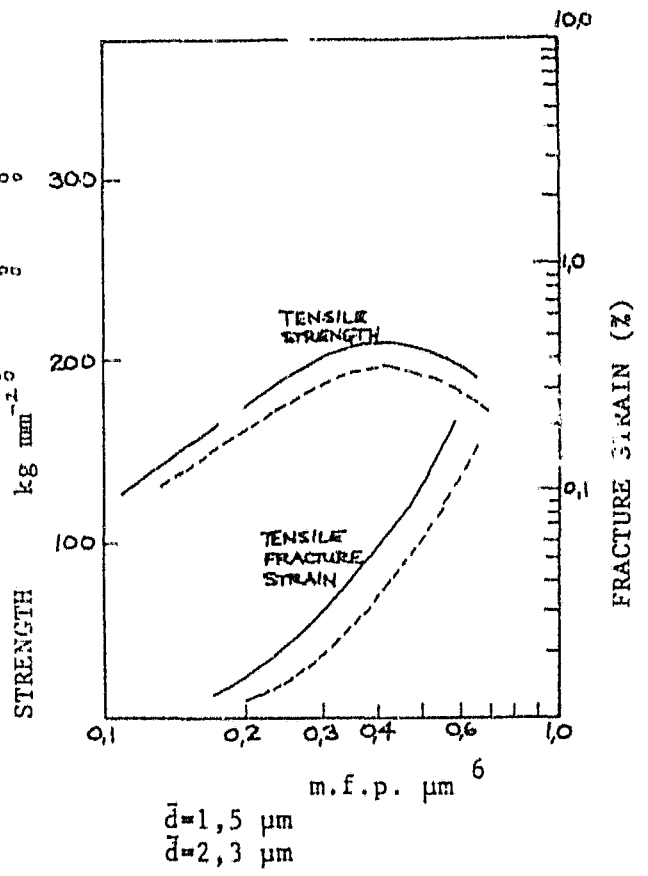


(b) Variation in transverse rupture strength with WC grain size. [59]

Figure 2.8 [1 kg mm^{-2} = 10 N mm^{-2}]

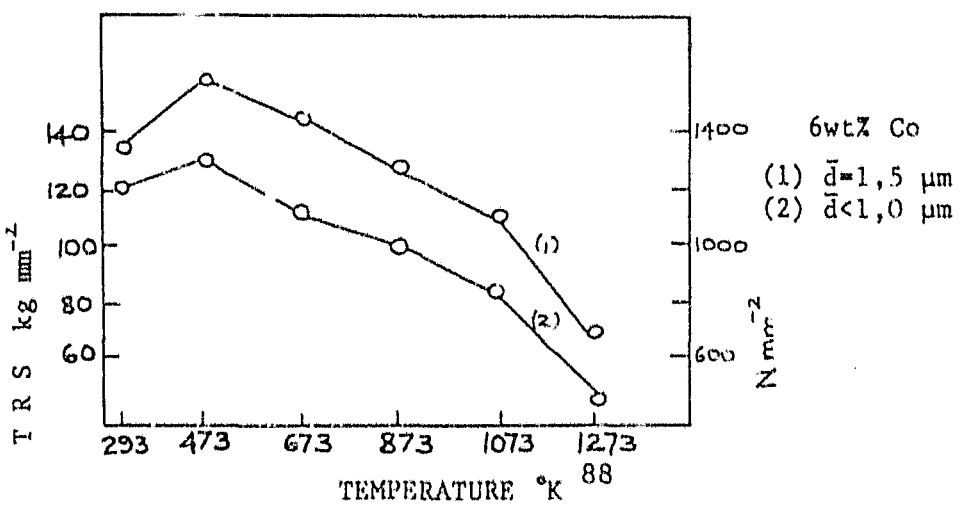


(1) 6wt% Co
(2) 12wt% Co
(3) 16wt% Co
(4) 20wt% Co
(5) 25wt% Co



$\bar{d}$=1,5 µm
$\bar{d}$=2,3 µm

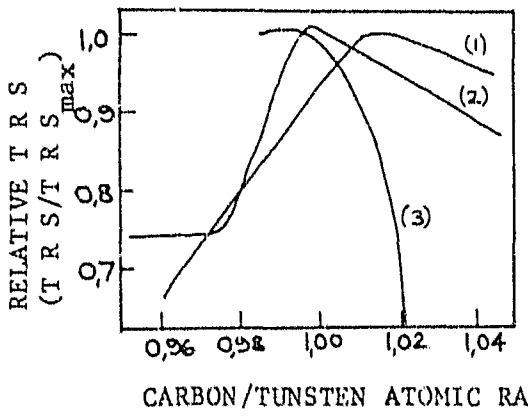
(c) Variation in the transverse rupture strength with mean free path of the cobalt binder.[6,57]



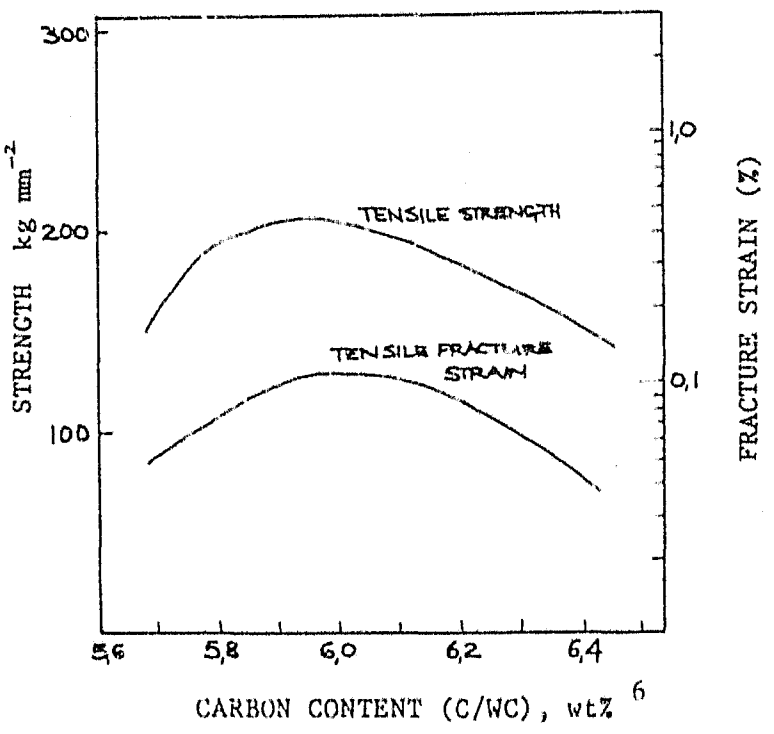
6wt% Co
(1) $\bar{d}$=1,5 µm
(2) $\bar{d}$<1,0 µm

(d) Variation in transverse rupture strength with temperature.[88]

Figure 2.8 [1 kg mm^{-2} = 10 N mm^{-2}]



(1) 10wt% Co $\bar{d}$=1-2 μm [92,93]
(2) 16wt% Co $\bar{d}$=2-3 μm [30]
(3) 10wt% Co $\bar{d}$=3 μm [94]



(e) Variation in transverse rupture strength with carbon content.[6,30,92,93,94]

Figure 2.8 [1 kg mm^{-2} 10 N mm^{-2}]

2.8.5 Fracture Toughness

There have been numerous studies investigating the fracture toughness of hardmetal alloys. Many of these have resulted in proposals for fracture mechanisms and models of varying complexity which attempt to correlate fracture toughness with microstructural parameters.

In general these relate, either directly or indirectly to the influence of the mean free path of the binder, as it is recognised that the energy expended in the flow and fracture of the ductile binder is the single most dominant factor in determining fracture toughness.[61,95-99]

It has recently been proposed that the volume of deformed binder per unit area of fracture surface has a significant influence on the fracture surface energy and hence the fracture toughness;[99] it being generally accepted that the transgranular fracture of carbide grains is a low energy fracture process.

This effect has been reported by Chermant and Osterstock[97] (and mentioned by Pickens[61]) who showed that the toughness of alloys with a large grain size is less than that of those with a small grain size for the same mean free path, large grains being more susceptible to transgranular fracture.

It is now possible, using Auger spectroscopy to measure the relative proportions of binder and fractured carbide grains on a fracture surface.[99] Viswanadham et al.[99] however concede that mean free path of the binder is the dominant parameter controlling toughness; despite the fact that increasing grain size (for a particular cobalt content) causes a greater proportion of cleaved carbide and hence reduction in surface energy, the simultaneous increase in mean free path leads to a net increase in fracture toughness.

A selection of the published results where mean free path is reported, or where there are sufficient data for

it to be calculated, is summarised in Table 2.3, Figures 2.9 - 2.12 and Appendix 1. Unfortunately, in many papers the mean free path is not reported and, if it is, there is often no indication of how it has been determined. In those cases where the values of nominal and true mean free path can be calculated the equations previously quoted are used, (Section 2.7.1). Where weight percentage binder is listed the volume fraction has been determined using density values for the individual constituents. Contiguity values (described in Section 2.6.3) required to calculate true mean free path have been obtained using Lee and Gurland's[66] graph relating contiguity to volume fraction of binder, except where values quoted are in close agreement with Lee and Gurland.[61,98,99]

Chermant Deschanvres and Osterstock[101] have attempted to measure the fracture toughness of the tungsten carbide crystals, i.e. pure WC, by preparing three-point bend specimens (4 x 8 x 40 mm) with no cobalt binder. They report however that the crack propagation was predominantly intergranular and conclude that the carbide crystals are stronger than the crystal boundaries. The value of 7,5 MNm $^{3/2}$ obtained is therefore more likely to be a measure of the toughness of a WC-WC interface with no binder than the fracture toughness of crystalline tungsten carbide.

Pickens[61] has summarised and assessed most of the research work on fracture toughness of hardmetal up to 1977. Subsequent investigations have done little more than add to the volume of results and increase the number of different models proposed.

Table 2.3

SUMMARY OF SELECTED FRACTURE TOUGHNESS INVESTIGATIONS

AUTHOR	SPECIMEN	DIMENSIONS [mm]	PRE-CRACKING TECHNIQUE	REMARKS
Chermant & Osterstock (1976)[97]	3-point bend	48 x 8 x 4	Diamond saw and spark erosion	Contiguity values reported are extremely high compared to other authors (Fig 2.5), therefore true mean free path is doubtful.
Ingelstrom & Nordberg (1974)[100]	3-point bend 4-point bend Compact tension	40 x 5 x 5 60 x 6 x 6 W=20 B=1,7-3,7	Knoop diamond indentation Wedge impact load	K_{IC} found to decrease linearly with hardness.
Lindau (1977)[95]	Compact tension	W=20 B=1,7-3,7	Wedge impact load	Lindau has determined mean free path using: $\lambda = \frac{\text{(vol fraction binder)(length of line)}}{\text{(number of binder layers)}}$ This formulation has been superceded.
Lueth (1974)[96]	Double cantilever beam	75 x 12,5 x 3	Wedge loaded	Lueth quotes mean free path vlaues but no formula to show how λ has been determined. Pickens[61] by direct measurement of grain size showed that nominal sizes quoted by Lueth were incorrect.
Nakamura & Gurland (1980)[98]	3-point bend	20 x 3,9 x 3	Electron discharge machining (EDM)	All microstructural variables reported. K_{IC} found to decrease linearly with hardness.
Pickens (1977)[61]	3-point bend	24,5 x 6,3 x 3,18 (1"x 1/4"x 1/8")	Electron discharge machining (EDM)	All microstructural variables reported. K_{IC} found to decrease linearly with hardness.
Viswanadham, Sun, Drake & Peck (1981)[99]	Short rod geometry	diameter = 12,7 height = 18,8	Not required	All microstructural variables reported.

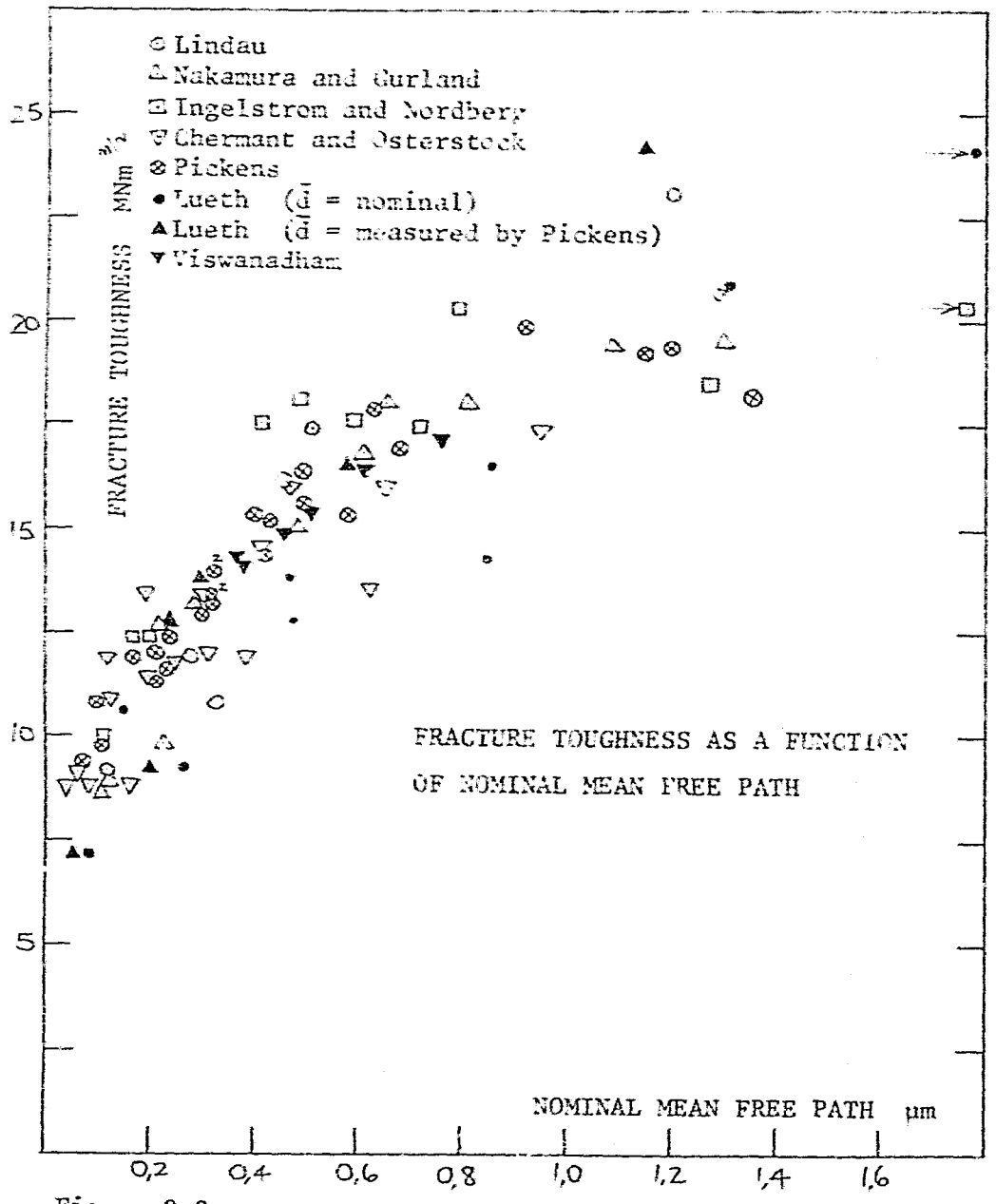


Figure 2.9

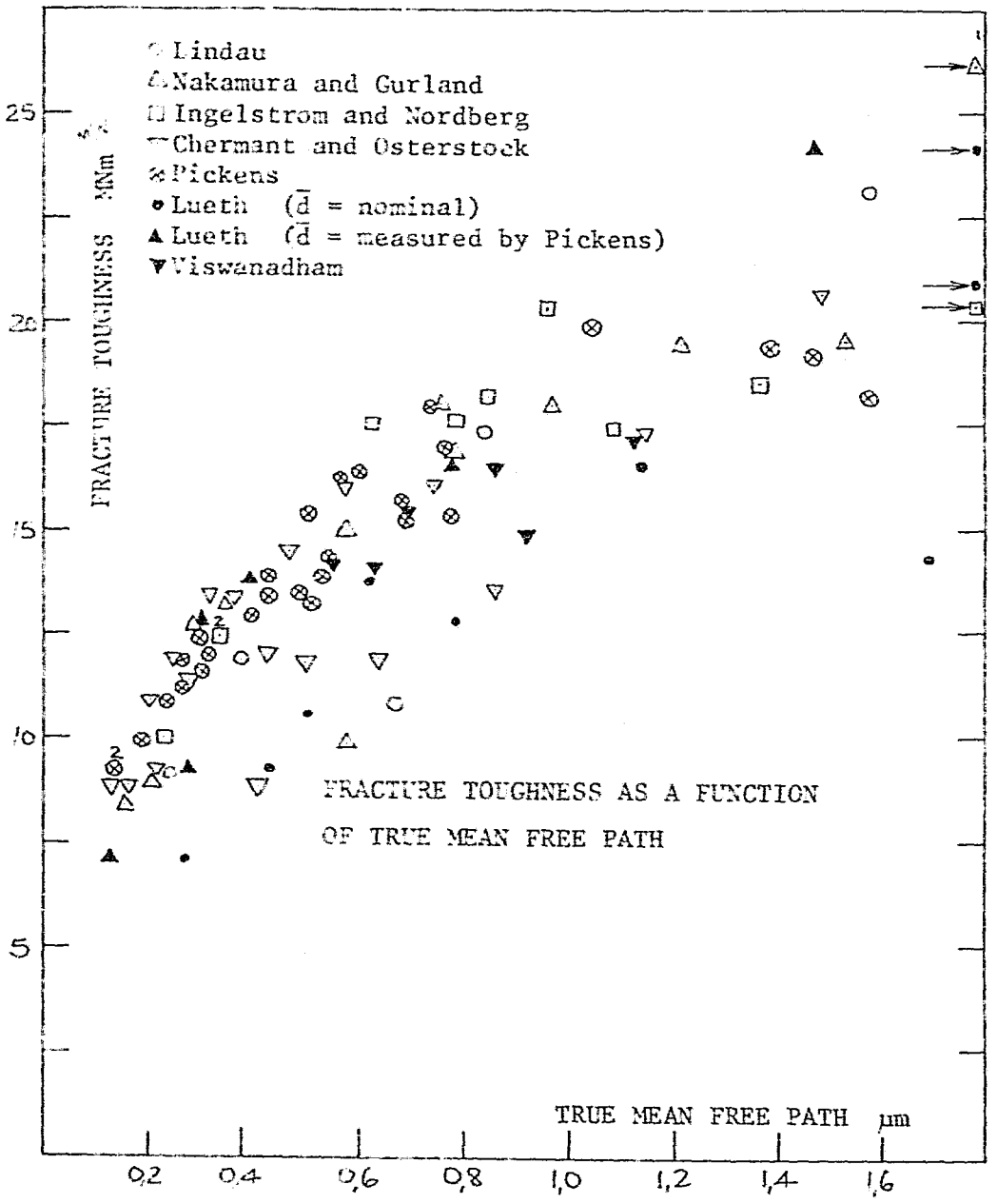


Figure 2.10

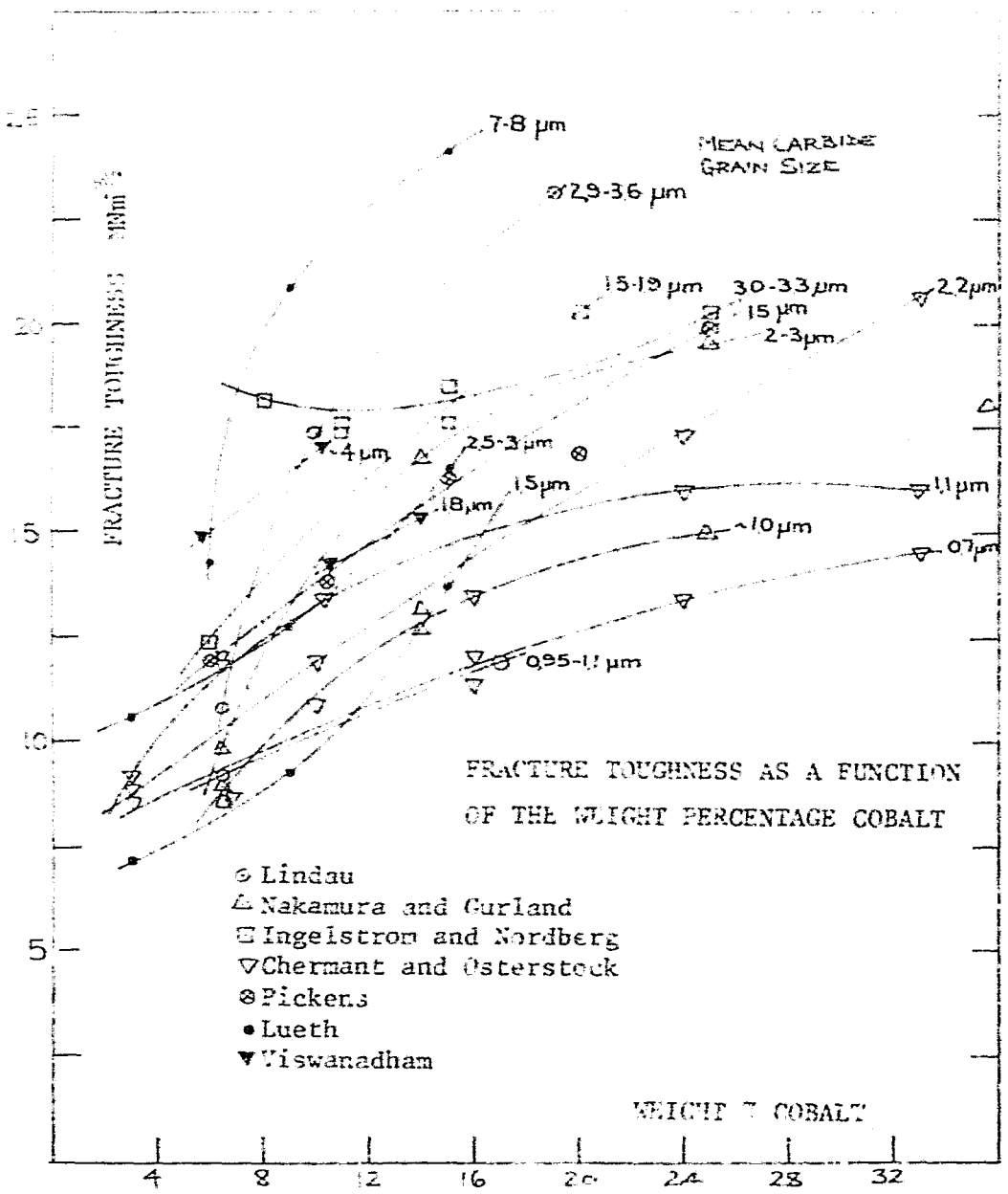


Figure 2.11

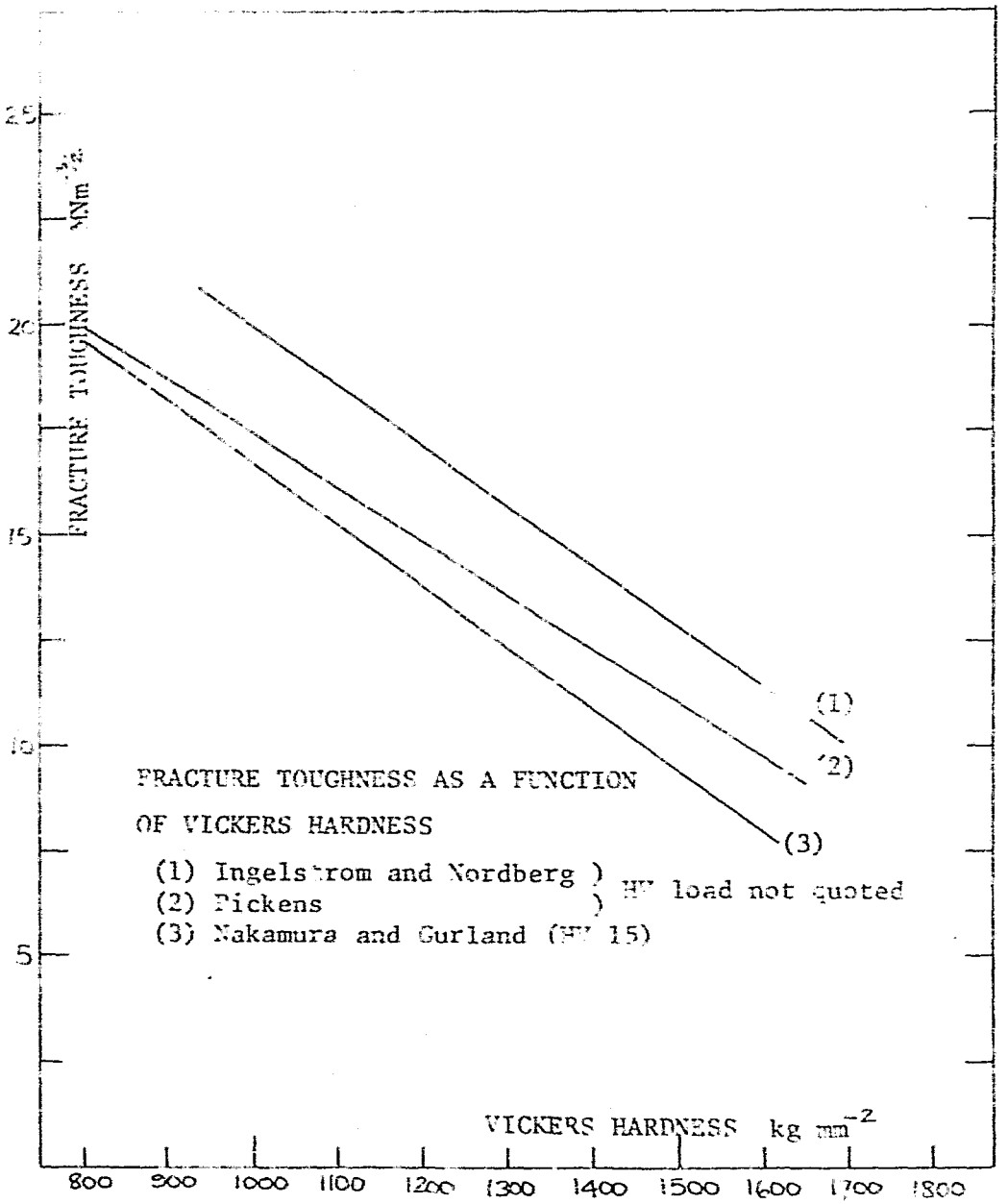


Figure 2.12

2.8.6 Poisson's Ration and Young's Modulus

Poisson's ratio and Young's modulus are relevant to some of the fracture mechanics equations and quantitative values are therefore required.[8] (Figures 2.13,2.14)

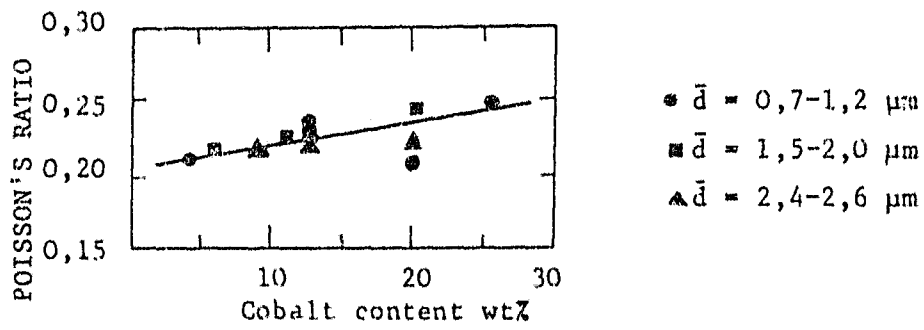


Figure 2.13 Variation of Poisson's ratio with cobalt content.[8]

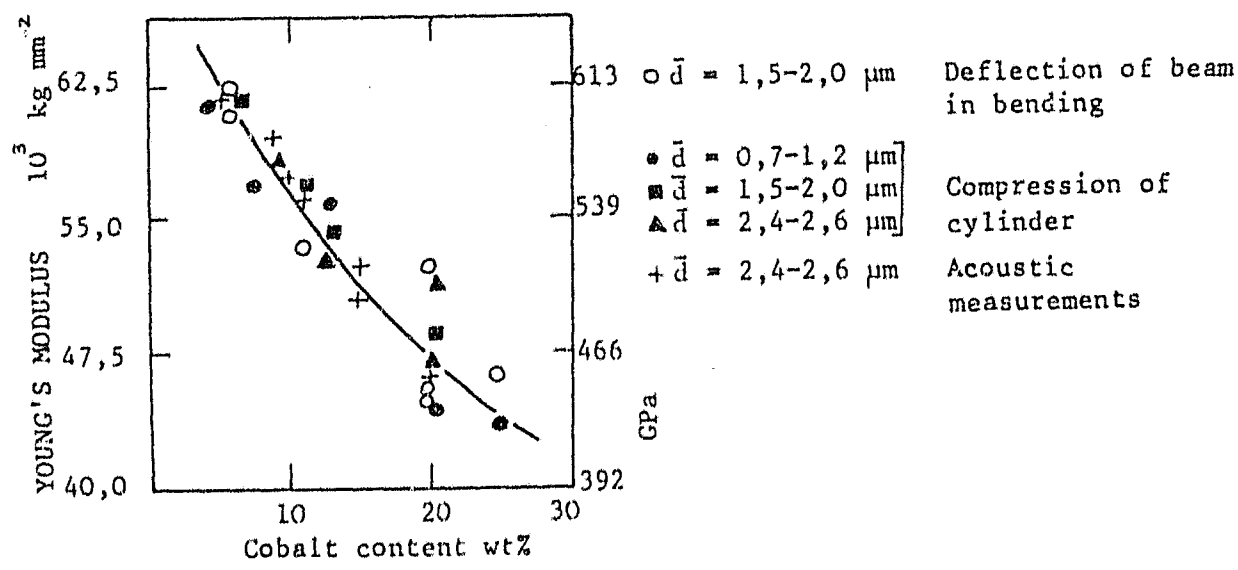


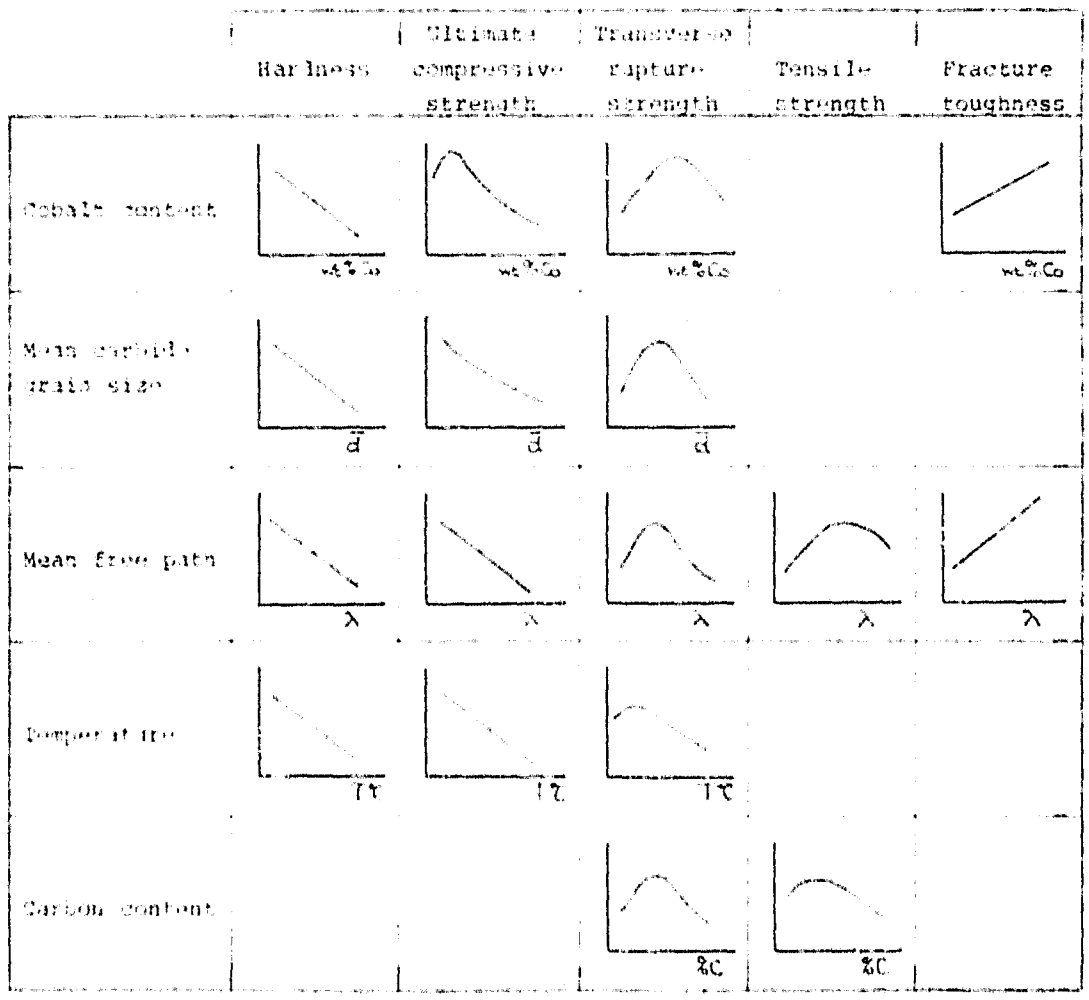
Figure 2.14 Variation in Young's modulus with cobalt content.[8]

2.8.7 Summary

The effect of cobalt content, tungsten carbide grain size, mean free path, temperature and carbon content on selected mechanical properties have been reviewed. The influence of these parameters are schematically represented in Table 2.4.

Table 2.4

SCHEMATIC REPRESENTATION OF VARIATION IN MECHANICAL PROPERTIES WITH MICROSTRUCTURAL PARAMETERS



2.9 SLOW CRACK GROWTH UNDER STATIC LOAD

Slow crack growth under monotonic loading in engineering applications (at ambient temperatures) is usually associated with environmental effects causing time dependent crack advance, for example by stress corrosion cracking.

Static crack growth rate can in general be characterised by an equation of the form:

$$\frac{da}{dt} = A(K_I)^n$$

where:

da/dt = crack growth rate w.r.t time
A = constant
K_I = applied stress intensity (mode I or tensile crack opening)
n = exponent

(This type of crack growth is sometimes, misleadingly, called 'static fatigue'; however the load is purely static with no cyclic component).

Studies into static crack growth effects in WC-Co alloys have been extremely limited. Braiden et al.[102] attempted to use the double torsion specimen to obtain crack velocity measurements but were unable to prevent fast fracture. They resorted to adopting a statistical approach using the strength and probability of failure in three-point bend tests. The specimens were held at subcritical loads for a given time, to achieve slow crack growth of existing flaws in the material, then loaded to failure. An extremely involved statistical analysis was used for data reduction. The existence of subcritical crack growth in air at room temperature was confirmed and a value for 'n' of 200 was calculated for a WC-6Co alloy. The author's state however that the accuracy is doubtful

due to the small sample size. At elevated temperatures, in an inert atmosphere, the following results, also using a small sample size, were obtained.[102]

WC-6Co	at 950°C	$n \approx 7$
WC-16Co	at 850°C	$n \approx 6$

Osterstock[103] has recently determined crack velocities using load relaxation measurements on double cantilever beam specimens for six different alloy grades. The results show that slow crack growth occurs in a very narrow range of stress intensity: $0,9\ K_{IC} \rightarrow K_{IC}$; below $0,9\ K_{IC}$ there is no crack advance. This obviously leads to very high 'n' values in the range $150 \rightarrow 200$. It was also found that the value of the exponent 'n' is not greatly affected by microstructure.

It is presumed that these tests were performed in a laboratory ambient air environment, although the relevant details were not reported.

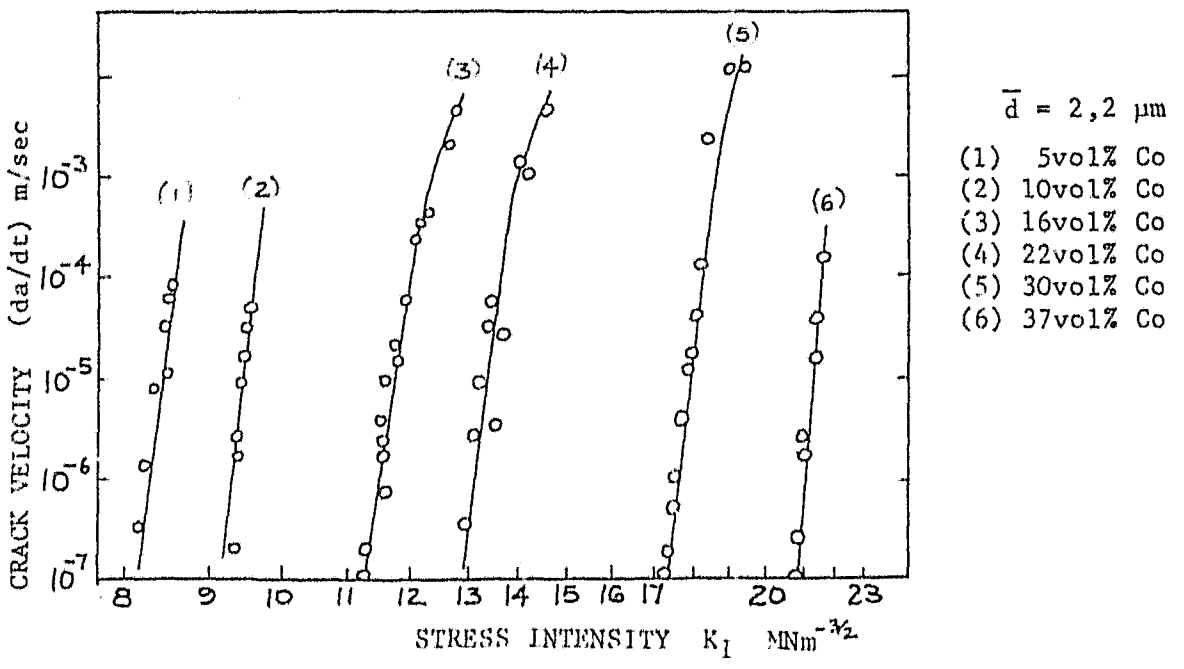


Figure 2.15 Static crack growth rates in WC-Co alloys[104]

2.10 FATIGUE

Traditional techniques for quantifying the fatigue properties of materials have employed, almost exclusively, the S-N curve under different loading modes. Though these are still widely used, particularly for engineering design, fracture mechanics is rapidly gaining acceptance as a more rational approach to the problem of fatigue failure. Fatigue data, plotted in the form of crack growth rate per cycle (da/dN) versus stress intensity range (ΔK_I), characterise the fatigue properties of materials and can in general be represented by an equation of the form:

$$\frac{da}{dN} = C(\Delta K_I)^m$$

where:

da/dN = crack growth per cycle
C = constant
ΔK_I = applied stress intensity range (mode I or tensile crack opening)
m = exponent

Experiments and analyses for tungsten carbide cobalt alloys have naturally followed this trend. Several early investigators of the fatigue process in these materials have obtained S-N curves[104-108] but very recently da/dN vs ΔK_I results have also been reported.[109-112]

2.10.1 S-N Data

The measurement of the number of cycles to failure at different stress levels requires relatively simple testing procedures.

2.10.1.1 Rotating Beam in Bending (R = -1)

Miyake et al.[104] used the rotating beam test to show that as the cobalt content increases the fatigue life increases (Figure 2.16)

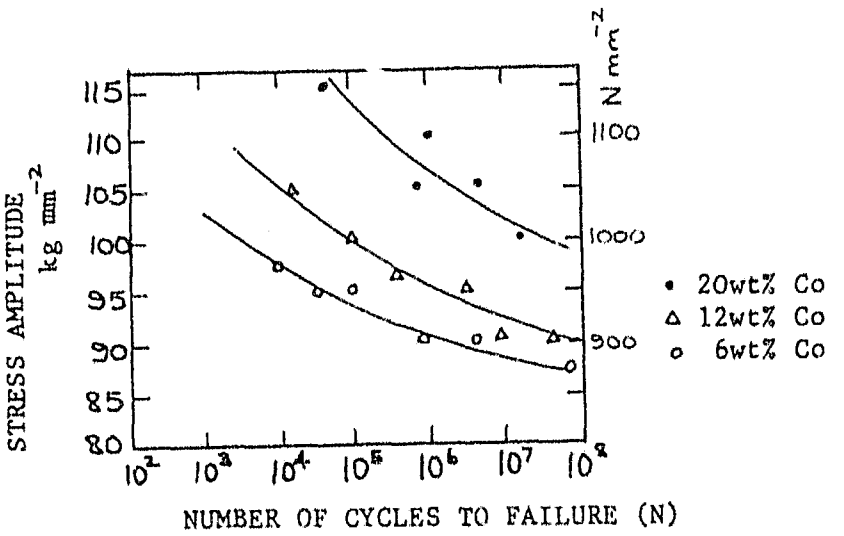
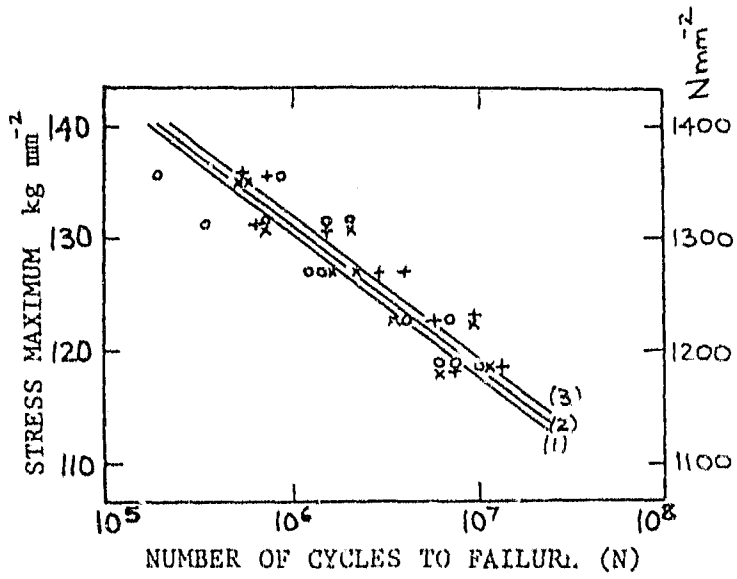


Figure 2.16 Effect of cobalt content on fatigue life using rotating beam test.[104]

Using the rotating beam the effect of surface finish has been investigated. Davies and Barhana[105] report that the quality of the surface finish does effect the life but there is considerable scatter in the results. (Figure 2.17).



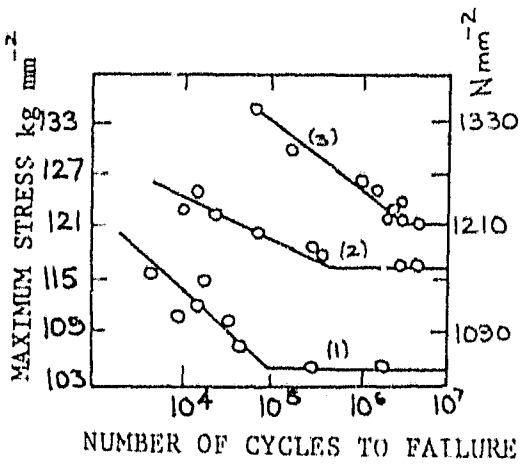
25 wt% Co $\bar{d}$ = 1,2 μm

(1) As ground finish
(2) 6 μm diamond polish
(3) $\frac{1}{4}$ μm diamond polish

Figure 2.17 Effect of surface finish on fatigue life.[105]

2.10.1.2 Three-Point Bend Tests (R = 0,1)

Kreimer et al.,[107] in agreement with Miyake et al.,[104] have shown that as the cobalt content increases the fatigue life increases, however their curves show a fatigue limit, i.e. there is a stress below which failure will never occur. (Figure 2.18)



(1) 4wt% Co
(2) 6wt% Co
(3) 8wt% Co

Figure 2.18 Effect of cobalt content on fatigue life using 3-point bend test.[107]

Kreimer et al.[106] using three-point bend tests confirm that surface finish influences fatigue life (Figure 2.19).

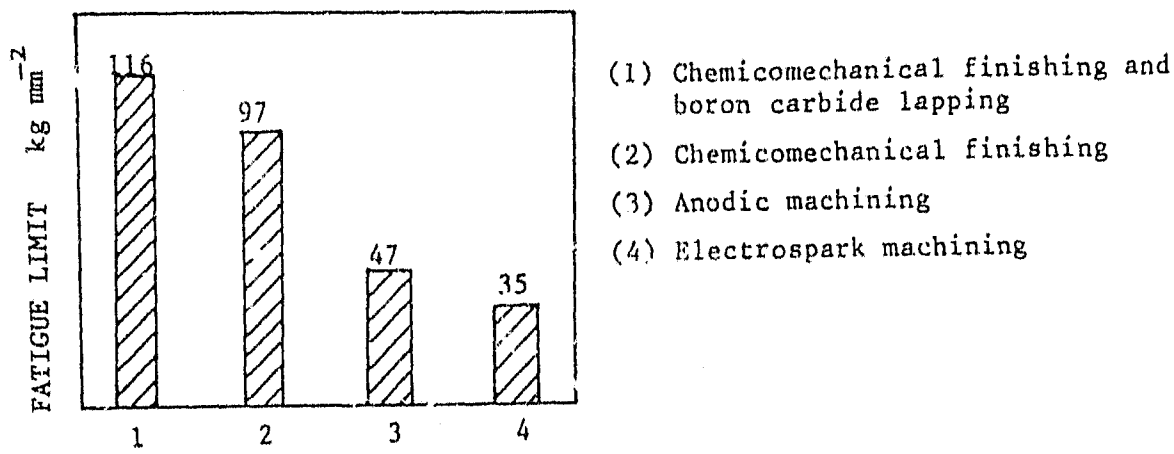


Figure 2.19 Effect of surface finish on fatigue life.[106]

2.10.1.3 Compression Tests ($R \leqslant 0,05$)

Here the results of Johansson et al.[108] seem to be contradictory to other investigations, since the fatigue strength is reported to decrease with increasing cobalt content. (Figure 2.20).[108]

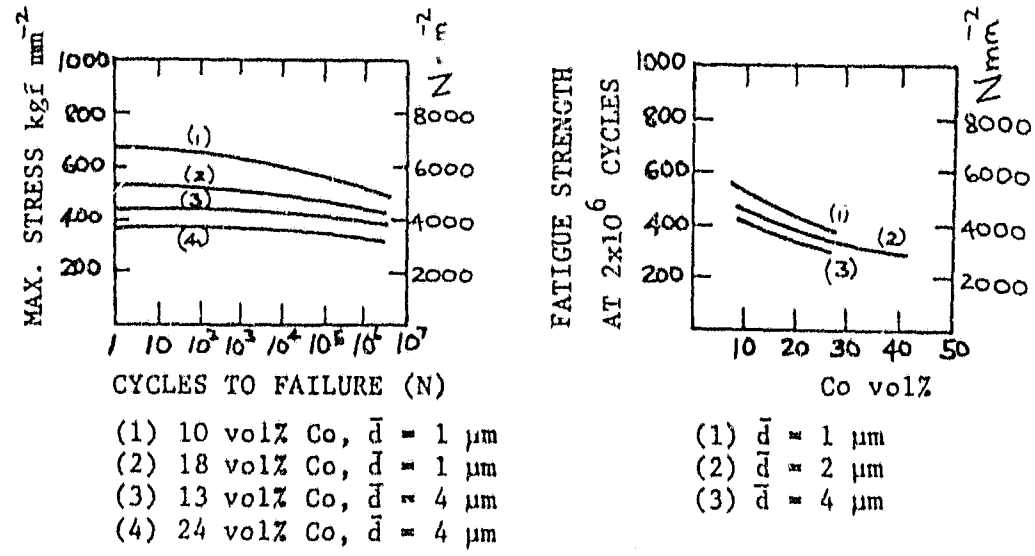
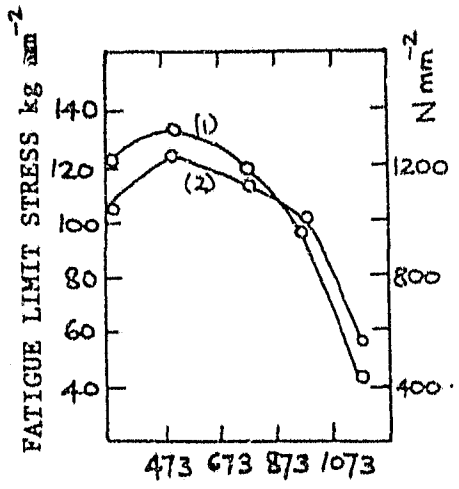


Figure 2.20 Effect of cobalt content on fatigue life in compression.[108]

2.10.1.4 Elevated Temperature Fatigue

Kreimer[107] has conducted elevated temperature tests on three-point bend specimens in an inert atmosphere (argon or helium). The fatigue limit (R = 0,1) for two alloys (4 wt% Co and 8 wt% Co, grain size not indicated) was determined at different temperatures.



(1) 8wt% Co
(2) 4wt% Co

Figure 2.21 Effect of temperature on fatigue life.[107]

2.10.2 da/dN vs K_I Data

Tests to obtain fatigue crack growth rate data in brittle materials are preferably performed on constant stress intensity specimen configurations. Thus, of the four investigations reported to date, two[109,110] employ the double torsion specimen. The four-point bend test has been used[111] and there is also work presently being carried out using the short rod geometry.[112]

Evans and Linzer[109] were apparently the first to obtain fatigue crack growth rates in hardmetal alloys.

Their experiments were aimed primarily at evaluating a fatigue testing machine and not at investigating the properties of WC-Co. The scatter in the results is considerable, (Figure 2.22) but a true fatigue mechanism, evidenced by frequency effects on the crack growth rate w.r.t time (Section 2.9.3) was reported.

Alloy: WC-6Co, grain size not stated
Test : Double torsion specimen, dimensions not stated
da/dN : measured by load relaxation
Frequency : 10 - 350 Hz
Loading : K_{Iav} constant
m values : (1) 12,44
(2) 10,6

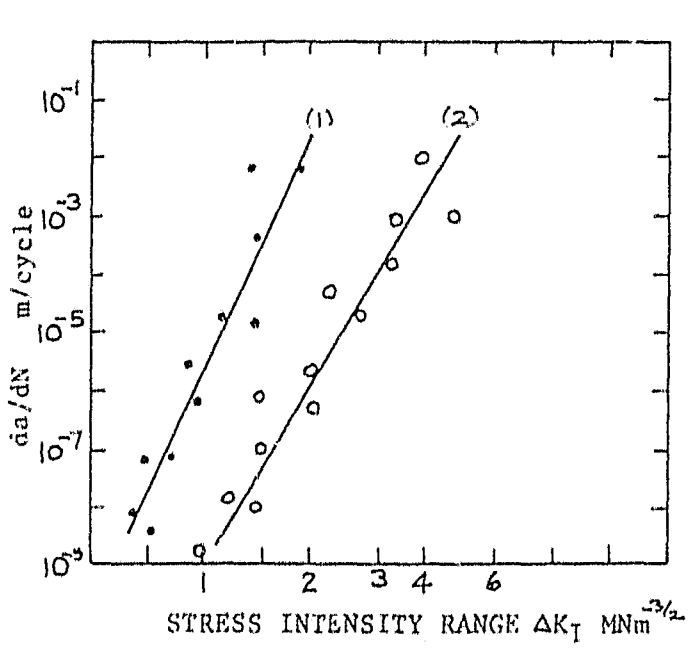


Figure 2.22 Fatigue crack growth rates measured by load relaxation in WC-6Co.[109]

A programme to measure systematically crack growth rates in WC-Co alloys, set up by Almond and Roebuck,[111] unfortunately produced only a single result before being

shelved for economic reasons.[113] (Figure 2.23).

Alloy : WC-11Co, coarse grained (≈ 3-4μm)
Test : three-point bend specimen, dimensions 38 x 7,2 x 2,4 mm
da/dN : measure crack length by potential drop method
Frequency : 20 Hz
Loading : R = 0,14 - 0,2
m value : 10

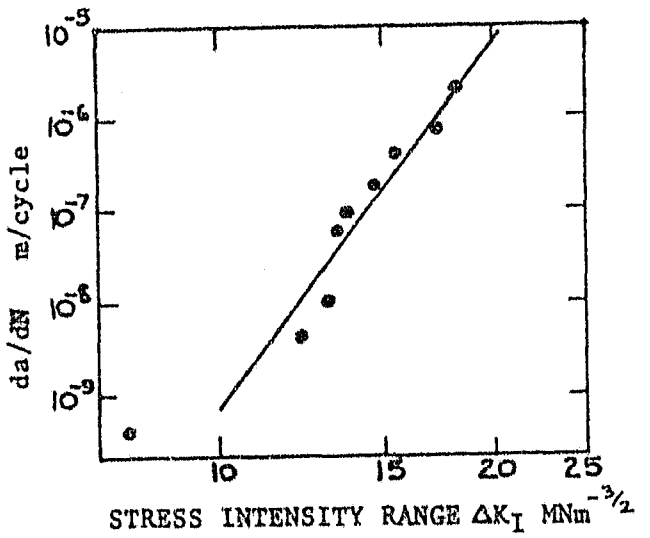


Figure 2.23 Fatigue crack growth rate in WC-11Co.[111]

Recently, results of crack growth rates on a range of alloy compositions have been reported by Lueth.[110] Unfortunately there is no indication of load range ratio (R value) or or mean stress intensity. Lueth states that the data fit an equation of the form $da/dN = C(\Delta K_I)^m$ (as would be expected) but straight lines appear on a graph which is plotted semi-logarithmically, i.e. K_I not on a log scale (Figure 2.24).

Alloy : WC-Co various Co contents, grain size not stated

Test : Double torsion specimen 76 x 43 x 3,2 mm (grooved)

da/dN : measure crack length directly with microscope

Frequency : 2 - 20 Hz

Loading : R values, K_{Iav} not stated

m values : (1) 22,85 (3) 18,44
(2) 19,36 (4) 12,42

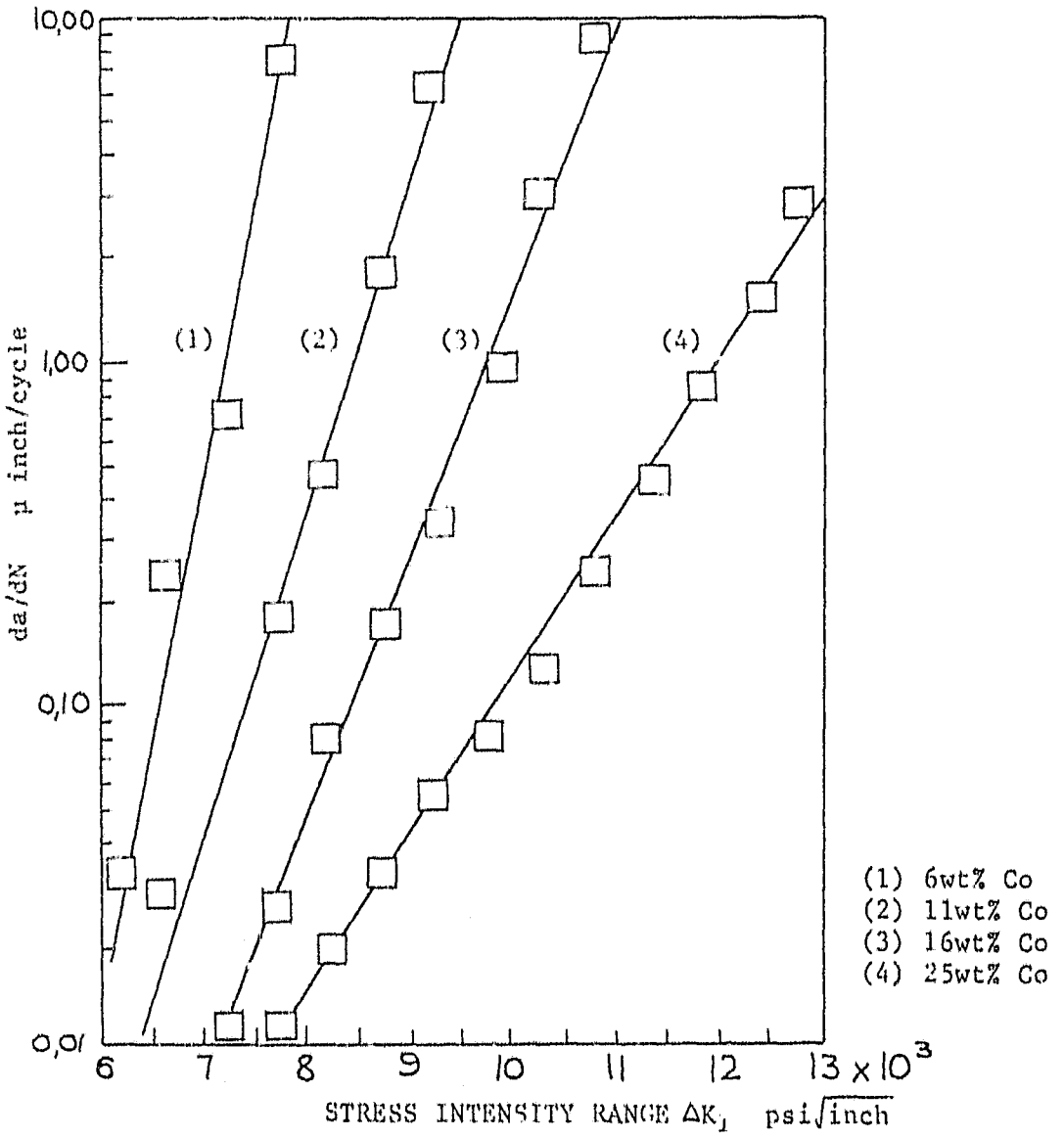


Figure 2.24 Fatigue crack growth rates measured using the DT geometry for a range of alloys.[110]

Viswanadham[112] using the short rod technique has carried out tests on alloys with fracture toughness values of approximately 17 $MNm^{-3/2}$. The results have been normalised as log da/dN vs log $\Delta K/K_{IC}$, thus combining data from different samples. (Figure 2.25).

Alloy : WC-Co (details not suplied) $K_{IC} \approx 17\ MNm^{-3/2}$, HV ≈ 1060 Kg mm^{-2}

Test : Short rod specimen. Diameter ≈ 12,7 mm height ≈ 18,8 mm

da/dN : measure crack length using compliance calibration

Frequency : 5 Hz

Loading : R ≈ 0,1

m : ≈ 15

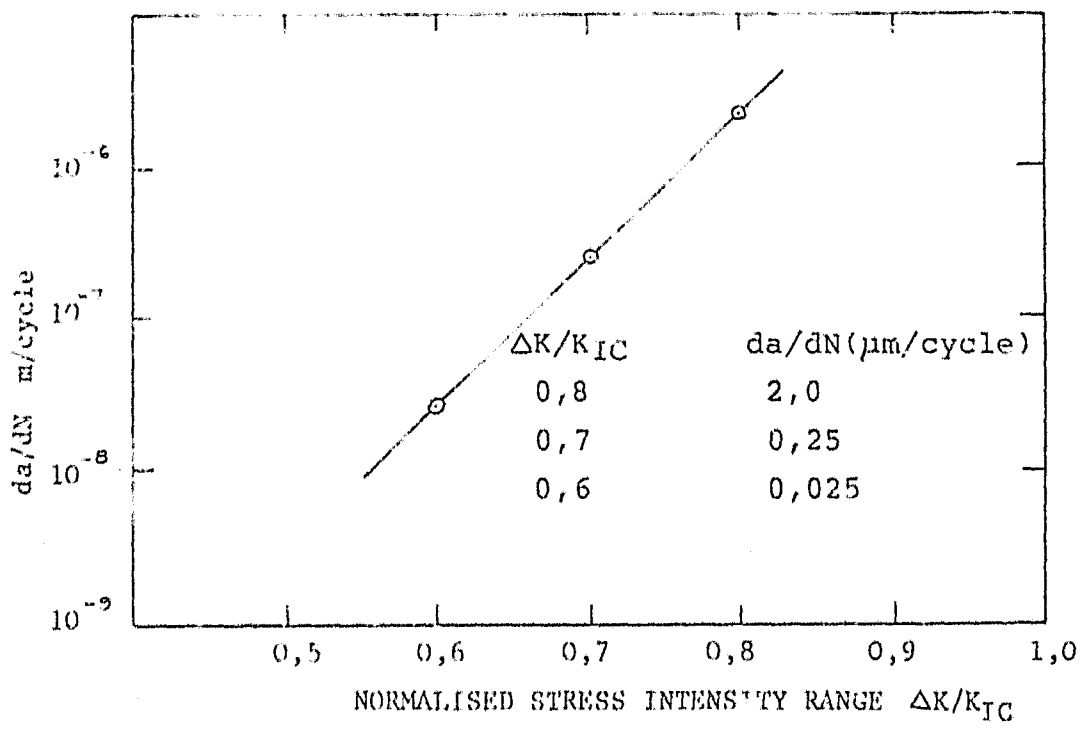


Figure 2.25 Normalised fatigue crack growth rate in WC-Co having $K_{IC} \approx 17\ MNm^{-3/2}$.

Limited studies have been made on the effect of R value up to R = 0,6 : as R increases crack growth rate increases.[112]

2.10.3 Frequency Effects

A range of frequencies have been used in fatigue investigations but no systematic study has yet been made of the effect of frequency changes on crack growth rate per cycle.

Evans and Linzer[109] have discussed frequency but no quantitative results are reported. The experimental technique they used was to monitor the rate of change in displacement of the load points with time, $\dot{y}_{av}$, under fatigue loading. If it is found that $\dot{y}_{av}$ is the same at all frequencies then the mechanism of crack growth is quasi-static. If there are significant effects of frequency on $\dot{y}_{av}$ then a true cyclic fatigue mechanism operates. Their results showed that the rate of change in compliance with time had a strong frequency dependence. Crack growth by fatigue is therefore a truly cyclic mechanism. Unfortunately they do not report any quantitative data nor do they discuss whether the crack growth is due only to cyclic mechanisms or whether there is also a static growth contribution.

Viswanadham[114] has examined, in a limited way, the effect of frequency - changing the frequency from 0,5 to 5 Hz decreased crack growth rates by a factor of 2 to 3.

2.10.4 Fractography and the Mechanism of Fatigue

Only some of the investigators have made an attempt to elucidate mechanisms of fatigue crack propagation. In essence mechanistic discussions have been based on experimental results and fractographic observations. Some controversy exists, however, as to whether there are any specific differences between fatigue and fast fracture surfaces.

Scanning election microscopy of surfaces from rotating beam tests[105] showed fracture to be

predominantly in the cobalt binder phase with characteristic ductile dimples. Lueth[110] supports this view and states that fatigue fracture surfaces are identical to those produced by a continuously propagating crack. Based on this fractographic evidence he concludes that fatigue is not an active failure mechanism, completely ignoring the da/dN vs ΔK_I data.

In contrast to this Almond and Roebuck[111] have reported that the binder-phase regions fail with little plastic deformation by a fracture mode that is probably partly cleavage and is characterised by surface markings that are crystallographic in nature. Their explanation for this more brittle failure of the binder in fatigue is the considerable work hardening of the cobalt resulting from the cyclic stresses at the crack tip.

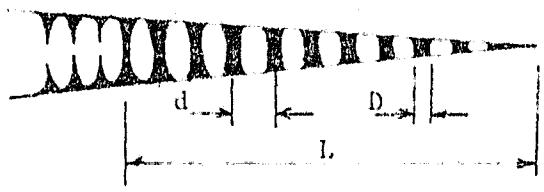
Viswanadham[114] has indicated that there is no significant change in the fracture topography of catastrophic and fatigue fracture except in a very limited number of cases observed in WC-6Co and WC-8Co alloys with grain size ~1μm. He feels that these differences are observed only under very restricted conditions which he has not yet been able to identify. The transition from fatigue to catastrophic failure can, however, often be distinguished visually, the effect it is felt[112] being due to deviations in the location of the crack plane.

Miyake et al.[104] using X-ray diffraction measurements, have shown that the binder transforms from the f.c.c to h.c.p structure during fatigue, with the proportion of h.c.p. increasing with the number of fatigue cycles.

Evans and Linzer[109] did not carry out any fractography but by analysing the effects of frequency on growth rates concluded that true cyclic mechanisms operate in hardmetal alloys.

Evans[115] has subsequently proposed a model for fatigue in ceramic-metal systems, with specific

application to WC-Co. The metal binder phase has a substantially higher toughness than the brittle carbide particles and even in fast fracture metal ligaments are expected to remain behind the primary crack front. Ductile failure of these ligaments as the crack opening displacement exceeds the strain for fracture produces the dimples and filaments observed on fast fracture surfaces.[116,117]



The formation and fracture of these ligaments provide the primary source of toughness, a view reinforced by the dependence of toughness on mean free path. Evans et al.[118] have shown that toughness depends on the yield strength and dispersion of the binder phase to an extent given by the relation: (derived by Evans, Heuer and Porter[118]).

$$K_C = K_O + \frac{\sigma_y}{(1 + d/D)^2}\left(\frac{\pi L}{2}\right)^{\frac{1}{2}}$$

where:

K_C = fracture toughness of composite
K_O = fracture toughness of ceramic constituent
d = separation between ligaments
D = ligament diameter
L = ligament zone size

Values for d and D cannot be related directly to the microstructural parameters of WC-Co alloys because an idealised composite of cylindrical ductile particles in a brittle matrix is assumed.

In a fatigue situation the unbroken ligaments most remote from the crack tip are subject to extreme plastic strain and can be expected to exhibit necking.[115] When the applied load is reduced and crack surface separation decreases, failure of the remote ligaments by plastic buckling is likely to occur. The effective, total, remaining ligament zone area and hence the force resisting crack opening is reduced, for unit width, by an amount ΔL.

Upon reapplication of tensile load the stress intensity at the crack tip becomes:

$$K = K_\infty - \frac{\sigma_y}{(1 + d/D)^2}\left(\frac{\pi L - \Delta L}{2}\right)^{\frac{1}{2}}$$

where:

K_∞ = applied stress intensity

If K exceeds the intrinsic toughness of the ceramic constituent, K_o, the crack extends until:

$$\begin{pmatrix}\text{applied stress} \\ \text{intensity}\end{pmatrix} - \begin{pmatrix}\text{force resisting crack} \\ \text{opening}\end{pmatrix} = K_o$$

Fatigue is therefore observed.

In terms of this model, the number of ligaments that fail by buckling during unloading will depends on the degree of crack of crack closure i.e. the minimum stress intensity of the load cycle (K_{Imin}). The subsequent crack advance during the loading half cycle then depends on the maximum applied stress intensity, K_{Imax}.

It is therefore evident that the crack growth per cycle da/dN is a function of the absolute cycle parameters K_{Imax} and K_{Imin} as well as the stress intensity range ΔK_I.

2.10.5 Summary

The published data on fatigue crack growth rates are summarised in Figure 2.26.

The various conflicting opinions on the nature of fatigue crack growth are tabulated to show the degree of controversy that exists. (Table 2.5).

Table 2.5

SUMMARY OF FATIGUE OBSERVATIONS

ISSUE	OBSERVATION	
Effect of increasing cobalt content	Fatigue life increased Kreimer[107] Miyake, Fujiwara and Nishigaki[104] Lueth[110]	Fatigue life decreased Johansson, Persson and Hiltscher[108]
Fatigue fracture surface	Ductile failure of binder i.e. same as fast fracture Davies and Barhana[105] Lueth[110] Viswanadham[114]	Brittle failure of binder Almond and Roebuck[111]
Mechanisms	Static effects Lueth[110]	True cyclic effect Almond and Roebuck[111] Evans and Linzer[109]
Fatigue limit or K_I threshold?	Does exist Kreimer[107] Lueth[110]	Does not exist Miyake, Fujiwara and Nishigaki[104] Davies and Barhana[105] Johansson, Persson and Hiltscher[108]

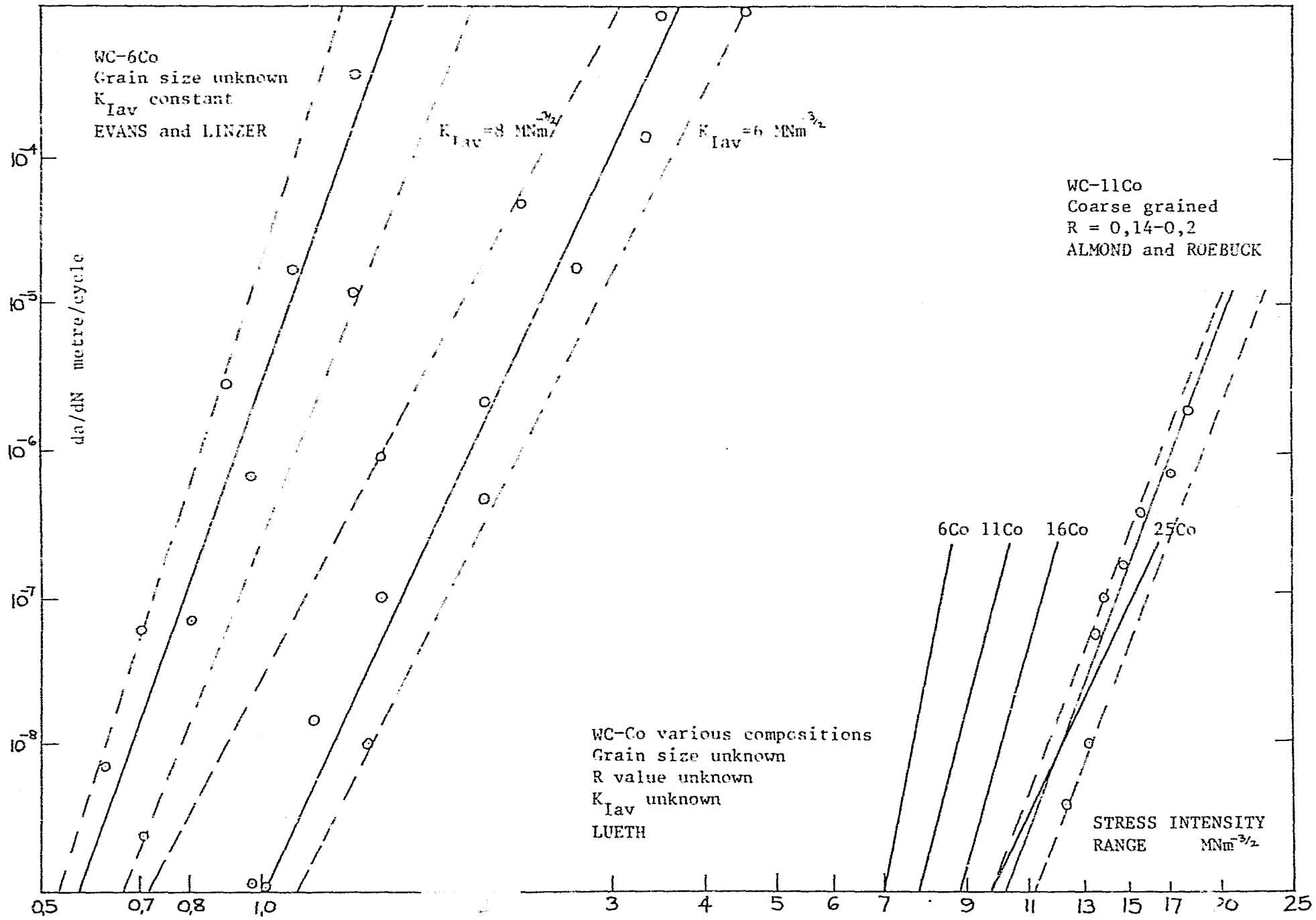

WC-6Co
Grain size unknown
K_{Iav} constant
EVANS and LINZER
K_{Iav}=8 MNm$^{-3/2}$
K_{Iav}=6 MNm$^{-3/2}$
WC-11Co
Coarse grained
R = 0,14-0,2
ALMOND and ROEBUCK
6Co 11Co 16Co 25Co
WC-Co various compositions
Grain size unknown
R value unknown
K_{Iav} unknown
LUETH
da/dN metre/cycle
10^{-4}
10^{-5}
10^{-6}
10^{-7}
10^{-8}
0,5 0,7 0,8 1,0
3 4 5 6 7 9 11 13 15 17 20 25
STRESS INTENSITY RANGE MNm$^{-3/2}$

Figure 2.26

3 REVIEW OF THE DOUBLE TORSION TEST METHOD

3.1 INTRODUCTION

A wide variety of specimen types can be used to obtain fracture mechanics information. The majority, however, have been developed and are ideally suited to relatively ductile materials and while most are satisfactory for determining fracture toughness values in brittle materials, slow crack growth measurements present a more complex problem. These materials can be very load sensitive and the stress intensity has to be carefully controlled to prevent fast fracture. For this reason the 'constant K' geometries are preferred. Evans[119] has summarised the optimum applications of various test methods for brittle ceramics (Table 3.1). All four geometries suitable for crack growth rate studies have the 'constant K' characteristic, which in addition to the simplified stress intensity control also permit measurements to be made over a relatively large crack propagation length within a single specimen.

In particular the double torsion test technique, first proposed by Outwater and Jerry in 1966,[120] has gained popularity and been used extensively by various authors to measure fracture toughness and to obtain slow crack growth data in brittle materials subjected to both monotonic and fatigue loading. The major advantages are that the specimen geometry is relatively simply and easy to manufacture, (Figure 3.1),[119,121] the analysis is supposedly straightforward and experiments are easily performed.[122] There are also unfortunately a number of unresolved questions concerning the technique.

Pletka et al.[123] have stated that:

(i) "certain precautions and special techniques are required to conduct the experiments properly,"

and (ii) "certain specimen and experimental conditions lead to data whose validity is (sic) questionable."

In addition there has been no standardisation of test procedure and as a result a wide variety of methods and geometries have been employed. A review of the many publications on the subject has therefore been made in order to systematically document all aspects of this useful test method.

Table 3.1

FRACTURE MECHANICS GEOMETRIES SUITABLE FOR TESTING BRITTLE MATERIALS

Data Required	Critical Stress Intensity Factor (Fracture Toughness), K_{IC}					Crack Growth Rate vs K_I or ΔK_I	
	Slow Loading Rate				Fast Loading Rate	Ambient Temperature	High Temperature
	Ambient Temperature		High Temperature				
	Porous Material	Non-Porous Material	Porous Material	Non-Porous Material			
Specimen Configurations	Double Torsion Tapered Cantilever Beam Constant Moment	Double Torsion Three (four) Point Bend Double Cantilever Beam Compact Tension	Double Torsion	Double Torsion Three (four) Point Bend	Three (four) Point Bend	Double Torsion Tapered Cantilever Beam Double Cantilever Beam Constant Moment	Double Torsion

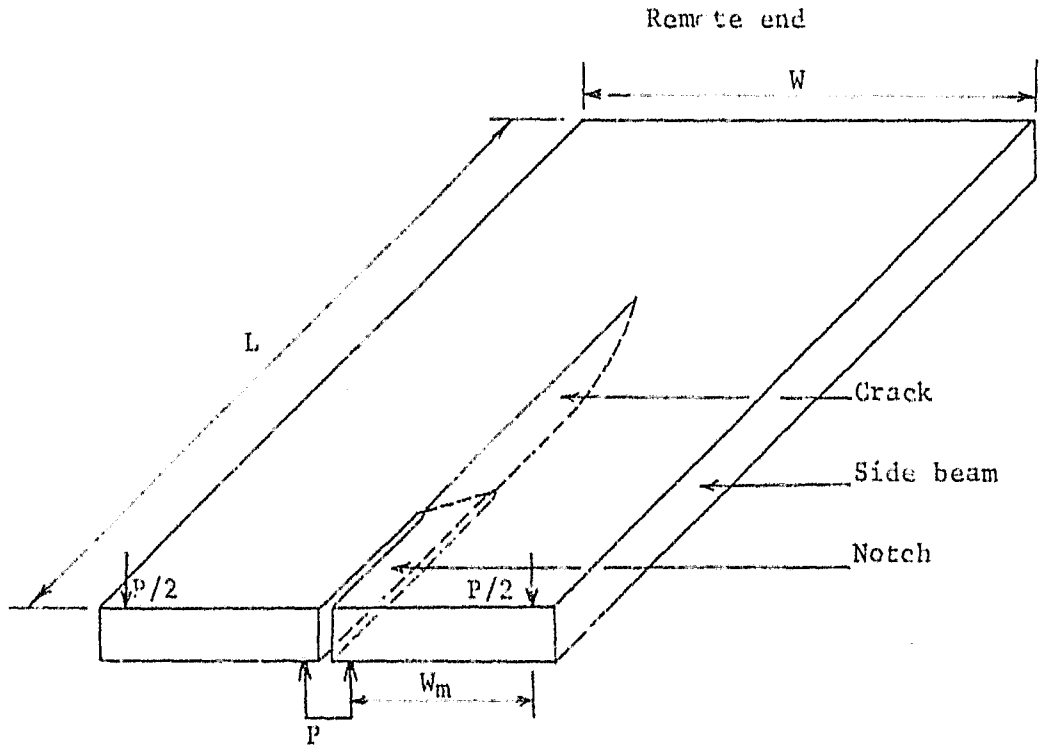
3.2 THEORETICAL ANALYSIS

3.2.1 Description of Test

The double torsion specimen consists essentially of a thin flat rectangular plate with a starter notch cut into one end (Figure 3.1). The co-linear point loads applied at the notched end effectively cause opposing torsional moments on each side of the plate resulting in crack propagation down the centre line of the specimen.

If, however, the torsional moments are not exactly equal, for example due to misalignment, the crack will deviate from the centre line. Some authors[125-129] have used grooves in the top and/or bottom surfaces to stabilise central cracking. The effect of these grooves is discussed in Section 3.3.4.

The remote end of the specimen (as opposed to the loaded end) is simply supported, the only load being the weight of the test piece.



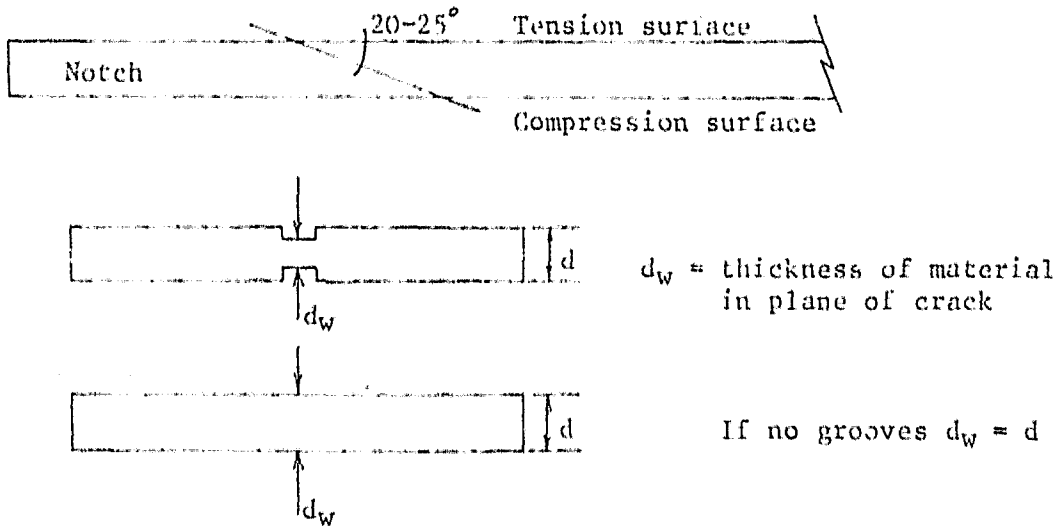


Figure 3.1 Diagram showing the basic geometry dimensions and terminology used in the double torsion test.

3.2.2 Derivation of the Stress Intensity at the Crack Tip

The following derivation shows that the stress intensity in the double torsion specimen is nominally independent of the crack length, i.e.: a so-called 'constant K' geometry. There is, however, some variation in the stress intensity due to end effects. These are discussed in Section 3.3.5.

The specimen can be considered as two rectangular elastic torsion beams of length, a, loaded as shown in Figure 3.2. The analysis assumes a vertical crack front (Section 3.4.3) beyond which the specimen is perfectly rigid. For a beam in torsion subjected to small deflections, y, and where width is much greater than specimen thickness, the following equation applies:[124]

$$\Theta \approx \frac{y}{W_m} = \frac{6Ta}{Wd^3G}$$

where:

Θ = torsional strain
T = torsional moment
G = shear modulus
a = crack length
C = elastic compliance

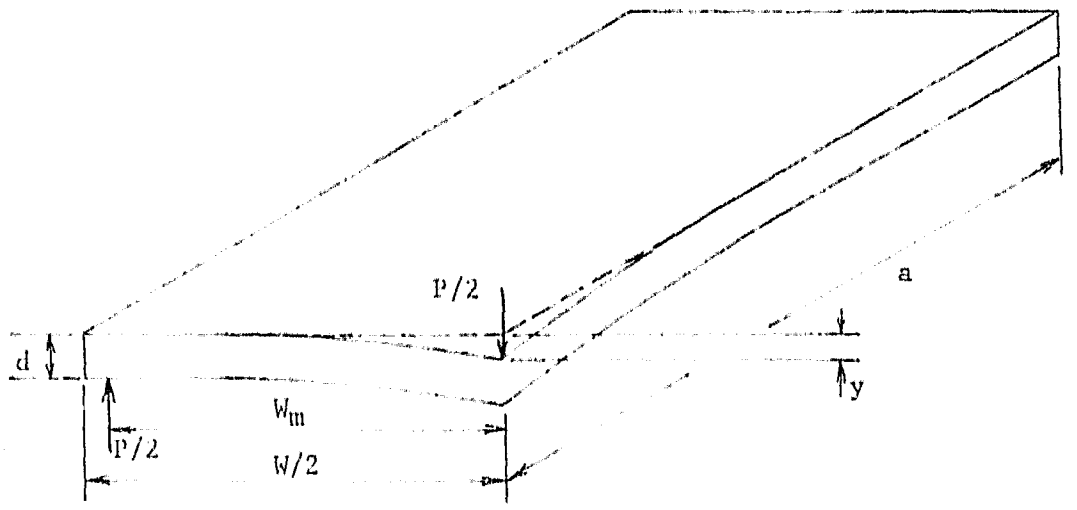


Figure 3.2

3.2.2 Derivation of the Stress Intensity at the Crack Tip

The following derivation shows that the stress intensity in the double torsion specimen is nominally independent of the crack length, i.e.: a so-called 'constant K' geometry. There is, however, some variation in the stress intensity due to end effects. These are discussed in Section 3.3.5.

The specimen can be considered as two rectangular elastic torsion beams of length, a, loaded as shown in Figure 3.2. The analysis assumes a vertical crack front (Section 3.4.3) beyond which the specimen is perfectly rigid. For a beam in torsion subjected to small deflections, y, and where width is much greater than specimen thickness, the following equation applies:[124]

$$\theta \approx \frac{y}{W_m} = \frac{6Ta}{Wd^3G}$$

where:

θ = torsional strain
T = torsional moment
G = shear modulus
a = crack length
C = elastic compliance

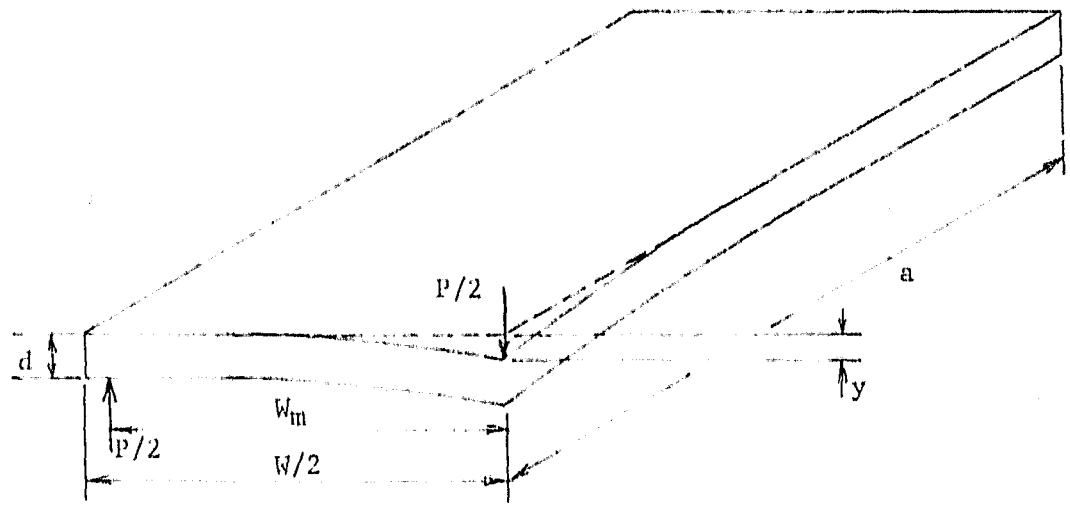


Figure 3.2

The elastic compliance is defined as the deflection, y, divided by the applied load, P. It is a function of the shear modulus of the material, G, and the dimensions of the assumed beam in torsion. Particularly, as the length of the beam increases, for a given applied moment and cross-sectional area the compliance will increase.[124] Hence:

$$C = \frac{y}{P} = \frac{3W_m{}^2 a}{Wd^3 G}$$

where:

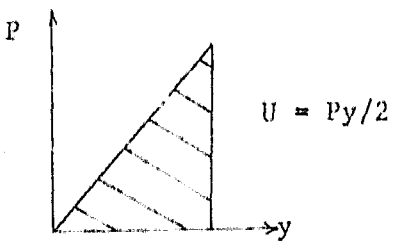
W_m = load moment arm
W = specimen width
d = specimen thickness
G = shear modulus
a = crack length

It is not a pre-requisite for the measurement of fracture mechanics parameters to have available a stress intensity calibration for the specimen. The relation between stress intensity, K_I, (or strain energy release rate $\mathcal{G}_I$) crack length and load can be obtained empirically:

$$\mathcal{G}_I = \frac{-dU}{dA}$$

where:

U = strain energy of specimen = area under load/deflection curve = Py/2
A = area of crack



It has already been shown that:

$$C = \frac{y}{P}$$

so that:

$$\mathcal{G}_I = \frac{-d}{dA}\left(\frac{CP^2}{2}\right)$$

at constant load:

$$\mathcal{G}_I = \frac{-P^2}{2}\left(\frac{dC}{dA}\right)$$

$$\frac{dC}{dA} = \frac{dC}{da} \times \frac{da}{dA} = \frac{1}{d_w}\left(\frac{dC}{da}\right) \qquad (da/dA = d_w, \text{ Section 3.3.6})$$

therefore:

$$\mathcal{G}_I = \frac{-P^2}{2d_w}\left(\frac{dC}{da}\right)$$

Deflections beyond the crack tip are assumed to be negligible.

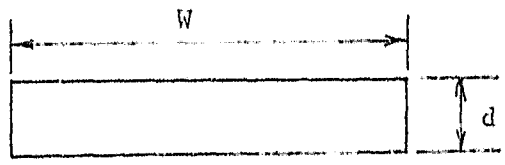
$$C = \frac{3W_m{}^2 a}{Wd^3 G}$$

Therefore the slope of the compliance curve = dC/da

$$\frac{dC}{da} = \frac{3W_m{}^2}{Wd^3 G} = B$$

B can be calculated or determined empirically (Section 3.4.3)

Fuller[8] in a more rigorous analysis includes a thickness correction factor, $\psi(t)$.



$$t = \frac{2d}{W}$$

$$\psi(t) \approx \xi$$

where:

$$\xi = 1 - 0{,}6302t + 1{,}20e^{\frac{-\Pi}{t}}$$

Hence:

$$G_I = \frac{BP^2}{2d_w}$$

$$= \frac{3P^2W_m^2}{2Wd^2d_wG\xi}$$

By substituting the following formulae,

$$K_I = (EG)^{\frac{1}{2}} \qquad \text{plane stress}$$

$$K_I = \left(\frac{EG}{1-\nu^2}\right)^{\frac{1}{2}} \qquad \text{plane strain}$$

$$G = \frac{E}{2(1+\nu)}$$

E = Young's modulus of elasticity

The stress intensity equation is obtained:

$$K_I = \left[\frac{3P^2 W_m^2 2E(1+\nu)}{2Wd^3 d_w (1-\nu^2) E\xi} \right]^{\frac{1}{2}}$$

$$K_I = PW_m \left[\frac{3}{Wd^3 d_w (1-\nu)\xi} \right]^{\frac{1}{2}}$$

NOTE: If a specimen without grooves is used the thickness in the plane of the crack, d_w, is equal to d.

In general the stress intensity formula is used as it stands but it is possible to use a value for B obtained experimentally.

$$K_I = P \left[\frac{EB}{2d_w(1-\nu^2)} \right]^{\frac{1}{2}}$$

Alternatively[127] the fracture toughness K_{IC} of the material can be determined by other techniques (e.g. SENB, CTS), and the load required for fracture of the double torsion specimen measured. Hence the constant of proportionality is determined empirically.

3.3 INFLUENCE OF SPECIMEN GEOMETRY ON THE FRACTURE MECHANICS MEASUREMENTS

3.3.1 Mode of Fracture

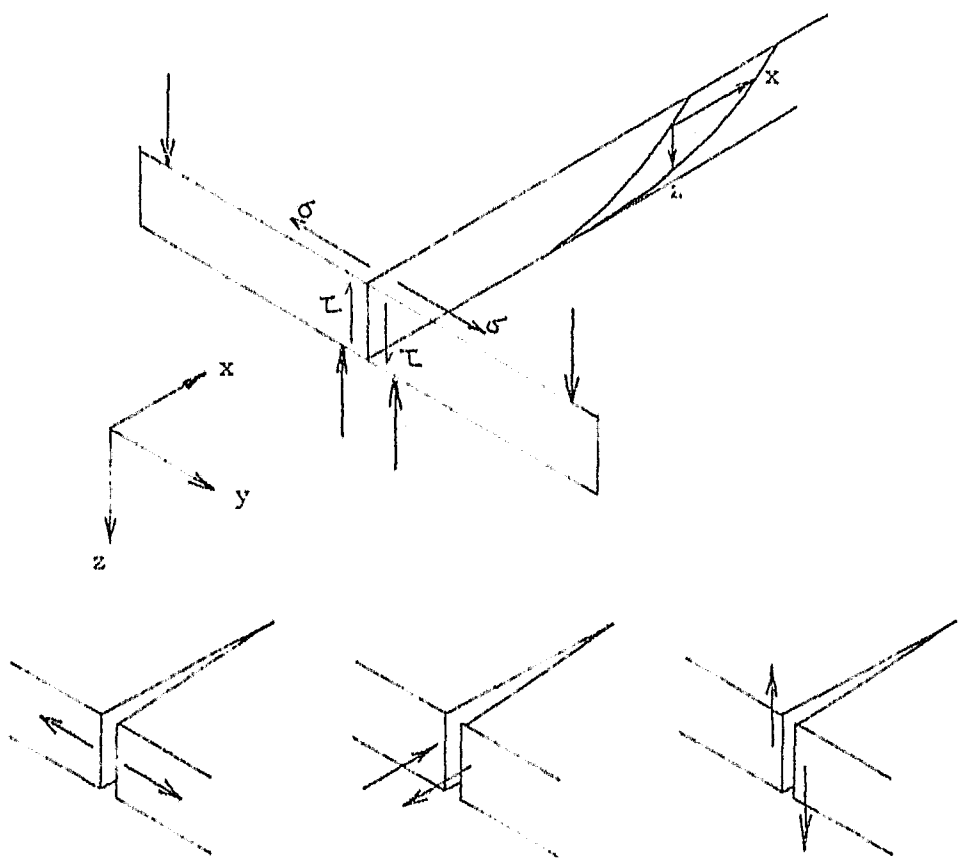
The theoretical analysis assumes a mode I, tensile crack opening, where in generalised fracture processes three modes are in fact possible. These have been classified as follows, (see also Figure 3.3):

I = tensile opening (most common)
II = pure shear
III = anti-plane sliding (torsion conditions)

Modes II and III are relatively uncommon and the fracture toughness of a material almost always refers to mode I. Values of K_{IIC} and K_{IIIC} are relatively large compared to K_{IC} for most materials and in service, failure will usually be by mode I, and it is therefore normal to measure K_{IC} as the fracture criterion.

The slightly unusual loading technique employed in the double torsion test requires that mode I fracture be validated. Fuller[130] has stated that this can be the only mode of crack propagation in an 'ideal' double torsion specimen since the loading configuration and specimen geometry are symetrical about the crack plane.

Evans[131] has acknowledged that the nature of the loading applied and the resultant apparent direction of crack propogation, x, suggest that fracture occurs due to the shear stresses, τ, i.e. mode III (Figure 3.3).



Mode I Mode II Mode III

Figure 3.3 Sketch showing different modes of fracture.

This would be the case if the crack front were parallel to the z direction propagating in the x direction, however the crack profile is closer to the x direction, except possibly at the tension surface. This indicates that the tensile stresses, σ, due to the applied bending moment are contributing to the crack growth so that fracture is by mode I or mixed mode I/III. Considerations of the critical strain energy release rates $\mathcal{G}_{IC}$ and $\mathcal{G}_{IIIC}$ using glass (a material which has $\mathcal{G}_{IIIC} >> \mathcal{G}_{IC}$) show that fracture for brittle materials is exclusively mode I.[131]

The four point loading applies equal torques to the side beams.[130] It has been shown by Fuller[130] that, if allowable the two separate beams would inter-penetrate

each other (Figure 3.4). Contact stresses would be generated by this action but are ignored for analysis; this is probably a good approximation for thin beams. (No indication is given of the thickness to width ratio, which is normally regarded as thin.) These contact stresses may be significant for thicker specimens increasing the effective stress intensity acting at the crack tip by causing additional, mode I, opening of the crack. It has been suggested by Fuller[130] that these stresses could explain why values of K_{IC} for polycrystalline alumina were under-estimated using specimens with thinness ratio $t = 2d/W \approx 1/4$, but were in good agreement with other methods of measurement for $t \approx 1/6$. A groove in the compression face reduces inter-action effects, but as discussed in Section 3.3.3, the stress concentrations due to grooves are unknown and therefore undesirable.

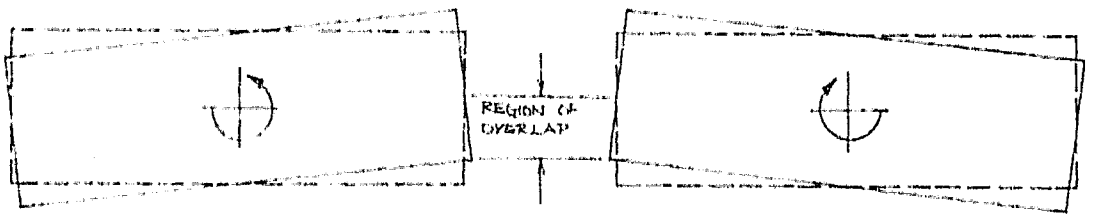


Figure 3.4

3.3.2 Specimen Geometry and Dimensions

No specific rationalisation of the dimensions of the double torsion specimen has been located in the literature. The majority of workers have used similar sized specimens (Table 3.2) either in the range 300 x 75 x 6 or 80 x 25 x 3, millimetres. Pletka et al.[123] state that "the specimen is a thin plate which usually has the dimensions of a microscope slide", it is quite clear

however that substantially larger sizes are used.

It is a requirement of the analysis[124] that the width be 'much greater' than the specimen thickness.

Recommendations on the dimension ratios have, however, been proposed by Pletka et al.[123] and Evans,[129] these are:

Length	Width	Thickness	Web thickness	Ref
> 2W	W	(1/12)W	1/2(thickness)	123
3W	W	(1/8 - 1/10)W	2/3(thickness)	129

These are based primarily on the good agreement of results obtained using the double torsion specimens of these geometries with other (e.g. D.C.B.[124,132]) techniques. There appears to be no mathematical basis for choosing these ratios.

Trantina[121] has carried out a finite element analysis of the double torsion specimens, using dimension ratios 2W : W :(1/10)W, his results and comments (Section 3.3.4) are therefore valid for most specimens listed in Table 3.2.

Table 3.2

TYPICAL DOUBLE TORSION SPECIMEN GEOMETRIES

REFERENCE NUMBER	DATE	MATERIAL	THICKNESS [mm]	WIDTH [mm]	LENGTH [mm]
148	1969	Glass	3,18	75	300
149	1970	Steel 4340	3,18	76,2	229
124	1973	Steel 4130	3,17	76,2	200
126	1973	Perspex (PMMA)	12,7	76,2	457
126	1973	Soda lime glass	6,35	76,2	609
126	1973	Glass ceramic	6,35	76,2	305
133	1973	Aluminium alloy	7,6	70,6	204
125	1974	Aluminium alloy 2124	6,35 - 13,2	71,1	203
144	1974	Cement paste	10	76	228
150	1976	Cement mortar	6	57	105
151	1979	Perspex (PMMA)	6	80	?
152	1973	Ceramic	3	25	75
143	1974	Vitreous carbon	3	25	?
128	1976	WC-Co	3	30	90
122	1980	Zirconia	2	23	80
153	1980	Ceramic	2	20	50

3.3.3 Thickness

The thickness of standard fracture toughness specimens is usually dictated by the fracture toughness (K_{IC}) and yield strength (σ_y) of the material. The usual requirement to ensure plane strain conditions is that:

$$\text{thickness} > 2{,}5\left(\frac{K_{IC}}{\sigma_y}\right)^2$$

If the material being tested is brittle this condition is usually satisfied as the size of the plastic zone at the crack tip is negligible. However questions remain concerning the range of dimensions for valid data, particularly in the case of brittle polycrystalline materials where microstructural interactions with the crack might be influenced by the specimen thickness and the state of stress.[130] The condition must therefore be imposed that the thickness of the section is sufficient to be microstructurally representative,[119] that is:
d_W >> dimensions of microstructural parameters e.g. grain size.

Outwater et al.[125] have used the double torsion method to determine the fracture toughness of a wrought aluminum alloy. The specimen thickness was approximately half that recommended by the formula above, no shear lips were observed on the fracture surface and the K_{IC} values were in good agreement with those obtained by more conventional (CTS) methods. Murphy et al.[133] have tested cast aluminium using double torsion specimen thicknesses as low as 0,25 the value recommended for plane strain.

It must be assumed therefore that plane strain conditions hold at least at the leading edge of the crack, even if the double torsion specimen is as little as half as thick as the recommended value.

3.3.4 Grooves

Grooves have frequently been cut (or cast) into the surfaces of the double torsion specimen to ensure that the fracture propagates down the centre line, where the stress intensity can be calculated. However "the centre slot causes certain intellectual discomfort because its effects, other than guiding the crack are not well understood."[134]

Almost every conceivable combination of grooves has been used in the past, for example:

(i) grooves in both surfaces, equal depths[125] and unequal depths[126]
(ii) grooves in the tension surface only[127,128]
(iii) groove in the compression surface only[123,129]
(iv) no grooves at all[124,134]

As with the overall dimensions there appears to be no mathematical or analytical base for selecting a particular groove geometry. There are several uncertainties relating to the effect of grooves, and a test piece with no centre grooves would be ideal.

Murray and Perrott[128] report that central cracking is not stabilised by a reduction in section thickness but rather requires the stress concentration effect of a sharp groove. On the other hand Pletka et al.[123] recommend that narrow grooves should be avoided and that if wide grooves are used[135] the crack is turned in the stress field of the specimen before it reaches the side of the groove. This eliminates the chance of the crack interacting with the side of the groove during propagation.

There are two principal reasons why the crack may deviate from the centre line. Misalignment of the specimen in the loading system results in unequal torsions and therefore uncertain crack front stress

intensity, it is quickly manifest as a deviation from the centre line.[134] However, careful machining and specimen alignment minimises the problem.[123] It has also been shown that microstructural discontinuities such as grain boundaries or second phase particles promote interaction of the crack with the side of the groove; this causes discontinuous cracking which has been attributed to the crack wandering into the wall of the groove.[135,136] The groove geometry may also introduce additional stress concentrations,[130] for example the existence of sharp corners can, because of the stress concentration effect, attract the crack to the side of the groove and it can then easily move into the full thickness side beam of the specimen (Figure 3.5).

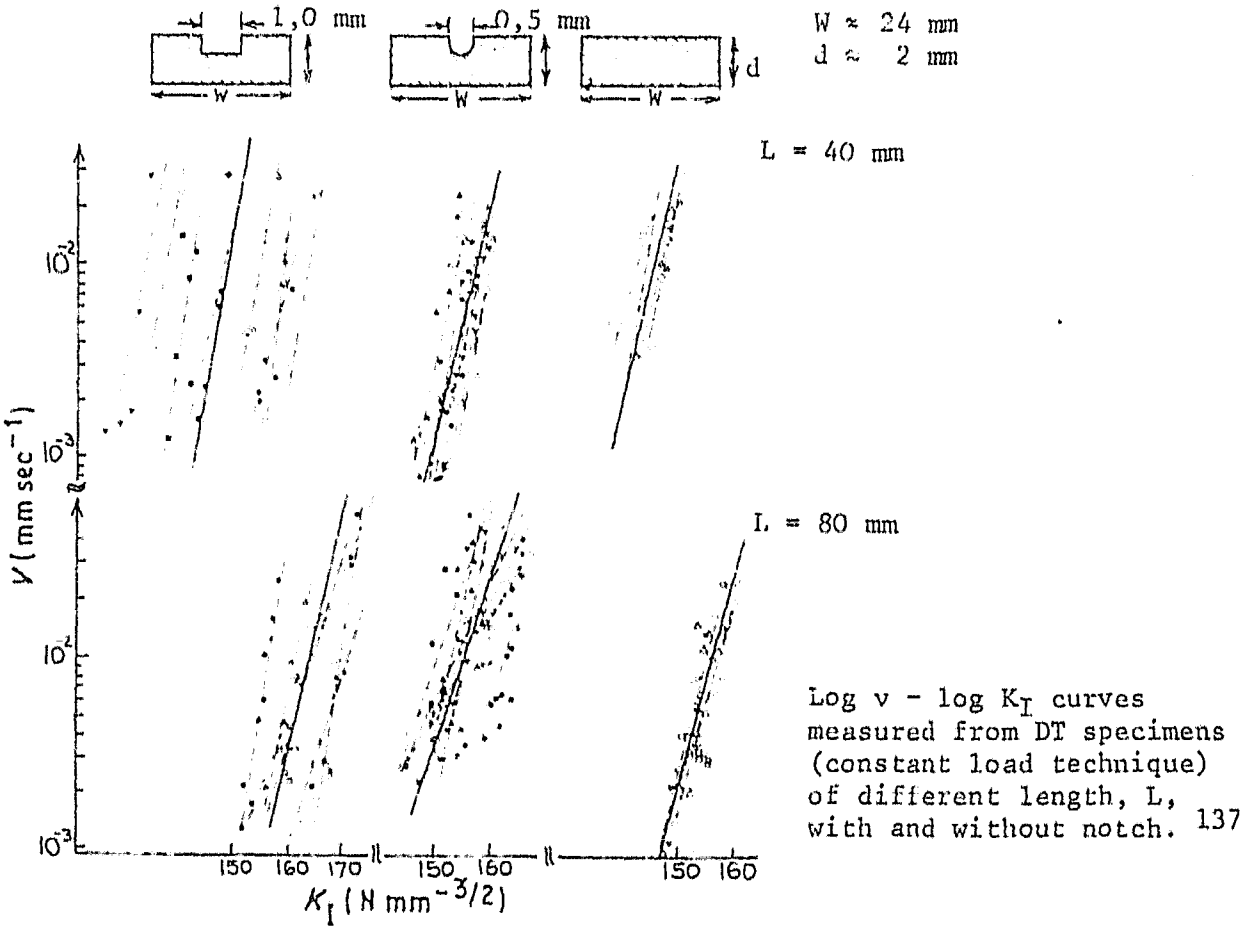


Figure 3.5

Li-Shing and Pabst[122] report that groove width and groove (tip) geometry influence the crack velocity behaviour; this contrasts the work of Pletka et al.[123] who found only a slight variation. Pabst and Weick[137] have shown by testing various groove geometries that the scatter of results in static crack growth rate tests is substantially decreased by using specimens without a groove. A rectangular groove, with two 90° corners causes so much scatter as to render the results almost useless. It is quite possible, therefore, that a groove in the tension surface alters the stress intensity at the crack tip. (Figure 3.6)

To avoid the uncertainty surrounding the effect of grooves it is possible to use specimens without them.[124,134] This requires well finished surfaces, an extremely well balanced loading device, a perfectly

dimensioned specimen, a homogenous material along the crack extension[124] and careful alignment.[134] Otherwise it is very likely that the crack will deviate from the midplane.



Log v - log K_I curves measured from DT specimens (constant load technique) of different length, L, with and without notch. [137]

Figure 3.6

3.3.5 Variation of Stress Intensity with Crack Length

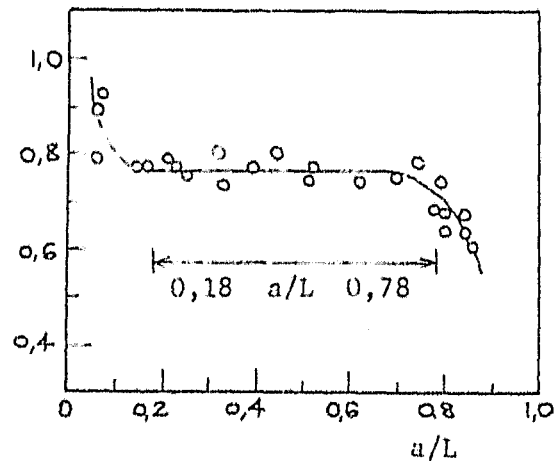
The "strength-of-materials" analysis of the double torsion specimen (Section 3.2.2) has indicated that it is a so called 'constant K' test i.e. the stress intensity at the carck tip is independent of the crack length. McKinney and Smith[126] first reported a departure from this situation due to end effects approximately one plate width from either end.

Experimental measurements of the fracture toughness

of glass by Shetty and Virkar[138] and Pletka et al.[123] have shown that the 'constant K' regime does not include the ends of the specimen. Pletka et al.[123] determined fracture toughness for crack lengths, a, in the range 0,05L to 0,85L.

The experimental evidence is in excellent agreement with the finite element analysis of Trantina[121] who predicted a valid range for a : 0,18L<a<0,78L, for a specimen with dimension ratio, length/width = 3.

These results are illustrated in Figures 3.7 and 3.8 which show the fracture toughness values obtained by experiment and the valid range predicted by finite element analysis.



Experimental results of Pletka et al.[123] for crack length, a, in the range 0,05L to 0,85L. Validity limits predicted by Trantina[123] also shown.

Figure 3.7 K_{IC} measured in toluene on soda-lime-silicate glass slides as a function of crack length.

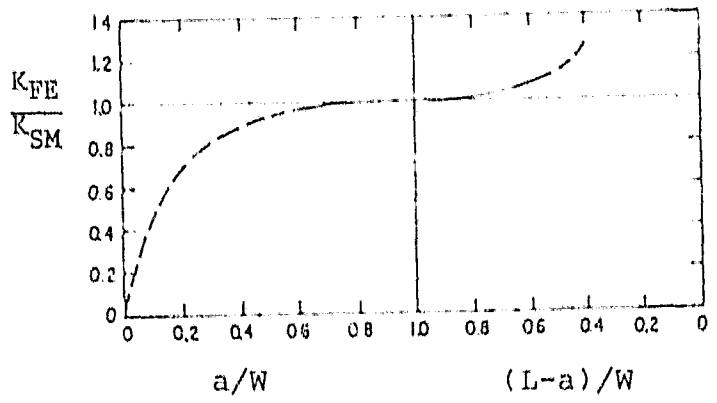


Figure 3.8 Relative stress intensity (finite element/ strength of materials) as a function of crack length and ligament length.

Trantina[121] originally quoted the valid range of crack length, a, in terms of the width, W, such that:

$0,55W < a < L - 0,65W.$

These limits are in close agreement with those set by Shetty and Virkar[138] for two different specimen sizes:

$0,5W < a < L - 1,0W$	1 : 31,25 : 75 mm
$0,4W < a < L - 0,8W$	1 : 50 : 75 mm

In Figure 3.8 the stress intensity computed by finite element technique for a given applied load is shown as a function of the value calculated by the 'strength-of-materials' approach. The implication of this is that the actual stress intensity acting at the start of the specimen is less than the value given by the strength of materials calculation. Hence loads higher than those required at the centre and end of the specimen will be needed to cause crack propagation in this region. This will result in apparently higher toughness values being calculated, as confirmed by Figure 3.7.

If constant load techniques are used to measure subcritical crack growth it is clear why catastrophic fracture can be difficult to prevent. At a constant applied load the actual stress intensity acting increases, remains constant at the middle of the specimen then increases again, as the crack extends.

These end effects also alter the compliance calibration curve so that it is not linear for short and long crack lengths.[130]

3.3.6 Crack Front Shape and Growth Rate Correction Factors

The analysis of the double torsion technique assumes a crack front perpendicular to the surfaces of the test specimen but practical observation show that the shape is curved extending further along the tension than the compression faces (Figure 3.9)

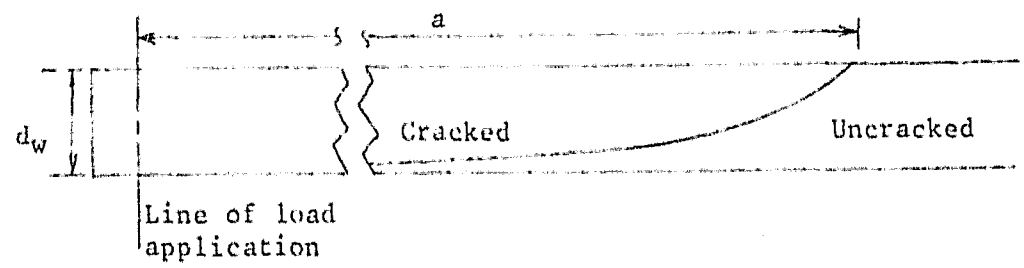


Figure 3.9 Schematic view of the curved crack front profile for the double torsion specimen.

For the purpose of strain energy release rate analysis it is necessary to determine the rate of change of crack surface area with increasing crack length. It is assumed, therefore, that the shape of the crack front remains unchanged over the length of the specimen as the crack propagates.

The increment in crack surface area, dA, that is produced by crack extension, da, at constant load, P, is:

$$(dA)_P = (da)(d_W)$$

$$\left(\frac{dA}{da}\right)_P = d_W$$

where:

d_W = material thickness in plane of crack

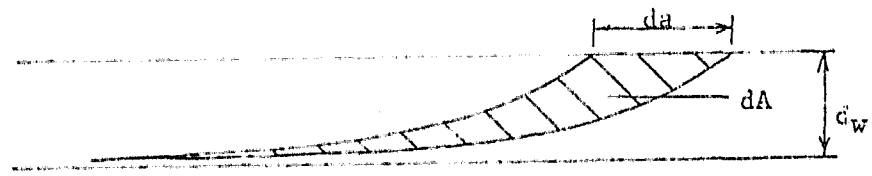


Figure 3.10

Williams and Evans[124] state that this shape is essentially independent of the crack length (except for cracks approaching the end of the specimen) for a given stress intensity, but varies marginally with stress intensity.

There are a number of problems associated with a curved crack front. Virkar and Gordon[139] have noted that the shape depends on the subcritical crack growth characteristics for a given material and environment, and that it is not coincident with the shape obtained by theoretical analysis assuming a constant K_I along the crack front.

The local direction of crack propagation must be orthogonal to the crack front, it is clear therefore that the velocity varies locally all along the front, (Figure 3.11)



Figure 3.11 Crack advance in Δt

The crack velocity is uniquely related to the stress intensity, by $V = A(K_I)^n$, or for fatigue $da/dn = C(\Delta K_I)^m$, where A, C, m and n are constants for a particular material and environment. Therefore the stress intensity must also vary along the crack front. It is concluded that the shape of the crack front depends on the value of the exponent. If the exponent varies with stress intensity i.e. a non-linear log V - log K curve, as typically found for stress corrosion cracking situations, then the crack front shape changes depending on the applied stress intensity.[139] It is then not possible to make accurate velocity determinations by simply introducing a crack front shape correction factor.

Trantina[121] using his finite element analysis of the double torsion specimen determined a unique crack front shape providing a constant K_I along the crack front to a depth of approximately half the thickness. He states that reasons for differences in crack shapes for different materials are not clear, it may be due to the groove depth but does not appear to be determined by the exponent (cf: Virkar and Gordon[139]). However, variations in stress intensity are small, and since the exponent is usually large ($n,m \gtrsim 10$) for brittle materials, small changes in the stress intensity can cause considerable variation in velocity and hence shape.

A correction factor can be introduced which will give a closer approximation to the velocity than that observed

on the tension surface. Evans[131] has recommended the measured velocities be reduced by a factor ϕ, where:

$$\phi = \frac{d_w}{(\triangle a^2 + d_w^2)^{\frac{1}{2}}}$$

However this is not really valid because the stress intensity is also decreasing.[121]

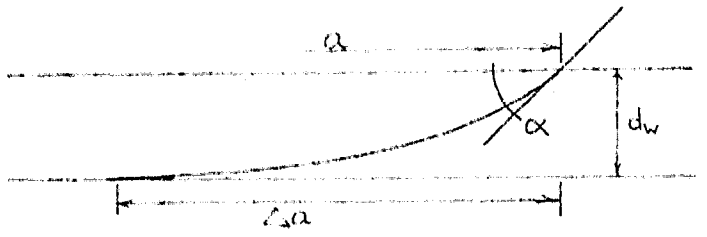


Figure 3.12

Trantina[121] and Virkar and Gordon[139] concede that further study of different materials and geometries, detailed evaluation of the crack front profiles and better averaging procedures are required to take into account more fully the effects of the curvature of the crack front.

It is assumed at this point that (a) the stress intensity in the double torsion specimen is given by the simple analytical solution (Section 3.2.2) and (b) the measured crack growth rate (da/dt or da/dN) is corrected by the sine of the angle of incidence, α , of the crack front with the specimen surface. (Figure 3.12)

3.4 EXPERIMENTAL TECHNIQUES

3.4.1 Precracking

In order to obtain valid fracture mechanics measurements it is necessary to start with an atomically sharp crack, this is usually recommended for all specimen geometries although some controversy exists. The requirement for an atomically sharp crack is especially evident in fracture toughness determinations, values obtained from blunt cracks are invariably too high.[123,128] Pletka et al.[123] have recommended two methods for precracking the double torsion specimen. These are: (i) a constant displacement rate and (ii) a fixed displacement, of the load points. Both methods employ a tapered starter notch (Figure 3.13) and initiation and propagation are detected by a rapid decrease in load.

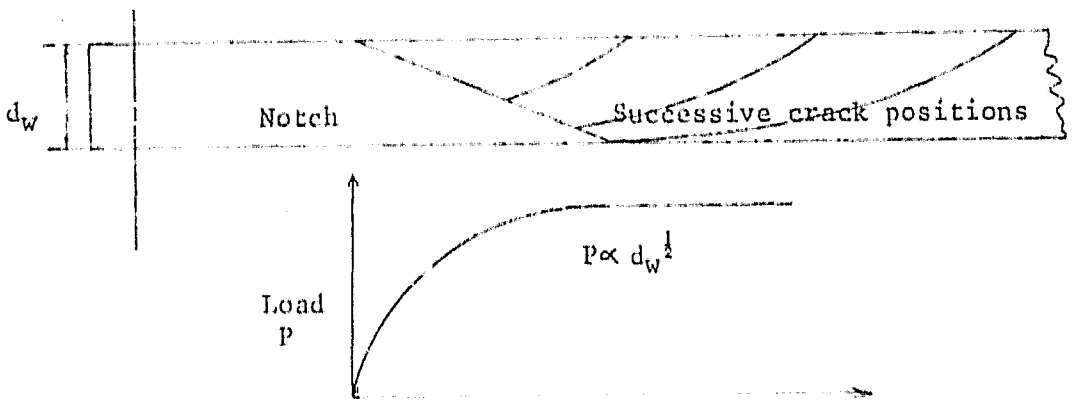


Figure 3.13 Sketch of load required for fracture using tapered starter notch.

Method (ii), whereby the displacement is occasionally increased but is then fixed and held at that value, is preferred because it requires a lower maximum load for initiation. More time is allowed for the slow crack growth mechanisms to form a crack and therefore a smaller

precrack is obtained. This is especially important for materials in which the precracking load can exceed the load for fracture of the complete specimen.

The stress intensity, K_I, in a double torsion specimen is a function of the load applied divided by the square root of the thickness seen by the crack, $K_I \propto P(d_w)^{-\frac{1}{2}}$. (If a specimen without grooves is used $d_w = d$). The effect of tapering the starter notch, initially very small d_w, is therefore to enable a crack to initiate by subcritical slow crack growth mechanisms at a suitable stress intensity but using loads well below the load required to cause fast fracture in the full thickness (Figure 3.13).

The stress intensity variations with crack length investigated by Pletka et al.[123] and Trantina[121] show that the loads required for a given stress intensity are higher at the start of the cracking than in the middle region (Section 3.3.5). This effect may counteract the benefits of the tapered notch and if load relaxation after initiation is insufficient total fracture of the specimen may occur.

In any event it is necessary to rely on subcritical slow crack growth mechanisms to intitiate a starter crack, which is then detected by a change in compliance.[124] For ceramic materials and for metals under environmental stress corrosion attack it is sufficient to use a static load. However, for metals in normal circumstances it is necessary to use cyclic fatigue either under controlled load or controlled displacement conditions,[124] as before crack extension is detected by a change in compliance, or by direct observation using dye penetrant techniques.(Section 3.4.2).

3.4.2 Direct Measurement of Crack Length (Position of crack tip)

Most of the test methods (detailed in Section 3.4.4) are such that the crack monitoring is not usually continuous, and measurements need only be taken before and/or after a test. For example the displacement controlled load relaxation technique requires a before or after measurement of the crack length in both the static[124] and fatigue[140] modes, fatigue crack growth, under constant load cycling however, requires measurement before and after a certain number of cycles have elapsed.

One of the primary advantages of the double torsion test is that crack length can be determined from the compliance of the specimen, once the compliance - crack length correlation has been obtained (Section 3.4.3). This means that the crack length can be measured without direct observation.[126,127,129]

Despite this extremely useful feature of the double torsion test, other techniques of measurement have been used, because the accuracy when using compliance may be insufficient for precise crack length determination. These have included such exotic ideas as silver grid lines evaporated on to the specimen surface in the line of the fracture,[126] as the crack propagates the resistance of the grid lines changes. The most successful however all rely on the ability to observe optically the position of the crack tip. In transparent materials (glass, perspex) this is no problem,[141,142] but in opaque materials a method is required which will reveal the position of the crack tip. For this purpose the use of dye penetrant seems to be most appropriate. Evans et al.[140] using a constant stress intensity under both fatigue and static loading measured the crack length increment, Δa, in a predetermined time, Δt, using fluorescent dye penetrants. Pletka et al.[123] have also recommended the use of dye penetrants, but comment that

checks need to be made to ascertain whether the dye actually penetrates to the crack tip. This can be done by turning the specimen over and loading to fracture. The crack profile and position of the original crack will be seen clearly, and the extent to which the dye has penetrated will also be visible.

A method which has been used with success by the author, for fatigue studies, but which is not reported in the literature, is the placement of a dye penetrant in the crack during testing. With the combination of capillary action and the opening and closing of the crack the liquid is drawn to the crack tip and on unloading cycles is squeezed out thus clearly showing its position, which is easily measured using a travelling microscope.

There is one problem however with the dye penetrant liquid capillary method. The substance used to reveal the crack may cause an environmental effect on the crack growth rates although specifications require that dye penetrants are totally non-corrosive.(Section 4.5.1).

3.4.3. The Use of Compliance to Measure Crack Length

The compliance, C, of a test specimen has previously been defined as the displacement of the load points, y, divided by the load applied at those points, P. (Section 3.2.2). The double torsion specimen is idealised as two rectangular beams fixed at one end with torsional moments applied. It is assumed that:

(i) the load point displacement is due only to purely elastic rotation of the side beams resulting from the applied torque i.e. the local stresses and deflections, due to the point loads, are neglected.[130]

(ii) the uncracked section of the plate is perfectly rigid i.e. no bending or torsional deflection beyond the crack tip.

(iii) the crack front is vertical and extends through the thickness of the plate (experimental observation shows that in practice the crack is curved extending further along the tension surface)(Figure 3.14).

(iv) the crack length, a, is measured in the tension surface.

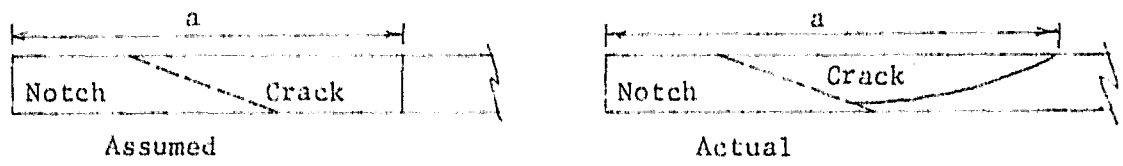


Figure 3.14

It is easily shown that the rotation of a beam fixed at one end, to which a torque is applied is a function of the length of the beam, the cross sectional dimensions and the elastic shear modulus. It follows, therefore, by the assumptions (i) to (iv) that the rotation of the side beams and hence load point displacement in the double torsion specimen is a linear function of the crack length, a,[124,126,130,135,143.144] and is given by:

$$C = \frac{y}{P} = \frac{3W_m{}^2 a}{Wd^3 G} = Ba$$

where:

$$B = \frac{3W_m{}^2}{Wd^3 G}$$

and:

W_m = moment arm of applied load
W = specimen width (side beam width = W/2)
d = specimen thickness
G = elastic shear modulus
a = crack length

Clearly the uncracked length of the specimen must deflect under the applied torque. However, if this length is 'long' it will have constant compliance, C_o, as is observed experimentally.[130] (No indication is given in the literature of the percentage of the specimen that must be uncracked.) This gives the very useful relationship:

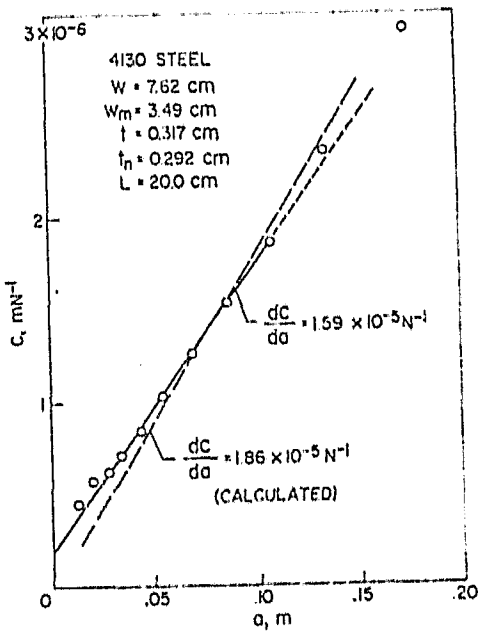
$$C = \frac{y}{P} = (Ba + Co)$$

where:

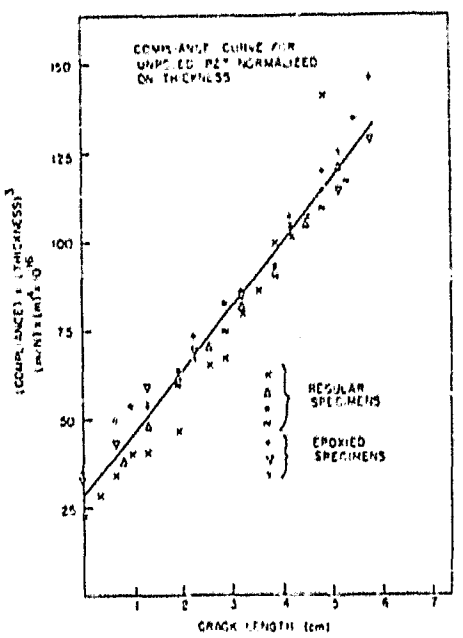
C = compliance
y = displacement
P = load
B = constant
C_o = constant
a = crack length

The values of B and C_o depend on the elastic moduli of the test material and the dimensions of the specimen and test device.[131] B can be calculated or determined experimentally by measuring the compliance at various crack lengths. The compliance of the side beams is usually much larger than the constant C_o ($Ba >> C_o$) therefore the stress intensity calculation which assumed $C_o = 0$ is not affected within the range of validity (Section 3.3.5) and crack velocity data is only slightly influenced.[130]

It is possible to use the compliance, $C = Ba + C_o$, to measure crack length indirectly once a calibration graph has been obtained. Figure 3.15 contains examples from the literature. Unfortunately the precision of measurement by this method is poor.

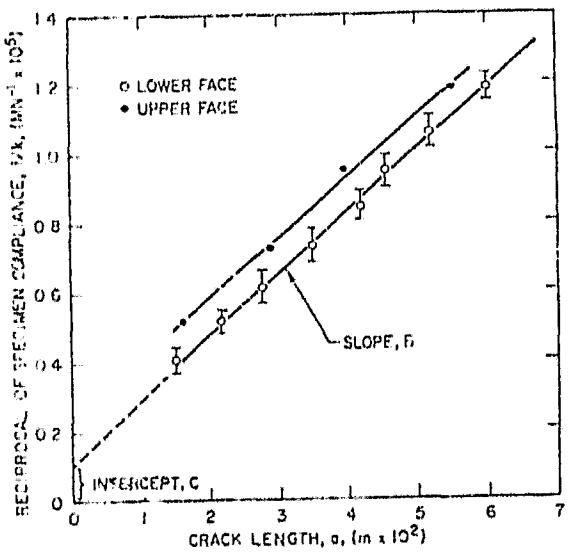


Williams and Evans[124]

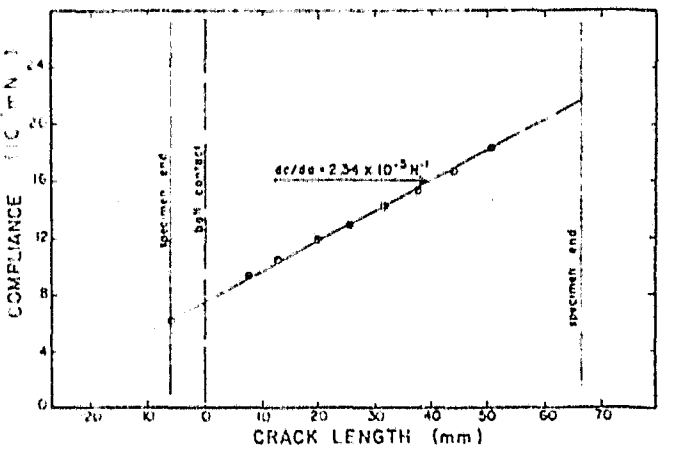


Bruce et al.[135]

Figure 3.15

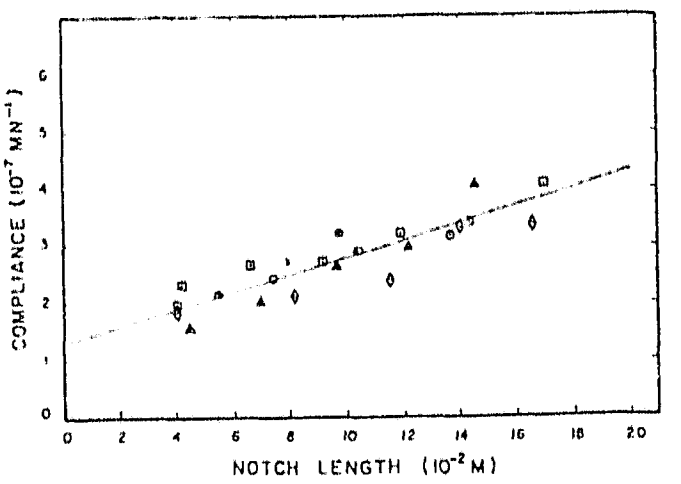


Evans[127]



Compliance plot obtained by cutting specimen along crack line.

Nadeau[143]



Compliance curve for notched cement-paste specimens. Data from 7 specimens.

Nadeau et al.[144]

The deflection of the side arms, due to load, is measured using linear variable differential transducers (LVDT). It is not stated explicitly[109,145] where this deflection should be measured but the implication is that it should be at the load points.

The criticality of where the LVDTs were placed was investigated using the relationship:

$$C = Ba + C_o \quad \text{where} \quad B = \frac{3W_m^2}{Wd^3G}$$

differentiating w.r.t. crack length, a:

$$\frac{dC}{da} = \frac{3W_m^2}{Wd^3G} = B$$

Therefore if the experimentally determined compliance value of B is to be compared with the analytical value, the deflection must be measured at W_m, i.e. at the load points.

If the LVDTs are placed outside the position of the load points i.e. W_m(LVDT) > W_m(load points) then the compliance graph will remain linear but the slope (dC/da) will be greater than calculated value of B.

3.4.4 Applications of the Compliance Relationship to Determine Crack Growth Rates Indirectly.

The compliance relationship of the double torsion specimen, already described, is, apart from the constant stress intensity characteristic, its most outstanding feature. It can be exploited in several ways to obtain static and fatigue crack growth data without continuous monitoring of crack length. Although not all of these have been attempted by the author all are detailed as it is foreseen that in future work, for example at elevated temperatures, remote sensing using these methods may be

The deflection of the side arms, due to load, is measured using linear variable differential transducers (LVDT). It is not stated explicitly[109,145] where this deflection should be measured but the implication is that it should be at the load points.

The criticality of where the LVDTs were placed was investigated using the relationship:

$$C = Ba + C_o \quad \text{where} \quad B = \frac{3W_m^2}{Wd^3G}$$

differentiating w.r.t. crack length, a:

$$\frac{dC}{da} = \frac{3W_m^2}{Wd^3G} = B$$

Therefore if the experimentally determined compliance value of B is to be compared with the analytical value, the deflection must be measured at W_m, i.e. at the load points.

If the LVDTs are placed outside the position of the load points i.e. W_m(LVDT) > W_m(load points) then the compliance graph will remain linear but the slope (dC/da) will be greater than calculated value of B.

3.4.4 Applications of the Compliance Relationship to Determine Crack Growth Rates Indirectly.

The compliance relationship of the double torsion specimen, already described, is, apart from the constant stress intensity characteristic, its most outstanding feature. It can be exploited in several ways to obtain static and fatigue crack growth data without continuous monitoring of crack length. Although not all of these have been attempted by the author all are detailed as it is foreseen that in future work, for example at elevated temperatures, remote sensing using these methods may be

necessary.

The equation $y = P(Ba + C_o)$ forms the basis for all these methods.

3.4.4.1 Constant Displacement Methods

(i) Static slow crack growth:[124]

Differentiate w.r.t. time:

$$\frac{dy}{dt} = (Ba + C_o)\frac{dP}{dt} + (BP)\frac{da}{dt}$$

If the displacement, y, of the low points is kept constant then:

$$\frac{dy}{dt} = 0, \text{ and}$$

$$P(Ba + C_o) = P_i(Ba_i + C_o) = P_f(Ba_f + C_o)$$

$$\frac{da}{dt} = \frac{-(Ba + C_o)}{BP}\frac{dP}{dt}$$

$$= \frac{-P_i}{P^2}\left(a_i + \frac{C_o}{B}\right)\frac{dP}{dt}$$

$$= \frac{-P_f}{P^2}\left(a_i + \frac{C_o}{B}\right)\frac{dP}{dt}$$

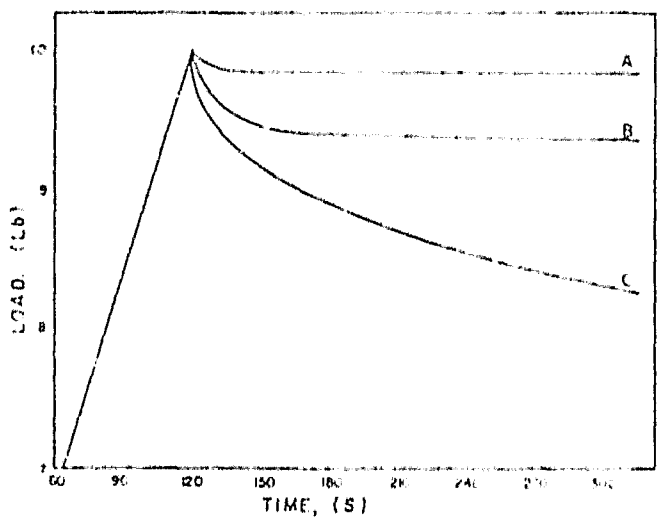
for large a_i, a_f these reduce to:

$$\frac{da}{dt} = \frac{-a_iP_i}{P^2}\frac{dP}{dt}$$

or $$\frac{da}{dt} = \frac{-a_fP_f}{P^2}\frac{dP}{dt}$$

Unfortunately no quantitative value or ratio for 'large' a_i in terms of specimen dimensions is given. However, the value of B can be determined and C_o obtained from the compliance graph. C_o/B can therefore be calculated and compared to the crack length, a_i or a_f.

These two equations are extremely powerful for measuring static slow crack growth rates. The specimen (previously precracked) is loaded rapidly under displacement control (0,25 - 0,5 mm/min) to a load P, which is slightly less than the critical load, P_{IC}. This displacement is fixed and as the subcritical slow crack growth proceeds the load decreases (Figure 3.16).



(A) Background
(B) Vitreous carbon + background
(C) Soda-lime glass + background

Figure 3.16 Typical load relaxation graph.[143]

Values of dP/dt can be taken off a strip chart plot at various loads, P, thus the crack velocity, V = da/dt, and stress intensity, K_I, acting can be calculated over a wide range of V and K_I. Alternatively automated data acquisition and reduction systems increase the accuracy and simplify the problem.[123]

Background load relaxation must also be taken into account, there are two techniques of doing this:

(i) The background relaxation is measured at 1/2 - 3/4 P_{IC} with no specimen in the test rig, this relaxation is subtracted from the total relaxation.

(ii) The background relaxation is minimised. The load fixture is preloaded using a dummy specimen to approximately twice the anticipated peak load, P_{IC}, and held until relaxation ceases. The actual specimen is then placed in the rig and loaded incrementally, to about 90% of the load required for subcritical growth, until no relaxation is noted.[123]

(ii) Fatigue crack growth:

Differentiate w.r.t. cycles, N:

$$\frac{dy}{dN} = (Ba + C_o)\frac{dP}{dN} + (BP)\frac{da}{dN}$$

the mean and cyclic displacement amplitude are kept constant, dy/dN = 0, so that:

$$\frac{da}{dN} = \frac{-a_i P_i}{P^2}\frac{dP}{dN}$$

where for one cycle ΔP, dP and P are defined as shown in Figure 3.17 below.

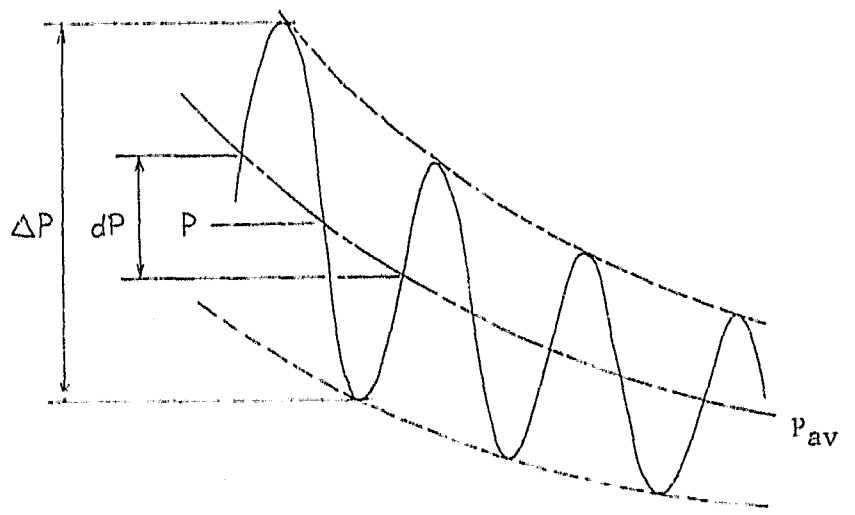


Figure 3.17

Alternatively, obtain load values at end of a cycle:

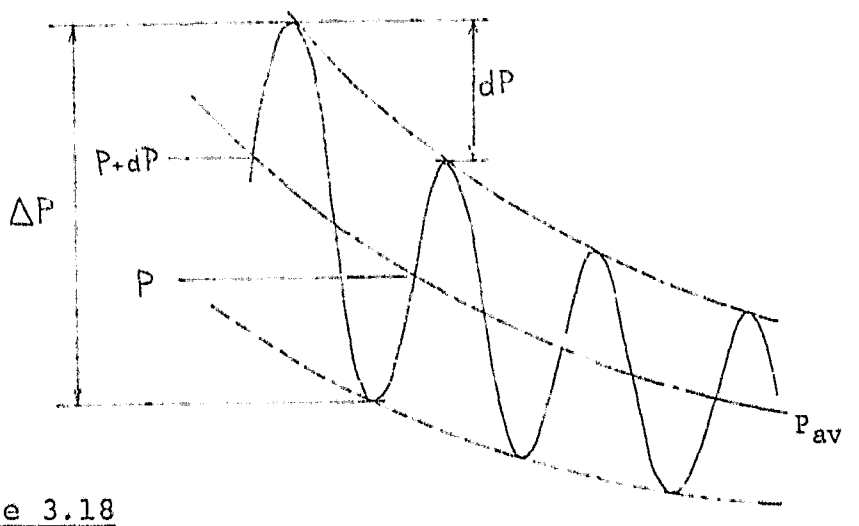


Figure 3.18

From the figure the mean load during the cycle is:

$$\frac{P + (P + dP)}{2}$$

$$\frac{[P + (P + dP)]^2}{2} = P^2 + PdP + \frac{dP^2}{4} \approx P^2 + PdP$$

$$\frac{da}{dN} = \frac{-a_i P_i}{P} \left(\frac{dP}{P + dP} \right)$$

There is one problem associated with this technique, the mean load and hence mean stress intensity is continuously decreasing. In a material where crack growth is by pure fatigue this is acceptable, $da/dN = C(\Delta K_I)^m$. However, if fatigue crack growth is assisted by static mechanisms and is mean stress intensity dependent it is not useful to plot a curve using data obtained by the load relaxation method. (Evans and Fuller[146] and Evans, Russell and Richerson[140] have derived a sophisticated technique of comparing static and fatigue crack growth rates to determine whether true fatigue occurs or if the crack growth is purely by static mechanisms operating over the cyclic stress intensity range.)

3.4.4.2 Constant Displacement Rate:

(i) Static slow crack growth:

$$\frac{dy}{dt} = (Ba + C_o)\frac{dP}{dt} + (BP)\frac{da}{dt}$$

If dy/dt is constant, i.e. constant displacement rate is applied, it is found experimentally that the crack propagates at constant load, (Figure 3.19)[127]:

$$\frac{dP}{dt} = 0$$

$$\therefore \frac{dy}{dt} = (BP)\frac{da}{dt}$$

$$\therefore \frac{da}{dt} = \frac{dy/dt}{BP}$$

This technique requires a new specimen for each da/dt value determined.

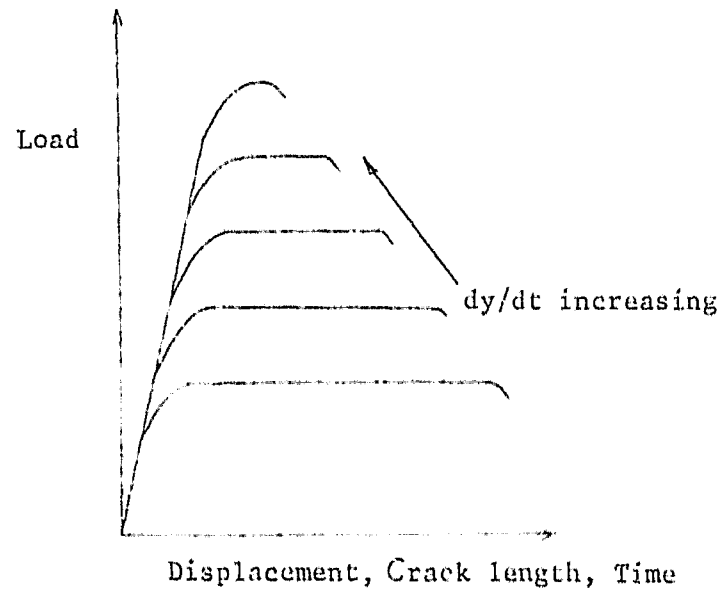


Figure 3.19

(ii) Fatigue crack growth

In materials where fatigue crack growth is mean stress intensity dependent it is possible that, with increasing mean displacement, the mean load and hence crack growth rate increases until da/dN matches dy/dN. The crack then propagates at a constant mean load, dP/dN = 0, and the following equation applies:

$$\frac{da}{dN} = \frac{dy/dN}{BP}$$

However, if fatigue is only dependent on the cyclic stress intensity, ΔK_I, it is not possible to set a predetermined cyclic and increasing mean displacement and expect a load plateau to occur. If dy/dN is too fast the mean load continuously increases and if dy/dN too slow it continuously decreases; at only one unique value is dy/dN exactly compatible with da/dN.

This method has not been used in the reported literature but despite the experimental problems that are apparent it is theoretically possible.

3.4.4.3 Constant load methods

(i) Static slow crack growth

A method almost equivalent to the constant displacement rate is to apply a constant load to the specimen and monitor the displacement continuously as a function of time.[119]

$$\frac{da}{dt} = \frac{dy/dt}{BP}$$

The value of B, as before, is calculated or obtained from the compliance - crack length relationship.

(ii) Fatigue crack growth

Load control techniques are probably the most useful for fatigue measurements as the mean and cyclic stress intensity can be accurately predetermined and once set are not affected by expansions and contractions due to temperature changes during testing. The crack growth rate must then be measured.

$$\frac{dy}{dN} = (Ba + C_o)\frac{dP}{dN} + (BP)\frac{da}{dN}$$

Using a constant mean load gives

$$dP/dN = 0$$

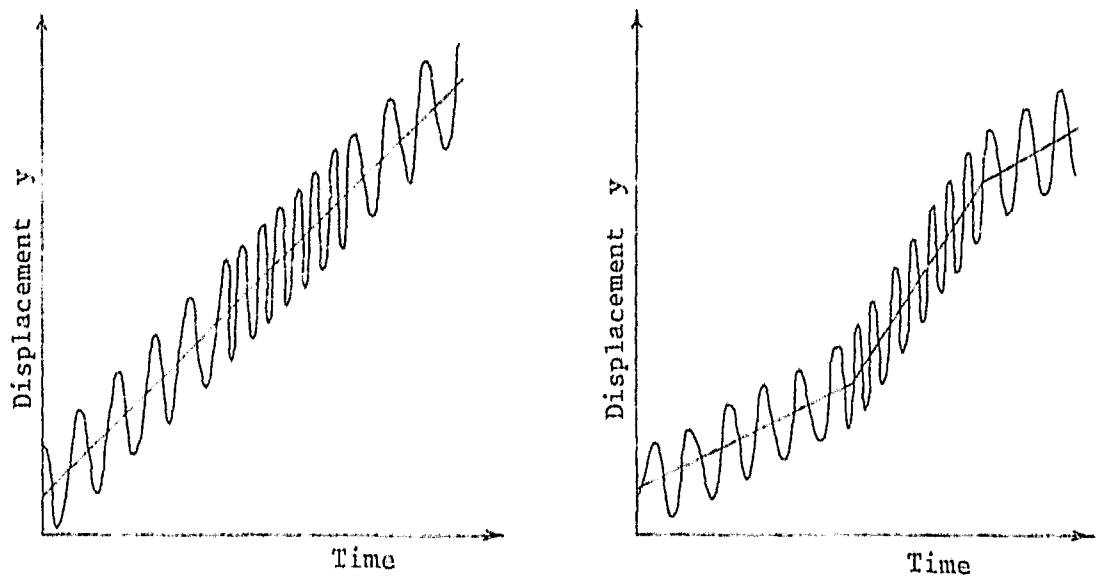
so that

$$\frac{da}{dN} = \frac{dy/dN}{BP} \qquad (P = \text{mean load})$$

dy/dN can be monitored (if necessary by measuring dy/dt and converting dy/dN since the frequency of cycling is known). Direct measurement of crack length, a, is eliminated.

The stress intensity range ΔK_I does not come into the formula but does not vary, hence crack velocity - stress intensity range graph can be determined.

Evans and Linzer[109,145] have described a very important aspect of this mode of measurement. By performing experiments at widely differing frequencies with the same ΔK_I and it is possible to identify whether true cyclic crack growth mechanisms occur. If it is found that the average displacement rate dy/dt is the same at all frequencies then the cyclic and quasi-static mechanisms must be identical, whereas if dy/dt is significantly affected by frequency a true cyclic fatigue process must exist, (Figure 3.20). (Alternatively measure da/dN if varies with frequency → quasi-static, if not → true fatigue.) The experiments should be performed over a range of ΔK_I and K_{Iav}, to examine the generality of the observations. Experiments can be performed in one specimen.



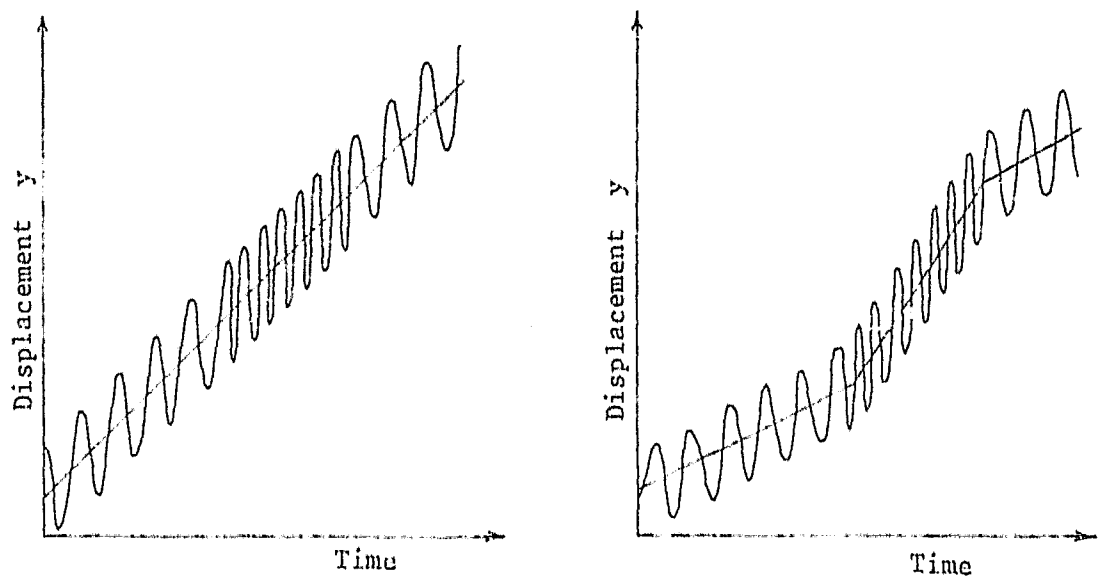
(a) quasi-static growth (b) fatigue growth

Figure 3.20

dy/dN can be monitored (if necessary by measuring dy/dt and converting dy/dN since the frequency of cycling is known). Direct measurement of crack length, a, is eliminated.

The stress intensity range ΔK_I does not come into the formula but does not vary, hence crack velocity - stress intensity range graph can be determined.

Evans and Linzer[109,145] have described a very important aspect of this mode of measurement. By performing experiments at widely differing frequencies with the same ΔK_I and it is possible to identify whether true cyclic crack growth mechanisms occur. If it is found that the average displacement rate dy/dt is the same at all frequencies then the cyclic and quasi-static mechanisms must be identical, whereas if dy/dt is significantly affected by frequency a true cyclic fatigue process must exist, (Figure 3.20). (Alternatively measure da/dN if varies with frequency → quasi-static, if not → true fatigue.) The experiments should be performed over a range of ΔK_I and K_{Iav}, to examine the generality of the observations. Experiments can be performed in one specimen.



(a) quasi-static growth (b) fatigue growth

Figure 3.20

Measurements of crack growth rate under fatigue loading can be obtained by selecting a predetermined ΔK_I and K_{Iav} for a set number of cycles, N. Direct methods (Section 3.4.2) or compliance (Section 3.4.3) are then used to measure the crack length and hence increase in length, Δa. Crack growth rate, da/dN, is then equal to $\Delta a/N$.

3.4.4.4 Displacement Rate and Constant Displacement Combination.

(i) Static slow crack growth rate.

Wiederhorn[147] has described a combination of the constant displacement rate and constant displacement techniques which totally eliminates the necessity of measuring crack length. Unfortunately, due to the problems associated with using the constant displacement rate with fatigue loading previously described, this is only suitable for static slow crack growth rate.

$$\frac{dy}{dt} = (Ba + C_o)\frac{dP}{dt} + (BP)\frac{da}{dt}$$

A constant displacement rate is used, when dy/dt matches da/dt a load plateau, P_i, occurs and dP/dt = 0. (Section 3.4.4.2).

$$\frac{da}{dt} = \frac{dy/dt}{BP}$$

and

$$\left(\frac{da}{dt}\right)_i = \frac{dy/dt}{BP_i}$$

If the displacement is then fixed while the load is at the plateau value, dy/dt = 0, the load will start decreasing as the crack propagates, so that:

$$\frac{da}{dt} = \frac{-(Ba + C_o)}{BP} \frac{dP}{dt}$$

and

$$\left(\frac{da}{dt}\right)_i = \frac{-(Ba_i + C_o)}{BP_i} \left(\frac{dP}{dt}\right)_i$$

At the instant of constant load, when the displacement is fixed constant two conditions apply:

$$\frac{da}{dt} = \frac{dy/dt}{BP}$$

and $y = (Ba_i + C_o)P_i = (Ba + C_o)P$

$$\frac{dy}{dt} = (Ba_i + C_o)\left(\frac{dP}{dt}\right)_i$$

$$(Ba + C_o) = \frac{P_i(dy/dt)}{P(dP/dt)_i}$$

$$\frac{da}{dt} = \frac{P_i(dy/dt)(dP/dt)}{BP^2(dP/dt)_i}$$

$$\frac{da}{dt} = \frac{P_i^2(da/dt)_i(dP/dt)}{P^2(dP/dt)_i}$$

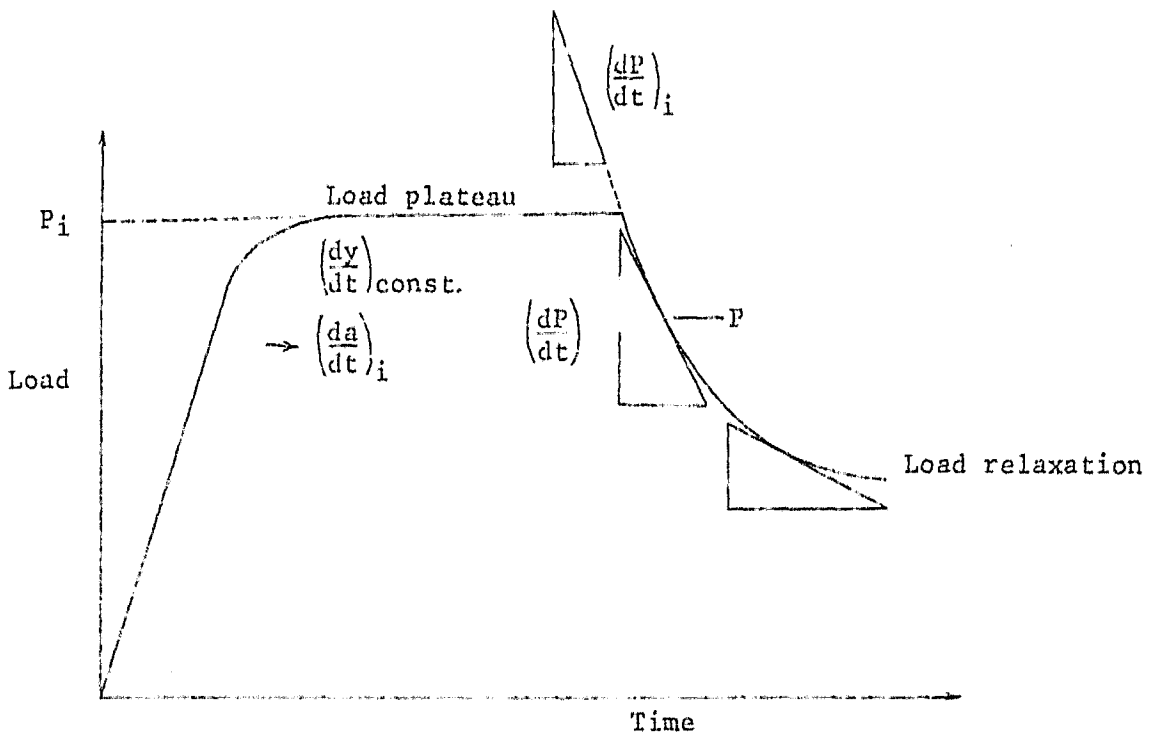

$\left(\frac{dP}{dt}\right)_i$
Load plateau
P_i
$\left(\frac{dy}{dt}\right)_{const.}$
$\rightarrow \left(\frac{da}{dt}\right)_i$
$\left(\frac{dP}{dt}\right)$
P
Load
Load relaxation
Time

Figure 3.21

3.5 SUMMARY

The double torsion test has been shown to be eminently suitable for fracture mechanics measurements in brittle materials. The stress intensity in the specimen is nominally independent of the crack length, i.e. 'constant K' geometry where:

$$K_I = PW_m\left[\frac{3}{Wd^3d_w(1-\nu)\xi}\right]^{\frac{1}{2}}$$

Several assumptions have been made in obtaining the equation above. Fuller[130] has rigorously assessed the double torsion specimen and tabulated the assumptions made and the consequences if these were to be invalid. These have all been discussed in the previous sections and are summarised in Table 3.3.

The extremely valuable compliance - crack length relationship of the double torsion geometry, $C = y/P = (Ba + C_o)$, has been used to derive the follwing equations for indirect measurement of crack growth rates.

(i) Slow crack growth rate under static load.

$$\frac{da}{dt} = \frac{-a_i P_i}{P^2}\left(\frac{dP}{dt}\right)$$ Constant displacement, measure load relaxation, dP/dt

$$\frac{da}{dt} = \frac{-a_f P_f}{P^2}\left(\frac{dP}{dt}\right)$$ As above

$$\frac{da}{dt} = \frac{dy/dt}{BP}$$ Constant displacement rate, measure load plateau, P

$$\frac{da}{dt} = \frac{dy/dt}{BP}$$ Constant load, measure displacement rate, dy/dt

$$\frac{da}{dt} = \frac{P_i^2 (da/dt)_i (dP/dt)}{P^2 (dP/dt)_i}$$

Constant displacement rate, followed by constant displacement, measure load plateau, P, and load relaxation, dP/dt.

(ii) Fatigue crack growth rate under cyclic load

$$\frac{da}{dN} = \frac{-a_i P_i}{P^2}\left(\frac{dP}{dN}\right)$$

Constant displacement, measure load relaxation, dP/dN

$$\frac{da}{dt} = \frac{-a_i P_i}{P}\left(\frac{dP}{P + dP}\right)$$

As above

$$\frac{da}{dN} = \frac{dy/dN}{BP}$$

Constant mean and cyclic load, measure increasing displacement rate, dy/dN

Alternatively crack growth rates can be measured directly using optical monitoring of the position of the crack tip.

Table 3.3

ASSUMPTIONS IN THE STRESS INTENSITY FACTOR ANALYSIS AND ANALYTICAL COMPLIANCE CALIBRATION FOR THE DOUBLE TORSION SPECIMEN AND POSSIBLE CONSEQUENCE OF THEIR INVALIDITY [130]

Section	Assumption	Consequence of Invalidity
3.3.6	Crack profile independent of crack length $(dA/da)_P = d_w$	Stress intensity factor depends on crack length
3.3.1	Mode I failure	Only G_I is given from analysis, K_I undetermined
3.3.2	Crack profile straight through the thickness	Unknown
3.4.1	Torsional deformation only	Unknown
3.3.1	Independent torsion beams with negligible contact stresses	Influence stress intensity factor determination
3.4.3	Specified distribution of applied shear stresses on loaded end of specimen	Unimportant for 'sufficiently long' crack lengths (Saint Venant's principle)
3.3.4	Specified applied forces and torques on end of specimen	Deviation of crack from centre of specimen
3.4.3	No deflections beyond crack tip	Unimportant to K_I calibration for 'sufficiently long' ligament lengths Unimportant to compliance calibration and crack propagation data for long crack lengths ($a \gg C_o/B$)
3.3.4	No side grooves	Additional stress concentrations that may influence stress intensity factor

4 EXPERIMENTAL DETAILS

4.1 INTRODUCTION

The selection of the double torsion technique in preference to other available fracture mechanics test configurations has already been fully discussed and appropriately justified in the literature survey, (Chapter 3). This present section describes, together with some of the less successful attempts, the methods used to obtain fatigue and static crack propagation data.

4.2 MATERIAL PROPERTIES

Hardmetal alloys, over a range of compositions and grain sizes, were supplied by Boart International.

The alloy designations with their respective microstructural parameters and hardness values are listed in Table 4.1. The mean linear intercept particle size, $\bar{d}$, has been measured directly from the micrographs (Appendix 2). It is assumed that contiguity is a function of the volume fraction of cobalt, as discussed in Section 2.7.3. The volume fraction was calcualted using the density of the two components and assuming the nominal weight fraction to be correct. The equations quoted in Section 2.7.1 were used to calculate both the nominal and true mean free path. The nominal mean free path assumes each carbide grain is surrounded by a binder layer. The true mean free path however recognises that cobalt free WC-WC boundaries exist in the microstructure and the equation includes a contiguity factor to account for this, both values have been tabulated.

Free carbon was present in the S10, G6, G10 (only small amounts), G15 and 25E grades, i.e. only the S6 did

not contain free carbon. Only one sample of each alloy was polished and etched for microstructural measurements, and although the S10 grade appeared not to contain free carbon a micrograph of the fatigue fracture path in another specimen of this grade proved that some samples did in fact contain free carbon. Without tediously checking every sample it was not possible to estimate the quality of alloy produced for testing. However, some of the scatter in the results may well be attributed to poor microstructural control during manufacture.

Some of the samples supplied were not tested due to the presence of large defects and obvious microstructural variations evident on the surface, (Appendix 3). The quality of production of these samples puts some doubt on the microstructural homogeneity of the rest of the specimens.

Table 4.1

DETAILS OF ALLOYS TESTED

Alloy: Boart grade designation	Cobalt content wt%	Cobalt vol. fraction f_{Co}	WC grain size nominal	WC ($\bar{d}$) measured [μm]	Contiguity	Nominal mean free path [μm]	True mean free path [μm]	Hardness VPN [kg mm^{-2}]
S6	6	0,101	fine	1,0	0,50	0,093	0,186	1541
S10	10	0,164	fine	1,1	0,36	0,216	0,338	1337
G6	6	0,101	coarse	2,9	0,50	0,327	0,654	1377
G10	10	0,164	coarse	3,1	0,36	0,608	0,950	1215
G15	15	0,227	coarse	3,5	0,25	1,090	1,453	1043
25B	25	0,370	coarse	3,2	0,13	1,882	2,163	798

Nominal mean free path: $\lambda_{nom} = \frac{f_{Co}\,\bar{d}}{(1-f_{Co})}$

True mean free path : $\lambda_{true} = \frac{f_{Co}\,\bar{d}}{(1-f_{Co})(1-C)}$

4.3 DOUBLE TORSION SPECIMEN

4.3.1 Geometry

A wide variety of double torsion shapes and sizes have been used in the past (Section 3.3.2). The specimen geometry used in the early stages of this investigation had dimensions 204 x 76,5 x 15,5 mm and contained trapezoidal grooves top and bottom, (Figure 4.1). The grooves caused a stress concentration effect and the crack very quickly moved into the sharp corner, and invariably continued to deviate from the centre line, (Figure 4.2). It was extremely difficult to observe the position of the crack tip, especially when it was moving up the wall of the groove. In addition, as the crack enters increasingly thicker material the stress intensity, for a set load, decreases. The effect of grooves on the stress intensity calculation has not been determined in any of the literature reviewed. The errors in stress intensity evaluation and crack length measurement imply a questionable validity for the fatigue crack propagation data from these early specimens. Somewhat surprisingly, however, the results obtained were not substantially different to those obtained from later specimens.

An extensive test programme using perspex, an approximately elastic-brittle and relatively cheap material, showed that, provided alignment was correct, centre line cracking could be achieved in double torsion specimens without the use of grooves. This is obviously a most desirable situation as the unknown effect of stress concentration and the problem of varying thickness, if the crack does deviate are at once eliminated.

Recommendations by Pletka et al.[123] and Evans[129] are that the specimen thickness should be in the range 1/12 - 1/8 of the width, considerably thinner than the original size tested.

The final geometry selected had no grooves and external dimensions, 200 x 75 x 6 mm. However, these dimensions varied by approximately 5 - 10% depending on the alloy composition, shrinkage and quality control in production. (This meant that every specimen had to be measured in order to calculate accurately the stress intensity.) Using an alignment procedure, described later, (Section 4.4.2), it was possible to achieve almost perfect centre line fracture, (Figure 4.3).

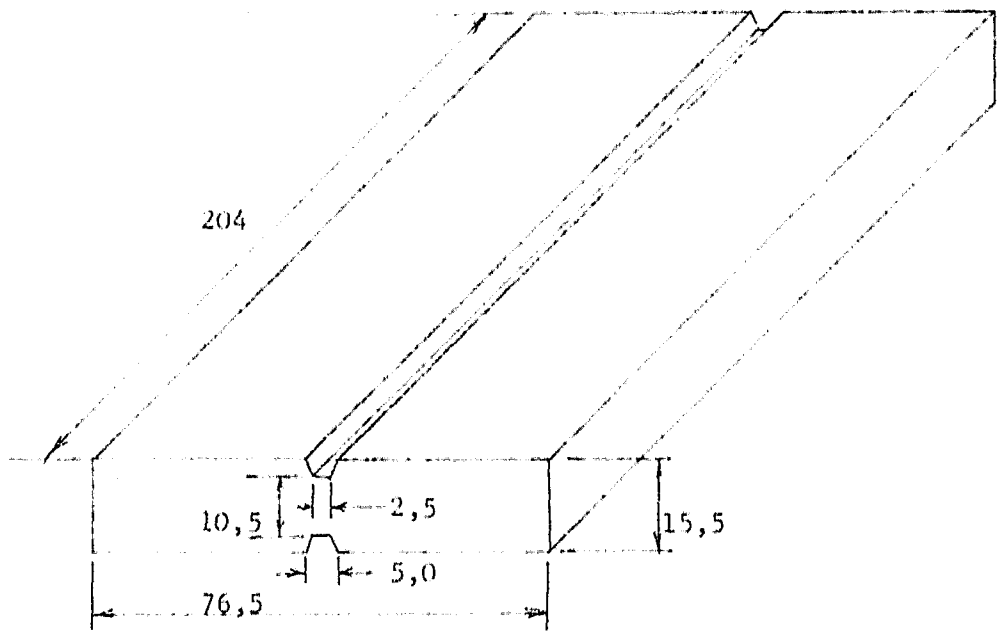


Figure 4.1 Dimensions of original test specimens

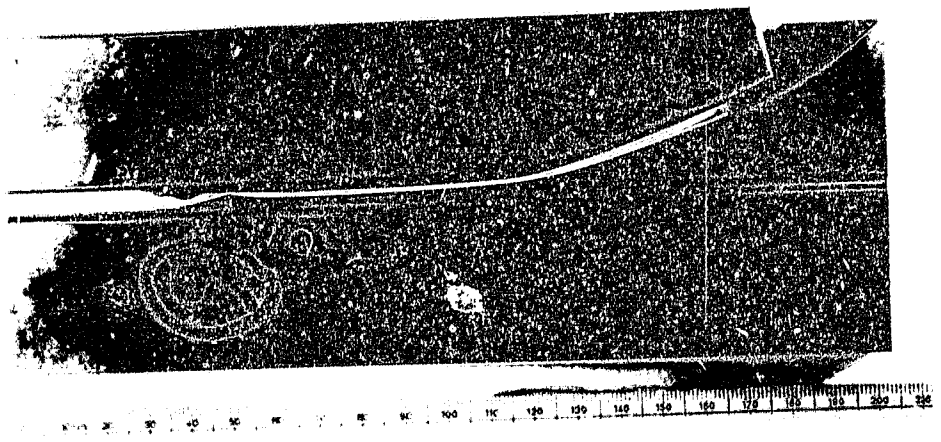


Figure 4.2 Typical deviation of crack from centre line.

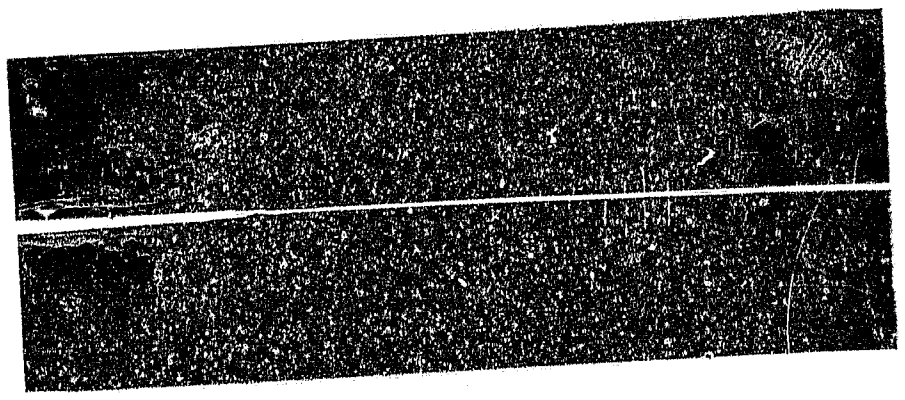


Figure 4.3 Centre line fracture in specimen without grooves

4.3.2 Notch Preparation

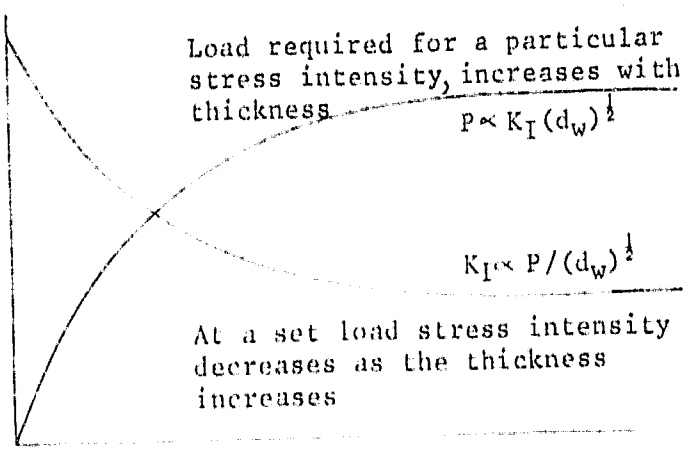
The double torsion specimen has a tapered starter notch from which the fatigue crack is initiated. The sole purpose for this shape is that the crack can be initiated at applied loads well below those required for propagation in he full thickness of the plate. The stress intensity is inversely proportional to the square root of the thickness, $K_I \propto (d_w)^{-\frac{1}{2}}$, so that as the crack enters increasingly thick material the stress intensity decreases, and uncontrolled fracture is therefore prevented. (Figure 4.4).

The notch was cut into the hardmetal plates using spark erosion (also called electron discharge machining, EDM) with a continuously moving electrode, on an Ekomix DC 310 machine, (courtesy of the de Beers Research Laboratories). The double torsion plate was set up in a jig to give a taper of approximately 20° - 25°. Spark erosion did not give a very sharp notch and an Isomet 11 - 1180 Low Speed Saw with a diamond wafering blade thickness 0,34 mm (Buehler Ltd No 11-4244) was used to complete the notching to a smaller radius. It was important to ensure that the notch was exactly central in the specimen. (Engineers blue or a marker pen and a scribe are recommended).

It was evident that in some cases spark erosion actually cracked the material ahead of the notch tip. Normally the crack had to be started by fatigue loading and an audible 'ping' could be heard as the crack initiated. On some occasions however a crack could be detected using dye penetrant (Section 4.5) before sufficient loading for initiation had been applied. It was likely that a damaged diamond blade used on some specimens also pre-cracked the material.



Tapered starter notch showing regions of:
(i) spark erosion machining: A
(ii) diamond blade cutting: B
(iii) fatigue fracture: C
Direction of propagation left to right, tensile stresses in top surface.



Increasing load required for crack propagation using tapered notch.

Figure 4.4

4.3.3 Crack Front Shape

The crack front shape is important in terms of correction factors to the measured crack growth rates, although there is still some controversy on this subject. (Section 3.3.6).

It has been assumed that the stress intensity calculated using the equation derived in Section 3.2.2 holds at the tensile (top) surface of the specimen. The crack growth rate can then be corrected by the sine of the angle of incidence of the crack front with that surface. The sine of the angle at any other point on the crack front corrects the growth rate at that point but for a stress intensity that is decreasing through the thickness.

Figures 4.5, 4.6 show that the angle of incidence was very close to 90^{o} and therefore, fortunately, no correction factor is required.

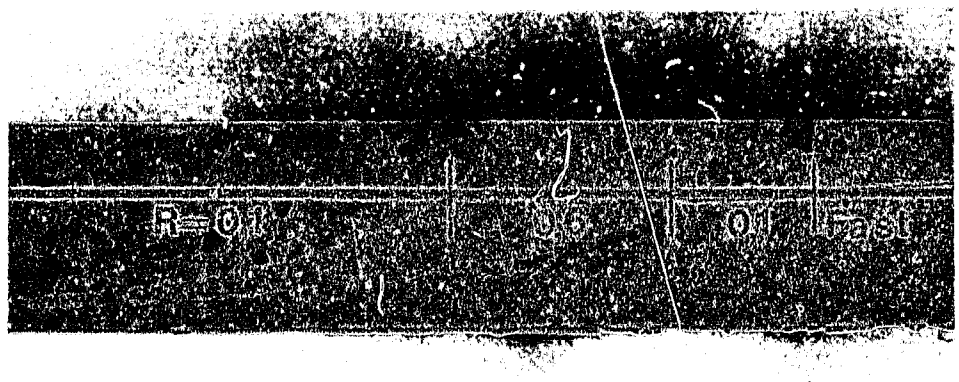


Figure 4.5 Crack front shape, in alloy 25E, successive positions revealed by zones of different R ratio fatigue loading.

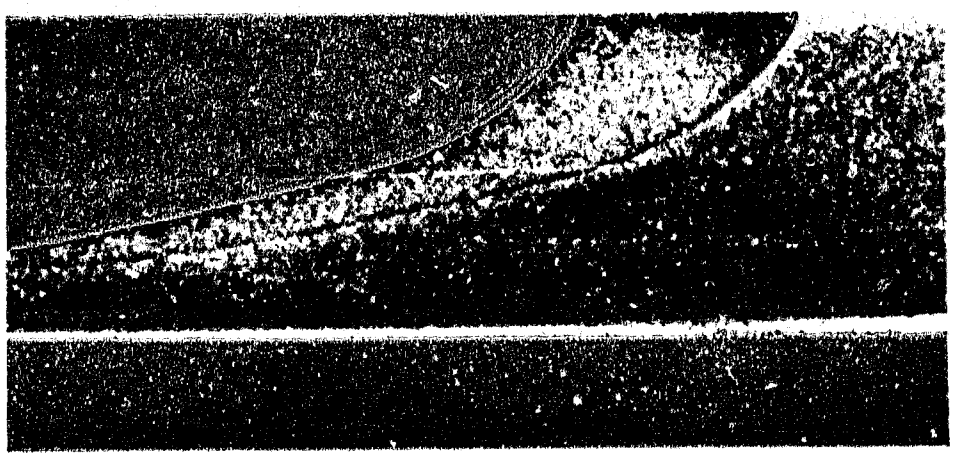


Figure 4.6 Crack front shape, in alloy S10, successive positions revealed by heat tinting.

4.4 PROCEDURE FOR OBTAINING CENTRE LINE FRACTURE

4.4.1 Loading System

The tests were carried out on a 50 kN capacity ESH Universal servo-hydraulic testing machine. (Figure 4.7).

A loading rig has been designed and built which permits easy alignment of the specimen, (Figures 4.8,4.9) (See also Appendix 4 for working drawings).

Two support 'pedestals' were fixed to a base plate which attached to the ESH machine. A platform which can be adjusted for alignment was bolted to each support pedestal. Figure 4.10 illustrates schematically the different parts of the loading rig.

Fatigue crack growth data was obtained using cyclic sinusoidal loading at a base frequency of 5 Hz.

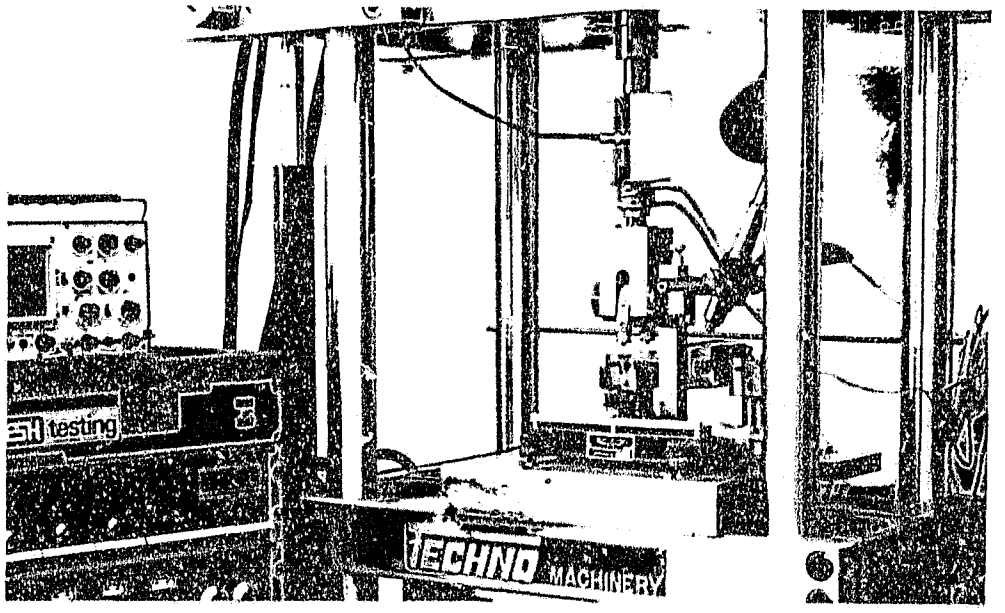


Figure 4.7 General view of test system.

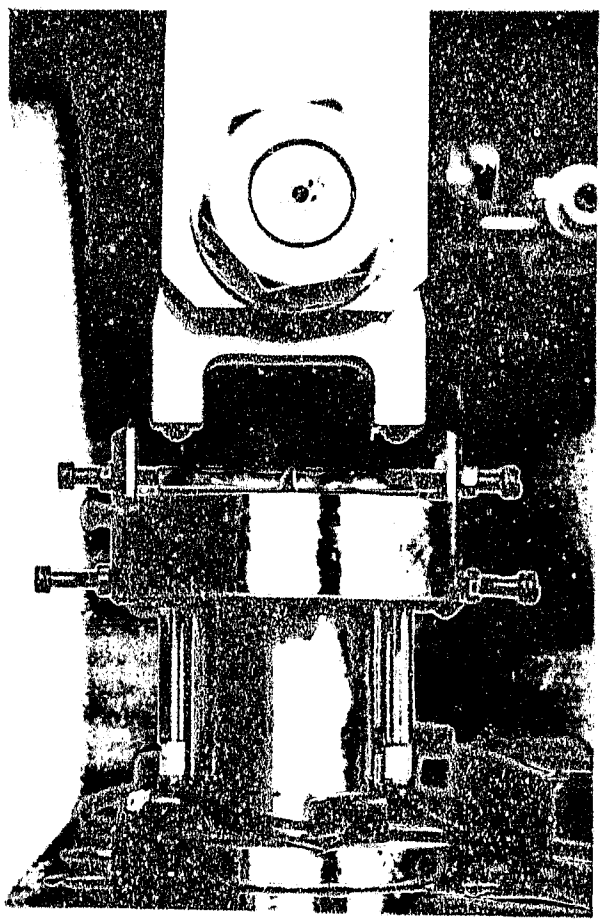


Figure 4.8

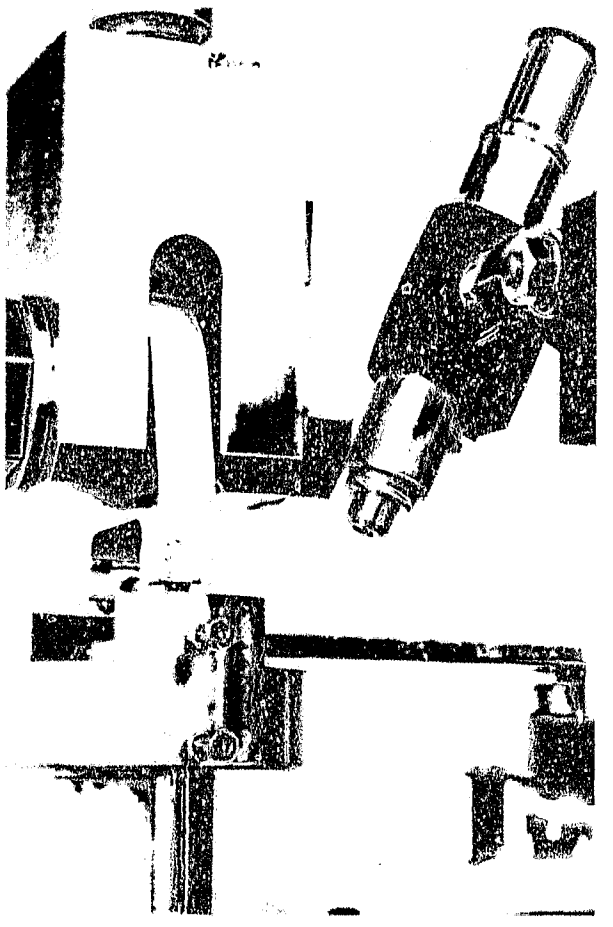


Figure 4.9

Close up views of the loading rig

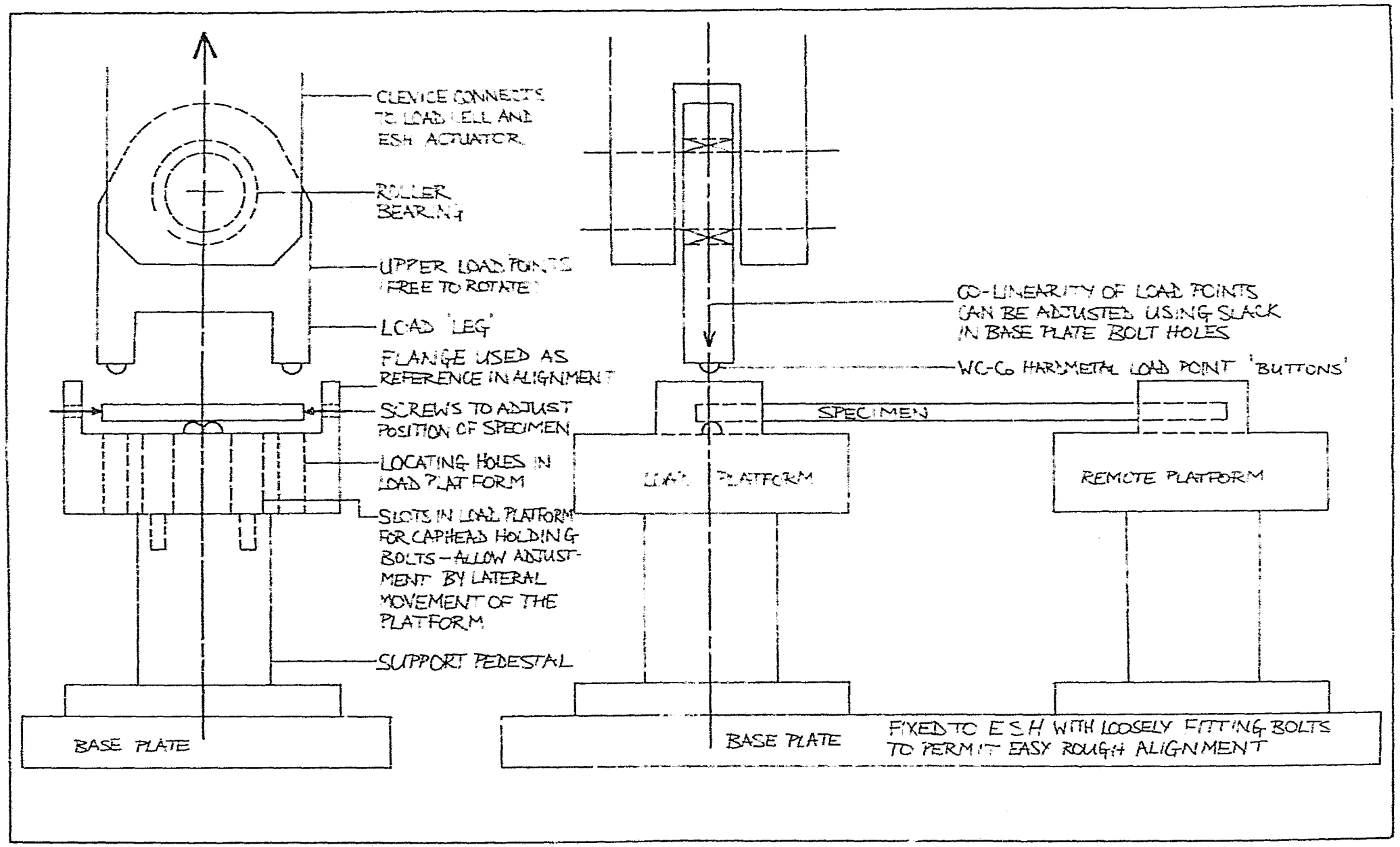


Figure 4.10 Schematic diagram of the different parts of the loading rig.

4.4.2 ALIGNMENT

It is generally accepted that alignment of the specimen and loading device are essential for obtaining centre line cracking. An imperfectly dimensioned sample or imbalanced load system will cause the crack to deviate from the midplane.[123,124,134] No reports are available, however, of allowable tolerances, degree of perfection or adjustments necessary to correct the problem.

Most of the samples supplied were slightly warped, almost inevitable in a sintered product with the dimensions specified, so it was vital to have a system to ensure fracture sufficiently close to the centre line for valid stress intensity values.

Through a comprehensive test programme firstly on perspex and then on hardmetal, it was found that fatigue crack directionality could be controlled, in the early stages of growth, by adjusting the position of the specimen with respect to the load points.

The procedure for proper alignment was therefore as follows, (refer to Figure 4.10):

(i) The base plate was set up so that it was roughly in position below the upper load points. The tungsten carbide load 'buttons' should then locate in holes drilled into the load platform. At this stage the primary objective was to ensure that the upper and lower load points were co-linear, (there was sufficient slack in the base plate bolt holes so this was normally not a problem). The base plate was then fixed in position.

(ii) Lateral movement (perpendicular to the centre line of the specimen) of the lower load platform has been designed into the system, so that centrality of the lower load points could be adjusted without affecting their co-linear

setting. These lower load points had to be located exactly central with respect to the upper whose position is fixed through the clevice, load cell, and actuator. Once again the locating holes were used. The cap-head holding bolts were loosened using Allen keys cut off to fit in the bolts with the upper load points in the locating holes. With the machine in 'stroke control' a cyclic displacement at approximately 5 Hz was applied and the mean position and cyclic amplitude adjusted so that a small (compressive) load of approximately 0,5 kN was reached, at the maximum displacement, when the base of the load legs contacted the surface of the load platform. The load platform could then be positioned so that the upper load points seated cleanly in the locating holes,without 'wobble' in the load train. Wobble could be observed by lateral displacement of the clevice and uneven displacement of the bases of the steel load legs, with respect to the load platform surface, as the carbide buttons located in their respective holes. When the alignment was estimated to be correct a small static load, was applied with the machine still in stroke control and the caphead bolts tightened, with the load maintained, until the platform was firmly fixed.

(iii) The remote platform was then aligned with the load platform. The flanges on the platforms and a straight edge were sufficient to carry out this simple final step.

(iv) The specimen was then positioned using vernier calipers and the locating screws in the flanges. All that had to be done was to shift the specimen until the gap between it and the flange was identical on both sides.

(v) The remote end of the specimen could be held in position, to prevent it 'walking', by lightly clamping it with the locating screws. Fatigue crack growth rates were not affected by doing this.

4.4.3 Precracking

In the early stages of fatigue cracking, particularly where the crack was still in the tapered notch region, it was possible to control the direction of propagation, by small adjustments in the alignment of the specimen.

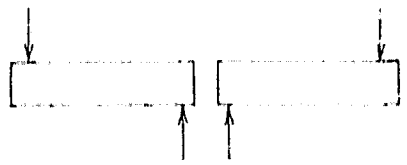
A travelling microscope with the vertical cross hair set exactly parallel to the centre line of the specimen was used to monitor the directionality of the fracture. (The horizontal cross hair was accurately set against an engineer's square held on the long edge of the specimen).

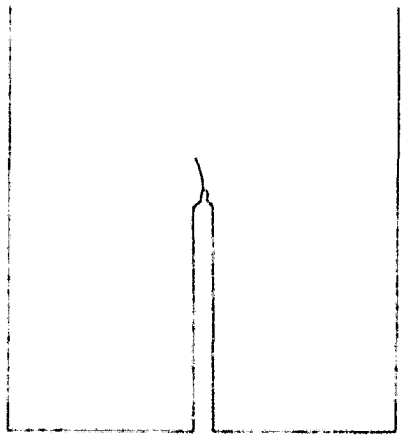
A fatigue load was applied (using load control) and the mean level and amplitude gradually increased until a crack was observed. If it did not initiate straight (w.r.t the vertical cross hair) the specimen could be moved using the locating screws (Figure 4.8) to adjust the direction of propagation. This could be done while the fatigue load was being applied if the minimum load was small, (approximately 0,2 kN).

It was found that by continuous observation and adjustment the required centrality could be obtained.

As represented diagramatically in Figure 4.11, if the crack deviated to the left of the centre (left for an observer looking in the direction of propagation) a shift of the notched end of the specimen to the right produced a direction change to the right.

It was apparent however that once the crack had extended a certain amount it could no longer be influenced by alignment and if straight would remain straight but if off line would continue in that direction.

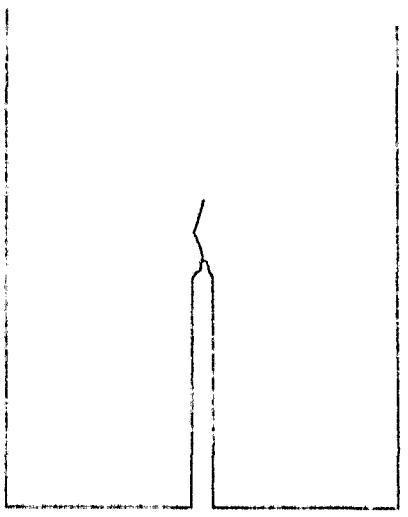




If original set up causes crack to initiate off-line, the loaded end of the specimen should be shifted in the direction the crack must move.

i.e.:





In this example the specimen is moved to the right and the crack bends right.
It may be necessary to make several adjustments as illustrated in the photograph, 4 changes in direction can be seen.

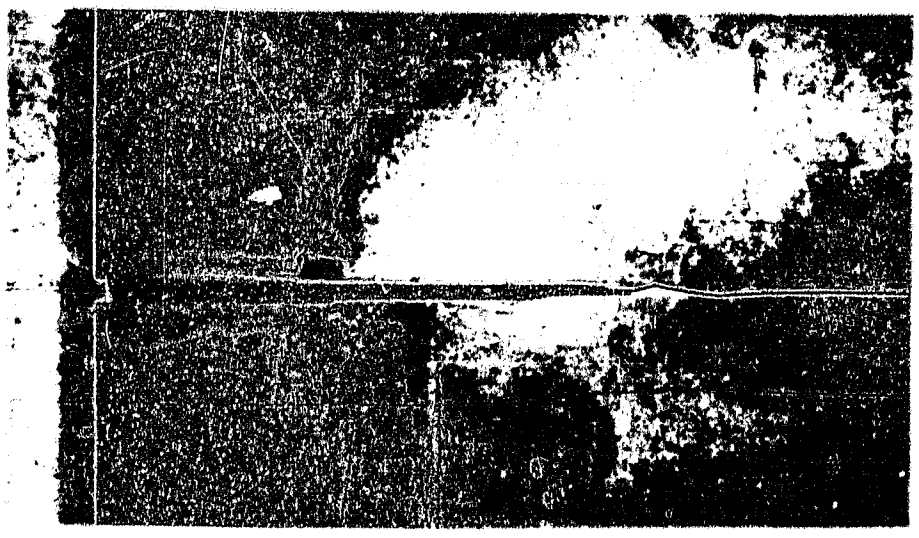


Figure 4.11 Procedure used to obtain central fracture by alignment adjustments.

4.5 CRACK LENGTH MEASUREMENT

4.5.1 General Background

The accurate measurement of the position of the crack tip was vital for determining crack growth data, particularly as the ability to measure small increments in crack length saved time and material. It being more efficient and economic to measure 0,10 mm in 5000 cycles than 1,0 mm in 50000 cycles, for the same precision.

There were essentially only two options available for measuring crack length: either by direct observation using an optical microscope or by the indirect compliance method.

It was recognised that some form of direct observation would be necessary, even if the compliance method was finally selected, as a compliance - crack length calibration would be required. An optical microscope was therefore used early on in the programme. It was found that it was impossible to detect the exact position of the crack tip without using a dye penetrant technique.

Subsequent efforts to measure crack length using compliance were unsuccessful, primarily because the technique was too insensitive to detect the small changes in crack length necessary for measuring crack growth rates in the 10^{-8} m/cycle range in a reasonable time.

Methods have been described in Chapter 3 whereby crack growth rates can be determined indirectly by monitoring, for example, load relaxation (Section 3.4.4.1) or, the rate of change in compliance, evidenced by the increasing displacement as the crack grows (Section 3.4.4.3). Efforts to use these techniques, as described in Section 4.5.2 and 4.5.3, were also completely unsuccessful.

For these reasons the dye penetrant technique, by which the position of the crack tip could be measured to 0,01 mm precision was selected early in the

investigation. The dye used was 'Magnaflux Spotcheck, Penetrant SKL-HF', it is essentially sulphur and halogen free the dyes and solvents being based primarily on large aliphatic and aromatic hydrocarbons. The exact details are not available from the manufacturers but it meets the following specifications:

(i) ASME Section 5, Article 6 Paragraph T630
(ii) Navships 250-1500
(iii) BS DTD 929

These specifications require that the penetrant does not cause any stress corrosion or fatigue corrosion effects.

The position of the crack tip was easily identified by smearing a thin layer of dye on the surface of the specimen and then applying a fatigue load. As the crack opens and closes under the cyclic load the dye could be seen 'pulsing'. It was not possible to see the crack under static load.

At the end of a test, whether monotonic or fatigue loading, the cyclic amplitude and mean level were reduced so that the crack did not grow while the position of the tip was being determined. Usually it took about 200 cycles to position the cross hairs exactly on the tip.

4.5.2 Fatigue Crack Growth Rate Measurement

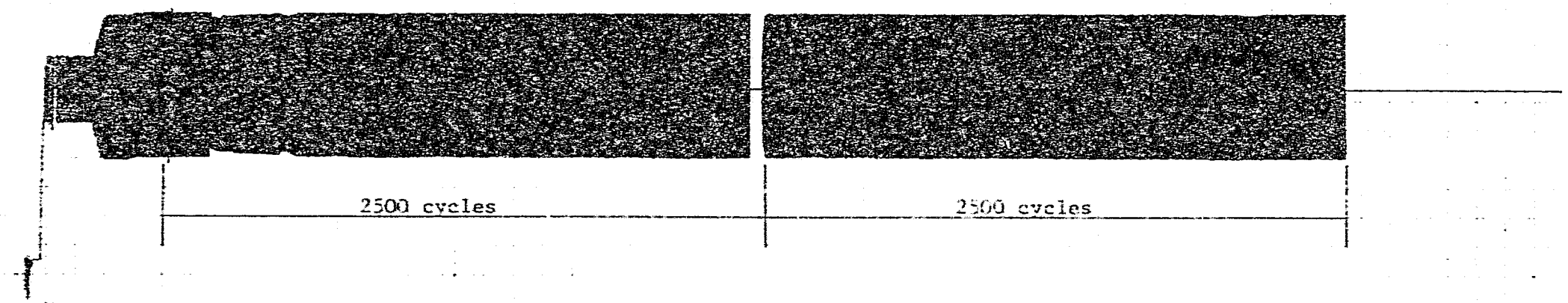
Before fatigue growth rates could be measured the crack had to be grown beyond the influence of the tapered notch. The experiments showed that once the crack tip was ~18 mm from the notch the growth rate stabilised and da/dN measurements could be taken. During preliminary studies, growth rate data were obtained by taking several readings at the same load range, plotting crack length, a, versus number of cycles, N, and determining the gradient, da/dN. This method is tedious and time

consuming so in later tests a load range was selected and the cycle counter set for a suitable number of cycles, depending on the growth rate. The increment in crack length was then measured when the pre-selected number of cycles had been completed thus eliminating the need for continuous monitoring.

The method of plotting crack length vs number of cycles, a vs N, however, proved extremely useful for investigating the effects of frequency and temperature changes on growth rate. The influence on growth rate being revealed by a change in the slope of the a vs N graph at the point of 'change over' to different conditions, frequency or temperature. An attempt was made to obtain fatigue data using the increasing compliance of the specimen as the crack grows. Under load control, an appropriate amplitude and mean level were selected, linear variable differential transducers (LVDT's) were used to measure the increasing deflection of the specimen (at the load points) as the crack grows. The LVDT's used were sensitive to 0,5 μm (5×10^{-7}m).

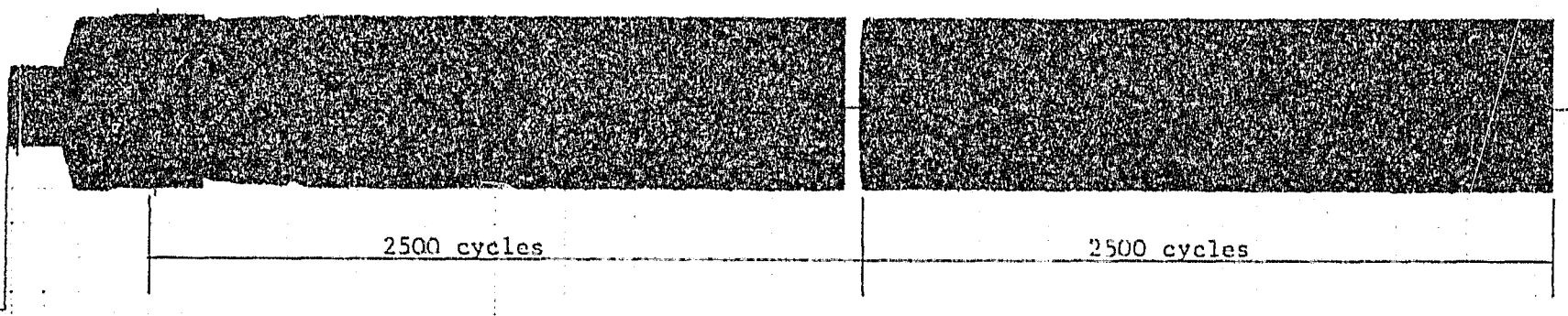
A chart recorder was used to monitor dy/dN but the increase in deflection was so small that it was impossible to obtain reasonable results. Calculations made using the best reasonable da/dN values from the plot gave results approximately 2 orders of magnitude different from the growth rates determined by direct observation, (Appendix 5). The primary reason for this discrepancy is thought to be the very high stiffness of WC-Co hardmetal alloy. The compliance values of between 2×10^{-8} and 50×10^{-8} mN^{-1} (Appendix 5) are approximately 10^2 smaller than those reported by other researchers for different materials. (Section 3.4.3), and consequently the increase in deflection with crack length was negligible.

A typical result is shown in Figure 4.12: despite a crack growth rate of $5,22 \times 10^{-7}$ m/cycle and an increment in the crack length of 2,61 mm there was no measurable increase in the mean displacement.



Alloy S10: WC-10Co fine grained.
Loading: ΔK_I = 7,618 $MNm^{-3/2}$, R = 0,056, Frequency = 5 Hz.
Crack growth: 2,61 mm in 5000 cycles, da/dN = 5,22 x 10^{-7} m/cycle.

Figure 4.12



Alloy S10: WC-10Co fine grained.
Loading: ΔK_I = 7,618 MNm$^{-3/2}$; R = 0,056, Frequency = 5 Hz.
Crack growth: 2,61 mm in 5000 cycles, da/dN = 5,22 x 10^{-7} m/cycle.

Figure 4.12

4.5.3 Static Crack Growth Data

Crack growth rates under static monotonic loading were measured for two grades of hardmetal alloy. Osterstock[103] has performed this type of work using the double cantilever beam technique. His results show that static crack growth only operates at stress intensities close to the fracture toughness, i.e. $K_I > 0,9\ K_{IC}$.

It was therefore necessary to use a test procedure that would prevent accidental catastrophic fast fracture of the specimen.

As described in Section 4.5.1 the exact position of the crack tip could only be detected using a fatigue load in combination with the dye penetrant. A small cyclic load amplitude (0,3 - 0,5 kN) was therefore superimposed on the mean load which was gradually increased until a growth rate of between 10^{-7} and 10^{-6} m/cycle was observed. The cyclic component was then taken out and the mean static load used to obtain the static crack growth rate. After a certain length of time, not cycles, the position of the tip was determined by decreasing the mean load to below fatigue crack propagation levels and applying a cyclic amplitude of 0,5 - 1 kN.

Load relaxation, under displacement control, which has been reported to be very successful by various authors[103,154] was attempted but failed to produce any meaningful results, even though a computer and chart recorder were used to monitor the decreasing load. (Appendix 5). Load relaxation was very limited due to the fact that crack growth stops as soon as the load has dropped below $\sim 0,9K_{IC}$. The background relaxation of the load system also contributes to the load decreasing; values were therefore unreliable and data limited. This method was abandoned because of the danger in breaking and wasting specimens.

4.6 DOUBLE TORSION AND FRACTURE IN A SCANNING ELECTRON MICROSCOPE

The constant stress intensity characteristic of the double torsion configuration has been exploited to study fracture, in situ, in a scanning electron microscope.

The technique was developed by Tait[155,156] for studying the fracture of cement mortar, it has been successfully adapted for testing WC-Co hardmetal.

The restricted space in the scanning electron microscope and size limitations previously designed into the loading rig dictated that small specimens, with dimensions 30 x 11 x 0,7 mm had to be used for this investigation. These specimens were grooved in the compression surface, primarily to reduce the loads required for static fracture, and notched using an Isomet 11-1180 Low Speed Saw with a 0,34 mm diamond wafering blade (Figure 4.13). It was apparent, incidentally, that in this case the fracture was directionally stabilised by the groove. The tension surface was polished, etched and gold coated. The etchant used a 1 to 1 mixture of $K_3Fe(CN)_6$ 10 wt% in water, and K(OH), also 10 wt% in water.

The loading rig, (Figure 4,14), has been modified from a Cambridge Instruments three-point bend test device. The load was applied to the specimen in the evacuated chamber via conventional screw threads and link rods from external controls.

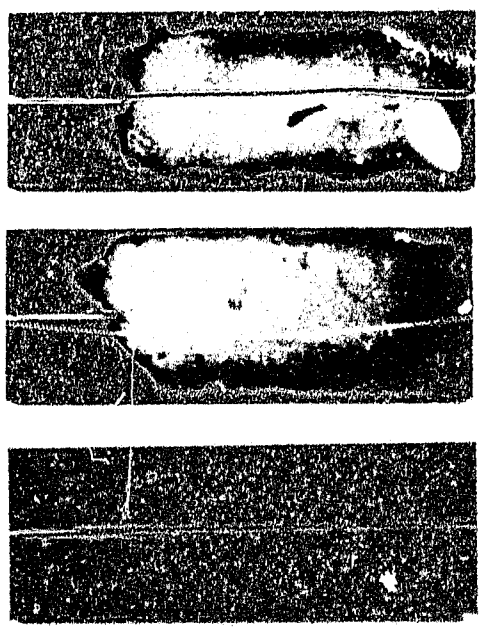
Obviously by using this method the load application was displacement controlled, and as the crack propagated the load decreased (load relaxation), and crack arrest occurred before complete failure of the sample.

The technique was used to

(i) observe the surface morphology of the fracture path;

(ii) study the effects, if any, of unloading and reloading;

(iii) investigate whether ligaments of cobalt binder spanned the crack behind the crack tip.



(a) Fractured specimen
Polished, etched and gold coated tension surface
Grooved compression surface



(b) Typical cross section showing very low angle taper used in these specimens

Figure 4.13 Details of specimens used in scanning electron microscope

1 Locking nuts
2 Loading plate
3 Plate pivot
4 Upper load points
5 Double torsion specimen
6 Lower load points
7 Retracting load system
8 Block mounting to SEM goniometer stage
9 Locating pin

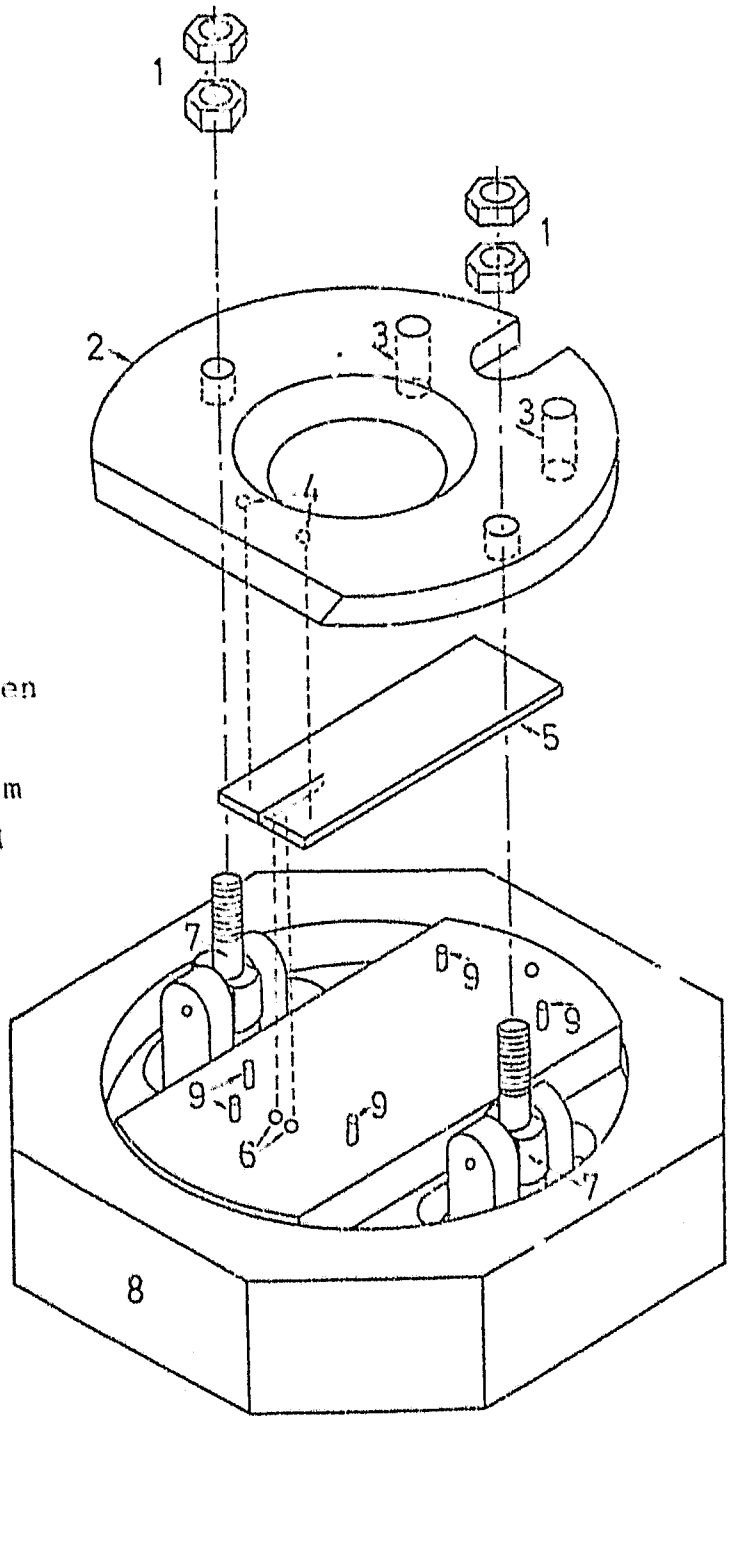


Figure 4.14 In situ SEM double torsion loading system

4.7 ELEVATED TEMPERATURE INVESTIGATION

The first objectives of this project were to establish a characterisation of the fatigue behaviour of selected hardmetal alloy grades at room temperature. This was obviously the necessary base for obtaining an understanding of the mechanisms that lead to fatigue crack propagation and failure in this material.

However, many hardmetal alloy components are used in service at elevated temperatures and data are therefore required to determine the influence of temperature on fatigue crack growth and hence life.

Using a simple heating element surrounding the double torsion specimen some preliminary observations were made on the effect of thermal cycling and elevated temperature fatigue.

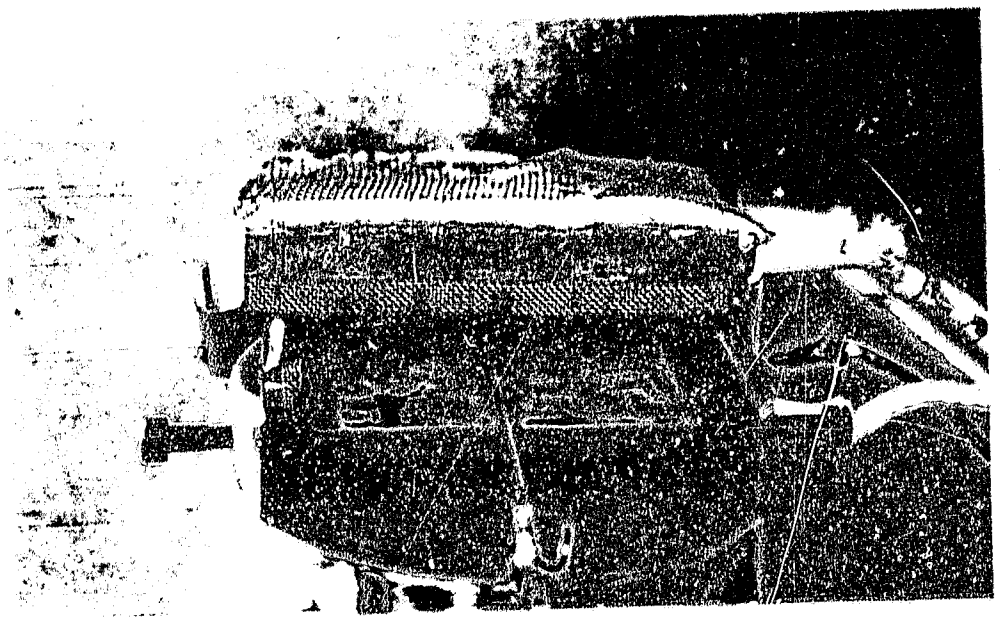
The heating unit consisted of two coil elements housed in ceramic insulators designed for this type of application (supplied by Heating Elements (Pty) Ltd., Johannesburg, SA). These were built into a stainless steel (AISI 316) box, (Figure 4.15), which fitted over the specimen and heated it approximately evenly from top and bottom. (A mild steel box originally supplied deteriorated rapidly in service due to oxidation at the elevated temperatures.) The specimen obviously acted as a heat sink and temperature decreased from a maximum at the centre of the element. The temperature distribution was determined using several thermocouples, K type chromel-alumel, which showed that over approximately 20 mm it was reasonably constant, (Figure 4.16).

The temperature was regulated using an on/off controller and was monitored using a digital thermometer and chart recorder, (Figure 4.17).

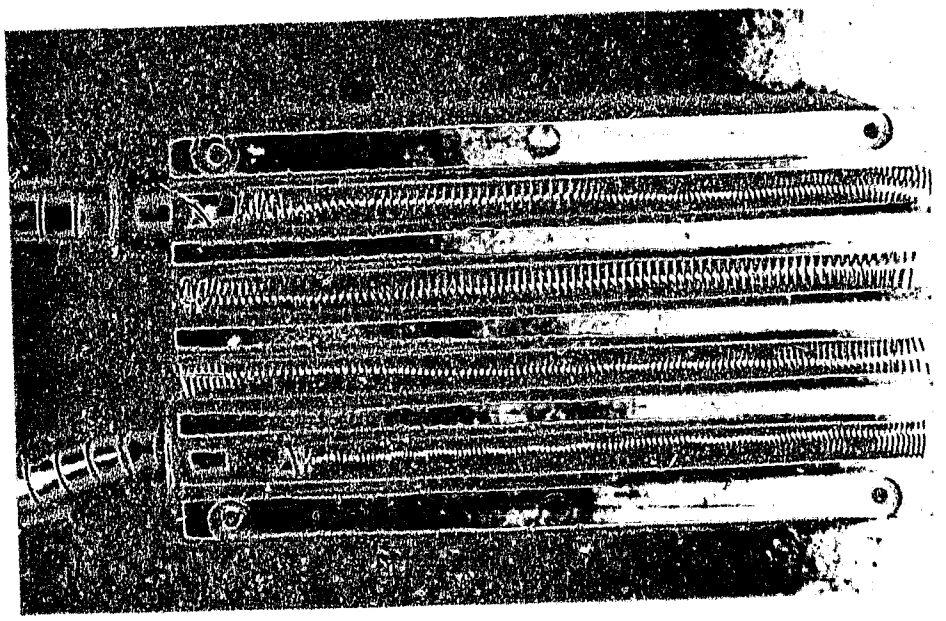
In a typical test the fatigue crack growth rate at room temperature was first measured in the normal way using the dye penetrant and travelling microscope cross hairs. The two thermocouples, connected to the

controller and thermometer, were then placed on the observed position of the crack tip. The heating element was then moved so that the crack tip was in the centre, and therefore in the region where temperature was a maximum and constant over a reasonable distance. It was then switched on and allowed to reach the required temperature. When it had stabilised fatigue loading was applied. After the selected number of cycles had been completed the element was switched off and the specimen cooled with a small fan. The new position of the crack tip was determined in the normal way once room temperature (or < 70°C) had been reached.

No attempt has been made to prevent oxidation or achieve entirely uniform heating of the specimen. These are obvious refinements for a more sophisticated study, but as a first approximation elevated temperature fatigue in a laboratory air oxidising atmosphere is probably representative of the working environment for many components.

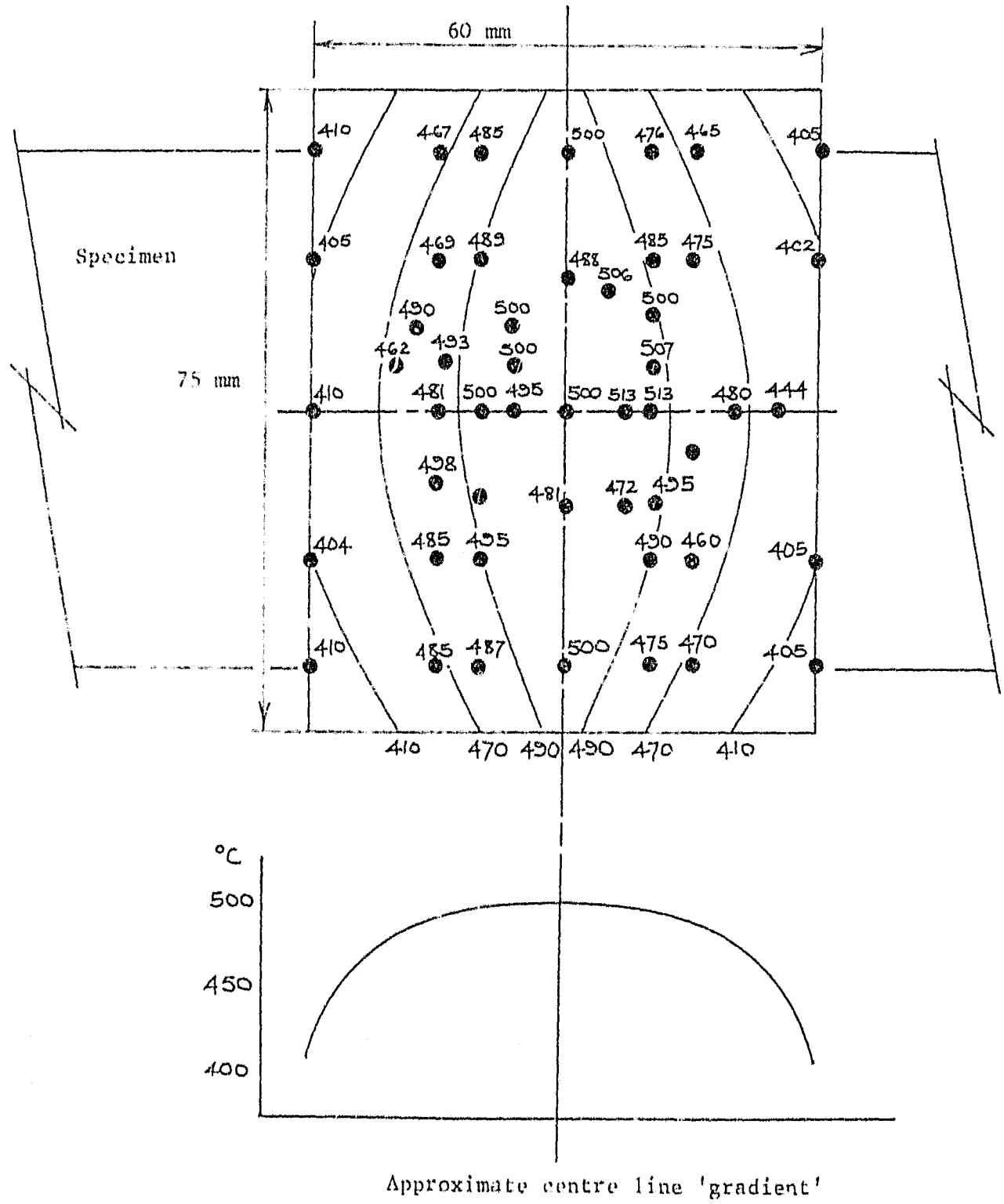


(a) Photograph showing heating unit in position around specimen.



(b) Photograph showing heating coils and ceramic insulator.

Figure 4.15



Approximate centre line 'gradient'

Figure 4.16 Details of temperature distribution in the specimen.

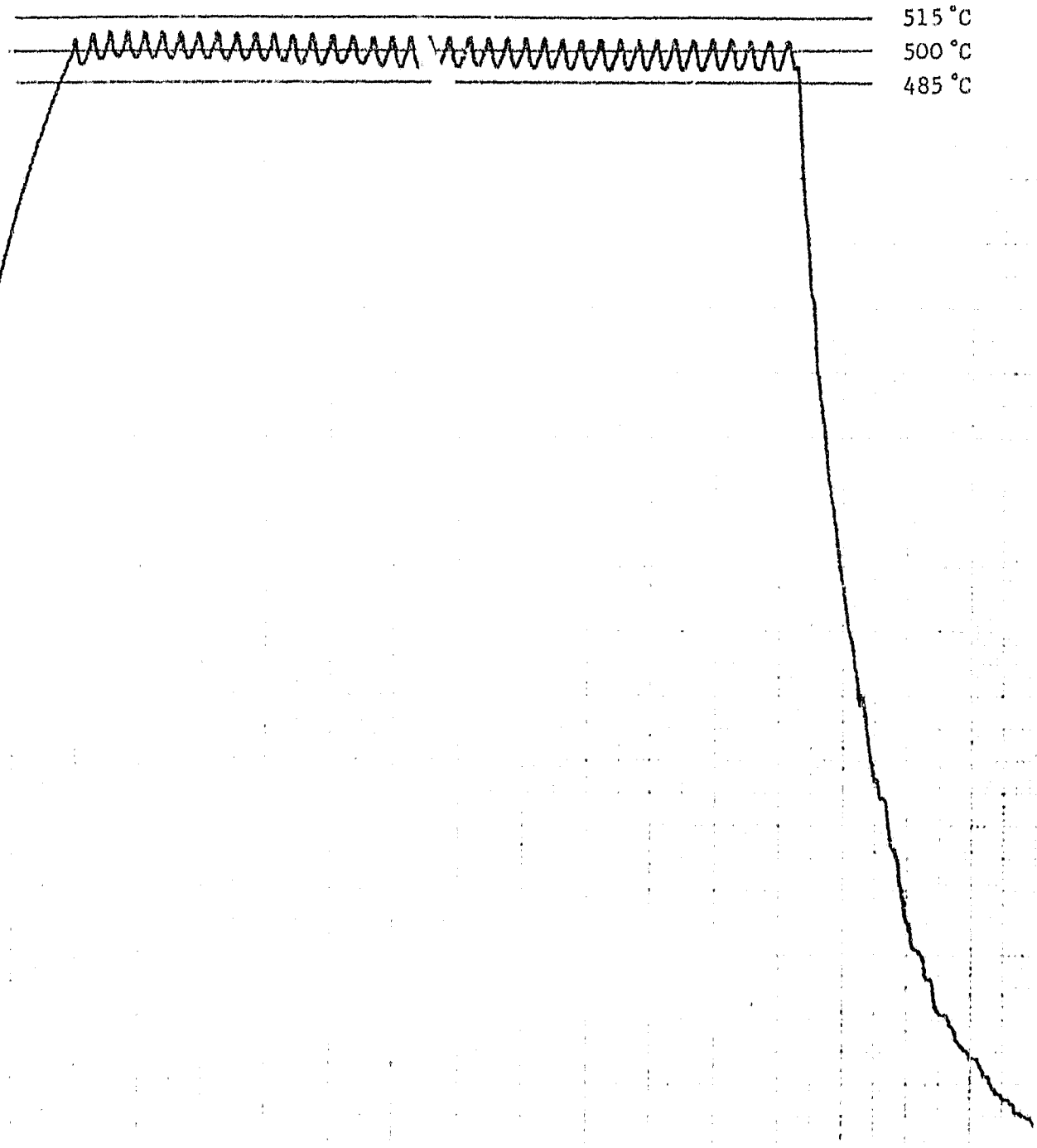


Figure 4.17 The ON-OFF controller does not maintain a constant temperature but the variation is small, ~ 15°C at 500°C.

4.8 PREPARATION OF SEM SAMPLES

Fractographic studies are a necessary and integral part of any investigation of this nature. The size of the test specimen was however too large to fit into most electron microscopes. This problem has not been reported by other researchers possibly on account of the different and smaller specimen geometries used. The required fracture area had to be cut out using either the spark erosion Ekomix unit (at de Beers Diamond Research Laboratories) or a Discotom saw with metal bonded diamond blade (at Boart Research Centre). Spark erosion was not successful, since the damage to the fracture surface as a result of sparking, thermal effects and the process liquid totally obliterated the surface features.

The diamond saw was water cooled and although some moderately successful fractography was carried out on specimens cut without protection from the water the majority suffered some surface degradation. It was therefore obvious that some form of protection had to be given to the fracture surface.

The following plastic coatings were tried but were unsuccessful because either the water seeped between the coating and the surface or the coating could not be perfectly cleaned off the surface.

Plastic	Solvent	Problem
Formvar	Chloroform	Insufficient adhesive strength
Lacomit	Benzene	Could not be perfectly removed
Lettraset 101 coating	Acetone	Insufficient adhesive strength and could not be perfectly removed
Dulux laquer	Acetone	Could not be perfectly removed

4.8 PREPARATION OF SEM SAMPLES

Fractographic studies are a necessary and integral part of any investigation of this nature. The size of the test specimen was however too large to fit into most electron microscopes. This problem has not been reported by other researchers possibly on account of the different and smaller specimen geometries used. The required fracture area had to be cut out using either the spark erosion Ekomix unit (at de Beers Diamond Research Laboratories) or a Discotom saw with metal bonded diamond blade (at Boart Research Centre). Spark erosion was not successful, since the damage to the fracture surface as a result of sparking, thermal effects and the process liquid totally obliterated the surface features.

The diamond saw was water cooled and although some moderately successful fractography was carried out on specimens cut without protection from the water the majority suffered some surface degradation. It was therefore obvious that some form of protection had to be given to the fracture surface.

The following plastic coatings were tried but were unsuccessful because either the water seeped between the coating and the surface or the coating could not be perfectly cleaned off the surface.

Plastic	Solvent	Problem
Formvar	Chloroform	Insufficient adhesive strength
Lacomit	Benzene	Could not be perfectly removed
Lettraset 101 coating	Acetone	Insufficient adhesive strength and could not be perfectly removed
Dulux laquer	Acetone	Could not be perfectly removed

Eventually a waterproof felt pen ink (Maruzen Wonder Marker, made in Japan) which could be ultrasonically removed with acetone was found to be virtually ideal, placing a thin tenacious layer on the surface which provided complete protection from water attack and left no deposit after cleaning.

The specimens were given a gold coating of ~ 20 nm to reduce charging distortion in the SEM.

It is impossible to distinguish between fatigue and fast fracture at high magnifications, although these different regions can sometimes be seen visually. (Figure 4.5). In order to establish which fracture mode was under observation an electric pencil was used to demarcate on the fracture surface the zones of fatigue at various load levels, and the fast fracture. (Figure 4.18).

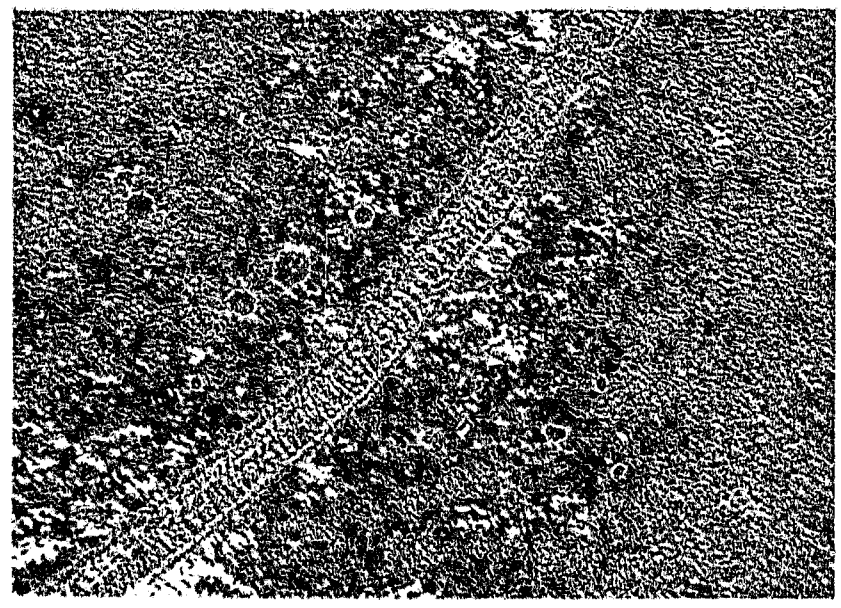


Figure 4.18 Electric pencil mark on fracture surface used to demarcate zones of different fatigue levels and fast fracture.

5 R E S U L T S

5.1 CRACK GROWTH UNDER STATIC LOADING

5.1.1 Static Load Crack Growth Rate

Static crack growth measurements have been made on two alloys, S10 and G10. The work confirms the results reported by Osterstock,[103] crack growth starts at approximately 0,9 K_{IC} and 'n' values are in the range 125 - 200 (where 'n' is described in the relation: $V = A(K_I)^n$). The technique used is described in Section 4.5.3 and the results are summarised graphically. (Figure 5.1).

It is not clearly understood how static growth occurs under monotonic loading as this type of crack propagation is normally associated with time-dependent environmental effects. The crack growth rate tests of Osterstock[103] and those carried out in the present investigation were performed in laboratory air which may constitute a sufficient environment to cause static crack growth by environmental attack at stress intensities close to K_{IC}. (In this investigation dye penetrant is also present in the crack.)

5 R E S U L T S

5.1 CRACK GROWTH UNDER STATIC LOADING

5.1.1 Static Load Crack Growth Rate

Static crack growth measurements have been made on two alloys, S10 and G10. The work confirms the results reported by Osterstock,[103] crack growth starts at approximately 0,9 K_{IC} and 'n' values are in the range 125 - 200 (where 'n' is described in the relation: $V = A(K_I)^n$). The technique used is described in Section 4.5.3 and the results are summarised graphically. (Figure 5.1).

It is not clearly understood how static growth occurs under monotonic loading as this type of crack propagation is normally associated with time-dependent environmental effects. The crack growth rate tests of Osterstock[103] and those carried out in the present investigation were performed in laboratory air which may constitute a sufficient environment to cause static crack growth by environmental attack at stress intensities close to K_{IC}. (In this investigation dye penetrant is also present in the crack.)

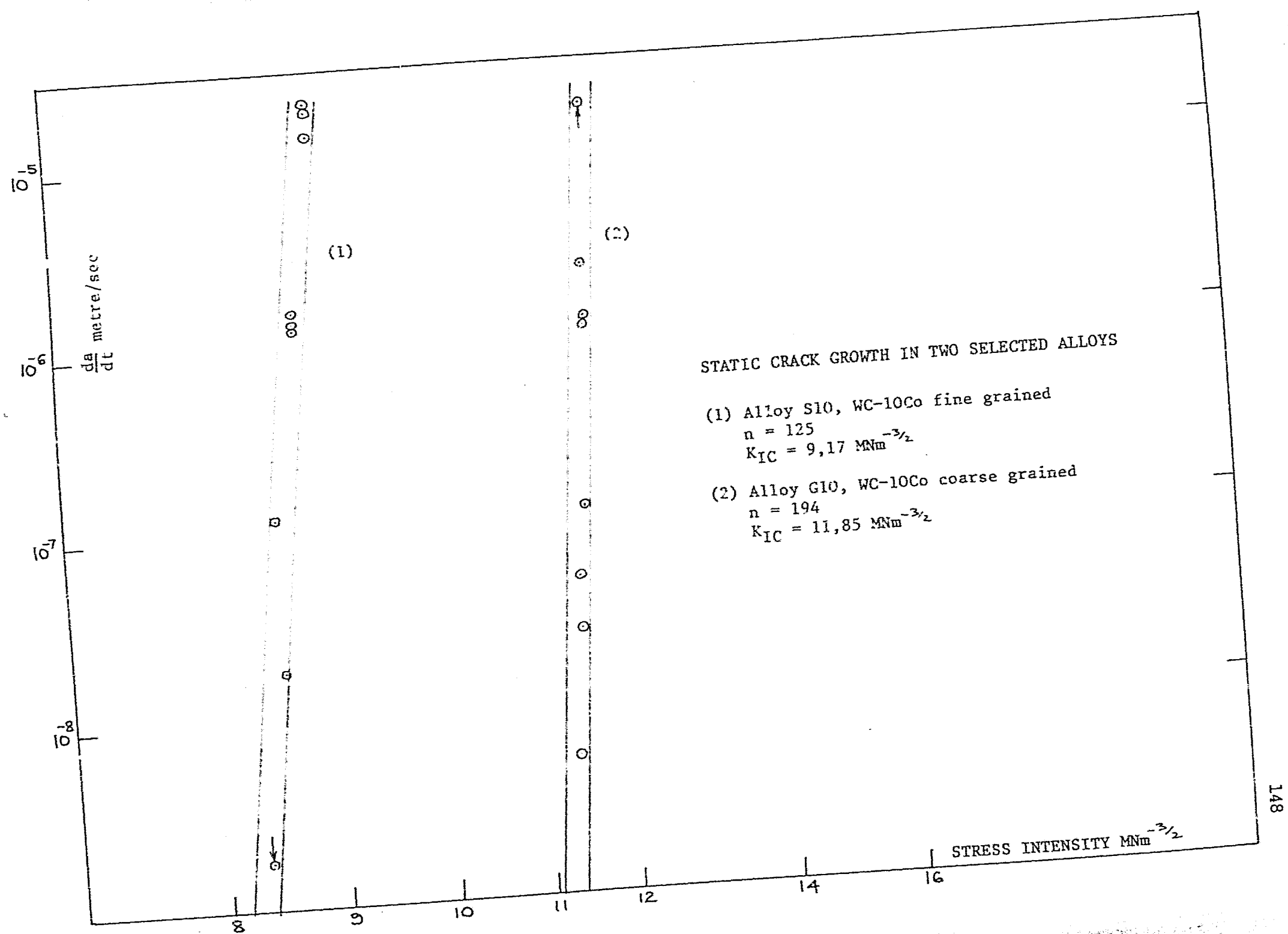

10^{-5}
10^{-6}
10^{-7}
10^{-8}
$\frac{da}{dt}$ metre/sec
(1)
(2)
STATIC CRACK GROWTH IN TWO SELECTED ALLOYS
(1) Alloy S10, WC-10Co fine grained
n = 125
K_{IC} = 9,17 $MNm^{-3/2}$
(2) Alloy G10, WC-10Co coarse grained
n = 194
K_{IC} = 11,85 $MNm^{-3/2}$
8
9
10
11
12
14
16
STRESS INTENSITY $MNm^{-3/2}$

Figure 5.1

5.1.2 Fracture Observations in SEM

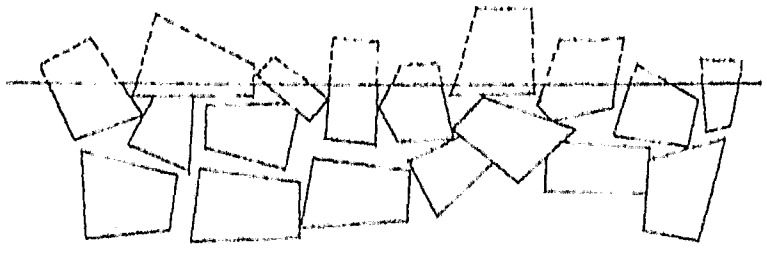
The objectives of the fracture studies carried out in the scanning electron microscope (Section 4.6) were:

(i) to establish whether static slow crack growth would occur in an inert (vacuum) environment, and

(ii) to observe mechanisms of static crack growth in tungsten carbide-cobalt alloys.

Figure 5.2 shows the crack path as manifest on the polished and etched surface. Figure 5.3 shows the extension of the crack before and after application of load. True slow crack growth, for example as reported by Tait[155] in cement mortar, using the same experimental technique, is not observed. Once the load has been applied the crack moves almost instantaneously to its next position at which point the stress intensity decreases to a value below that required for growth and the crack arrests.

The fractographic observations made indicate that the path of the crack is similar to that in fatigue fracture (Section 5.2.6) i.e. primarily intergranular but with transgranular fracture occurring, particularly in the large carbide grains. Surface observations unfortunately suffer from the "inverted iceberg" problem so that apparently large grains may in fact only be very thin wafers:



Load-unload-reload tests were performed on two specimens in order to assess whether or not ductile failure of the binder could be observed in situ. The results, as shown in Figures 5.4, 5.5 however, are not particularly conclusive. There is no indication of binder ligaments spanning the crack although some plastic deformation of the binder, as a result of closing of the crack, can be seen by comparing Figures 5.4(a) and (c) and also Figures 5.5 (a) and (c), sites of possible deformation are indicated with arrows. It is also shown that even with no load applied the crack does not close completely (Figures 5.4(b) and 5.5(b)).

The fine grained low cobalt (6 wt%) grade used for this work was not ideal for two reasons:

(i) it was necessary to use magnifications close to the limit of resolution of the microscope to observe effects, and

(ii) the mean free path and hence ductility of the binder is small in a fine grained low cobalt alloy.

A coarse grained, 10-15 wt% cobalt alloy would be more suitable.

In conclusion it should be noted that this technique has considerable potential and, with an alloy in which mechanisms can be observed at lower magnifications and higher resolution, could prove to be useful for determining fracture processes in this material.

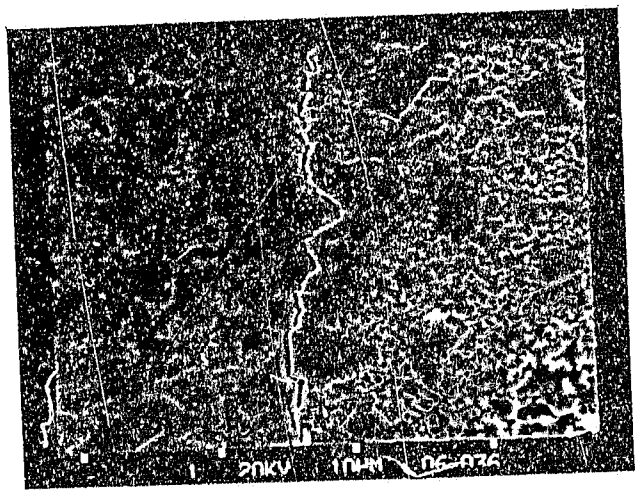
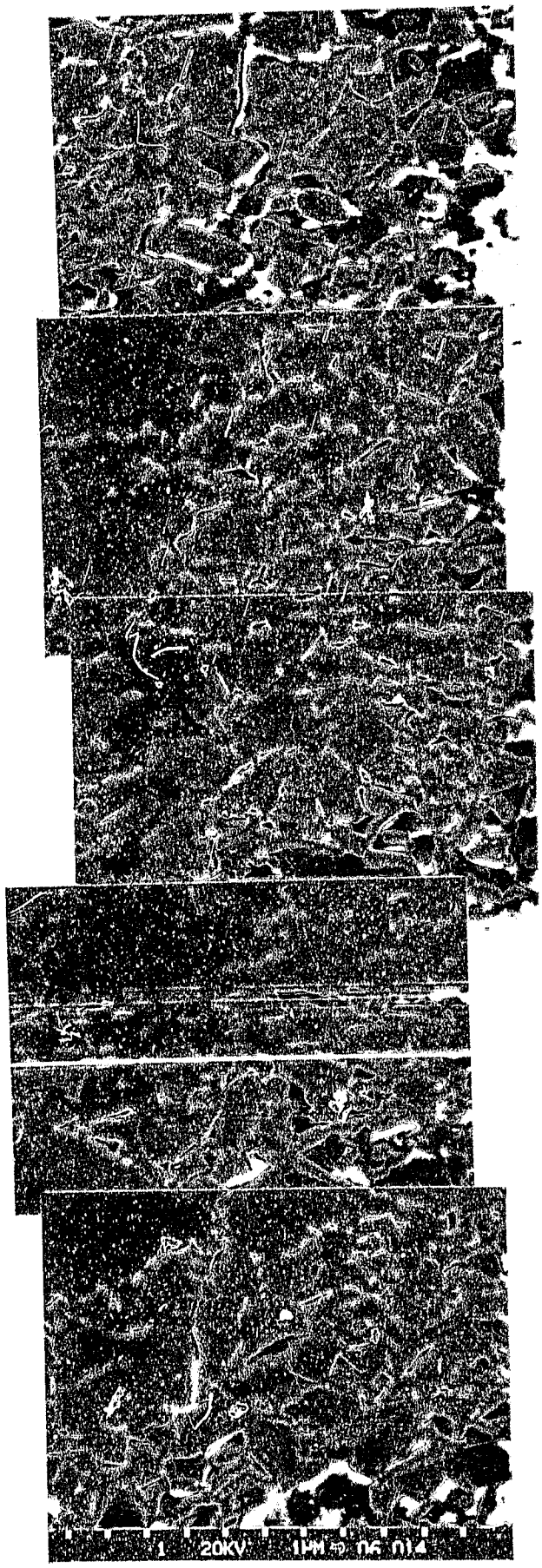
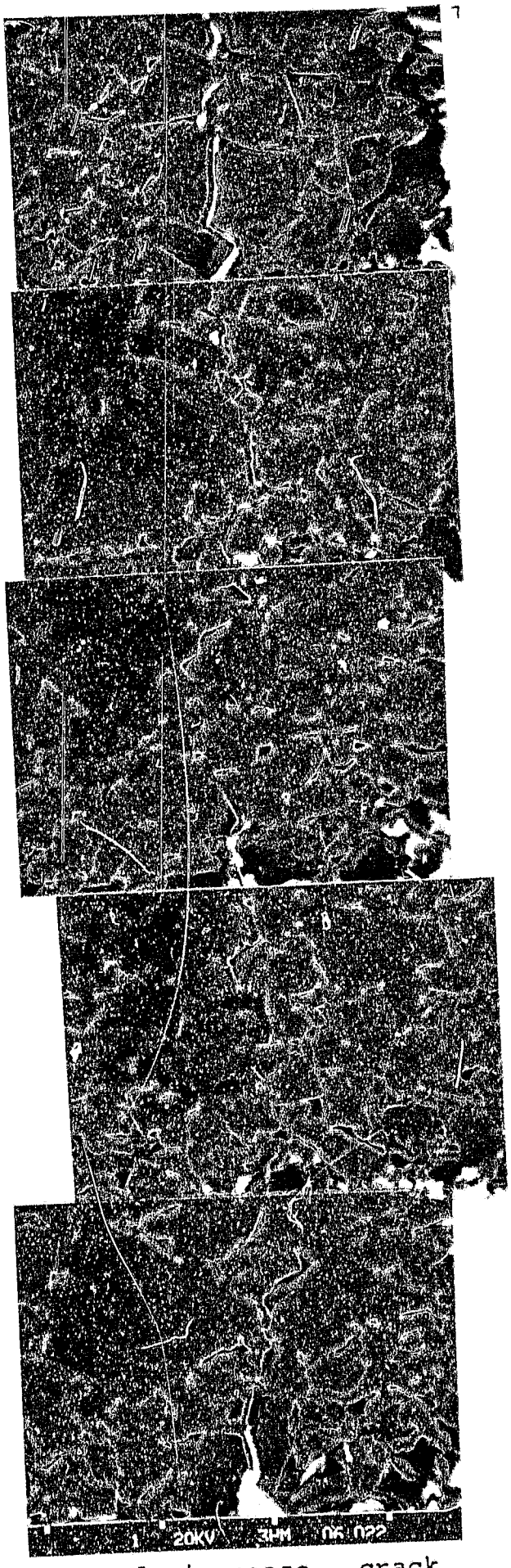


Figure 5.2 General view of fracture.



Before load increase.



After load increase, crack advances and crack opening displacement increases.

Figure 5.3

Author Fry P R
Name of thesis Fatigue crack growth behaviour of tungsten carbide-cobalt hardmetal alloys 1982

PUBLISHER:
University of the Witwatersrand, Johannesburg
©2013

LEGAL NOTICES:

Copyright Notice: All materials on the University of the Witwatersrand, Johannesburg Library website are protected by South African copyright law and may not be distributed, transmitted, displayed, or otherwise published in any format, without the prior written permission of the copyright owner.

Disclaimer and Terms of Use: Provided that you maintain all copyright and other notices contained therein, you may download material (one machine readable copy and one print copy per page) for your personal and/or educational non-commercial use only.

The University of the Witwatersrand, Johannesburg, is not responsible for any errors or omissions and excludes any and all liability for any errors in or omissions from the information on the Library website.